Turun yliopisto
University of Turku

VMAT2 AND GLP-1R TARGETING TRACERS FOR PANCREATIC BETA CELL IMAGING

Kirsi Mikkola

TURUN YLIOPISTON JULKAISUJA - ANNALES UNIVERSITATIS TURKUENSIS
Sarja - ser. D osa - tom. 1293 | Medica - Odontologica | Turku 2017

Turun yliopisto
University of Turku

VMAT2 AND GLP-1R TARGETING TRACERS FOR PANCREATIC BETA CELL IMAGING

Kirsi Mikkola

TURUN YLIOPISTON JULKAISUJA – ANNALES UNIVERSITATIS TURKUENSIS
Sarja - ser. D osa - tom. 1293 | Medica - Odontologica | Turku 2017

University of Turku

Faculty of Medicine
Institute of Clinical Medicine
Department of Clinical Physiology and Nuclear Medicine
University of Turku Doctoral Programme of Clinical Investigation
Turku PET Centre
MediCity Research Laboratory

Supervised by

Professor Pirjo Nuutila, MD, PhD
Turku PET Centre
University of Turku
Department of Endocrinology
Turku University Hospital
Turku, Finland

Professor Olof Solin, PhD
Turku PET Centre
University of Turku
Department of Chemistry
Turku, Finland

Veronica Fagerholm, PhD
Turku Centre for Biotechnology
University of Turku and
Åbo Akademi University
Turku, Finland

Reviewed by

Professor Timo Otonkoski, MD, PhD
Clinicum
Hospital for children and adolescent
University of Helsinki
Helsinki, Finland

Associate Professor Irina Velikyan, PhD
PET-Centre
Centre for Medical Imaging
Uppsala University Hospital
Uppsala, Sweden

Opponent

Assistant Professor Danielle J. Vugts, PhD
Department of Radiology and Nuclear Medicine
VU University Medical Center Amsterdam
Amsterdam, the Netherlands

Cover image: Kirsi Mikkola

The originality of this thesis has been checked in accordance with the University of Turku quality assurance system using the Turnitin OriginalityCheck service.

ISBN 978-951-29-6863-3 (PRINT)
ISBN 978-951-29-6864-0 (PDF)
ISSN 0355-9483 (Print)
ISSN 2343-3213 (Online)
Painosalama Oy - Turku, Finland 2017

To my family and friends

ABSTRACT

Kirsi Mikkola, MSc

VMAT2 and GLP-1R targeting tracers for pancreatic beta cell imaging

University of Turku, Faculty of Medicine, Institute of Clinical Medicine, Department of Clinical Physiology and Nuclear Medicine; University of Turku Doctoral Programme of Clinical Investigation; Turku PET Centre, Turku, Finland

Annales Universitatis Turkuensis, Medica-Odontologica, Turku, Finland 2017

Diabetes is characterized by hyperglycemia associated with beta cell dysfunction in type 2 diabetes (T2D) or loss in type 1 diabetes (T1D). Positron emission tomography (PET) could provide a possibility for the *in vivo* imaging of beta cells. This could be used for pathogenetic studies and to monitor therapeutic interventions. Currently, such a radiotracer is not clinically available.

In this thesis, the vesicular monoamine transporter 2 (VMAT2) and glucagon-like peptide-1 receptor (GLP-1R) were investigated as targets for beta cell imaging using [^{11}C]DTBZ, [^{68}Ga]NODAGA-exendin-4, [^{64}Cu]NODAGA-exendin-4, [^{64}Cu]NODAGA-MAL-exendin-4 and [^{18}F]exendin-4. The biodistribution and kinetics of the radiotracers in healthy and T1D animals was investigated by *in vivo* PET/CT imaging and *ex vivo* radioactivity measurements. The spatial distribution of radioactivity in pancreatic tissue sections of experimental animals and humans was analyzed by autoradiography.

The results showed that [^{11}C]DTBZ accumulation in pancreas is mainly nonspecific and does not represent specific binding to beta cells. [^{18}F]exendin-4, on the other hand, is a promising candidate for beta cell imaging. [^{18}F]exendin-4, produced at high specific activity, specifically labeled the islets in both human and rat pancreas, while exhibiting low binding in the exocrine pancreas. Unlike the metal-labeled exendin tracers investigated, excretion of [^{18}F]exendin-4 *via* the kidneys was rapid, resulting in a relatively low estimated absorbed radiation dose.

In conclusion, [^{18}F]exendin-4 is a promising radiotracer for beta cell imaging due to its specific labeling of the islets and concomitant low kidney retention. These properties make it suitable for further clinical development. For preclinical research, [^{64}Cu]NODAGA-exendin-4, with its long radioactive half-life, is also a useful tool.

Keywords: beta cell, pancreas, DTBZ, exendin, VMAT2, GLP-1R, PET, diabetes

TIIVISTELMÄ

Kirsi Mikkola, FM

VMAT2 ja GLP-1R kohdentuvat merkkiaineet haiman beetasolujen kuvantamisessa

Turun yliopisto, Lääketieteellinen tiedekunta, Kliininen laitos, Kliininen fysiologia ja isotooppilääketiede; Turun yliopiston kliininen tohtoriohjelma; Valtakunnallinen PET-keskus, Turku, Suomi

Annales Universitatis Turkuensis, Medica-Odontologica, Turku, Finland 2017

Diabetekselle on ominaista veren kohonnut glukoosipitoisuus sekä beetasolujen toimintahäiriö (T2D) ja tuhoutuminen (T1D). Positroniemissiotomografialla (PET) voitaisiin kuvantaa beetasoluja, edistää sairauden tutkimusta ja hoitokeinojen kehitystä. Tällä hetkellä ei ole olemassa merkkiainetta, jolla voitaisiin kuvantaa beetasoluja kliinisesti.

Tässä väitöskirjatyössä tutkittiin vesikulaarista monoamiini transportteri 2 (VMAT2) kuljetusproteiinia ja glukagonin kaltaisen peptidi-1 reseptoriin (GLP-1R) kohdentuvaa kuvantamista. Tutkimuksessa hyödynnettiin [^{11}C]DTBZ sekä [^{68}Ga]NODAGA-exendin-4, [^{64}Cu]NODAGA-exendin-4, [^{64}Cu]NODAGA-MAL-exendin-4 ja [^{18}F]exendin-4 merkkiaineita. Merkkiaineiden soveltuvuutta haiman beetasolujen kuvantamiseen tutkittiin merkkiaineen koko kehon jakaumana elävässä terveessä eläimessä ja T1D tautimallissa PET/CT kuvantamisella *in vivo*, kudosmittauksilla *ex vivo* sekä autoradiografialla radioaktiivisuuden paikkajakaumaa ihmisen ja rotan haimakudosleikkeillä.

Tutkimustulokset osoittivat, että [^{11}C]DTBZ kertymä haimassa on epäspesifistä eikä kuvasta spesifistä sitoutumista beetasoluihin. Peptideistä [^{18}F]exendin-4 sen sijaan on lupaava beetasolujen kuvantamiseen soveltuva merkkiaine. [^{18}F]exendin-4 merkkiaineella saavutettiin korkea ominaisaktiivisuus, se leimasi saarekkeet sekä ihmisessä että rotassa ja sitoutui vain vähän haiman eksokriiniseen osaan. Toisin kuin metalli-leimatut peptidit, [^{18}F]exendin-4 eritettiin nopeasti munuaisten kautta virtsaan. [^{18}F]exendin-4 säderasitus oli alhaisin.

[^{18}F]exendin-4 on lupaava merkkiaine haiman beetasolukuvantamiselle. Korkea ominaisaktiivisuus, spesifinen sitoutuminen haiman saarekkeisiin ja alhainen munuaiskertymä tekevät [^{18}F]exendin-4 merkkiaineesta lupaavan kliinistä kehitystä varten. [^{64}Cu]NODAGA-exendin-4 sen sijaan soveltuu pitkän puoliintumisajan ansiosta työkaluksi prekliiniseen tutkimukseen.

Avainsanat: beetasolu, haima, DTBZ, exendin, VMAT2, GLP-1R, PET, diabetes

TABLE OF CONTENTS

ABBREVIATIONS

AHH	adult hyperinsulinemic hypoglycemia
ATP	adenosine triphosphate
BB-DP	biobreeding diabetes prone
BF	blood flow
BID	twice a day
CHI	congenital hyperinsulinism of infancy
CT	computed tomography
DTBZ	dihydrotetrabenazine
EOS	end of synthesis
FOV	field of view
GLP-1	glucagon like peptide-1
GLP-1R	glucagon like peptide-1 receptor
HLA	human leukocyte antigen
HPLC	high performance liquid chromatography
HPTLC	high performance thin layer chromatography
5-HTP	5-hydroxytryptophan
IC_{50}	half maximal inhibitory concentration
i.p.	intraperitoneal
i.v.	intravenous
IVGTT	intravenous glucose tolerance test
L-DOPA	L-dihydroxyphenylalanine
MAO-A	monoamine oxidase A
MRI	magnetic resonance imaging
NaOH	sodium hydroxide
OGTT	oral glucose tolerance test
PET	positron emission tomography
p.i.	post injection

PSL	photostimulated luminescence
PVE	partial volume effect
ROI	region of interest
SA	specific activity
s.c.	subcutaneous
SD	standard deviation
SPECT	single photon emission tomography
STZ	streptozotocin
SUV	standardized uptake value
$T_{1/2}$	physical half-life
T1D	type 1 diabetes
T2D	type 2 diabetes
TAC	time-activity curve
TFA	trifluoroacetic acid
TLC	thin layer chromatography
VMAT2	vesicular monoamine transporter 2
VOI	volume of interest
ZDF	zucker diabetic fatty

LIST OF ORIGINAL PUBLICATIONS

This thesis is based on the following original publications, which are referred to in the text by their Roman numerals I–IV.

I Fagerholm V, Mikkola KK, Ishizu T, Arponen E, Kauhanen S, Någren K, Solin O, Nuutila P & Haaparanta M Assessment of islet specificity of dihydrotetrabenazine radiotracer binding in rat and human pancreas. *Journal of Nuclear Medicine* 2010; 51:1439–1446.

II Mikkola K*, Yim C-B*, Fagerholm V, Ishizu T, Elomaa VV, Rajander J, Jurttila J, Saanijoki T, Oikonen V, Tolvanen T, Tirri M, Gourni E, Béhé M, Gotthardt M, Reubi JC, Mäcke H, Roivainen A, Solin O & Nuutila P ^{64}Cu- and ^{68}Ga-labelled [Nle^{14},Lys^{40}(Ahx-NODAGA)NH$_2$]-exendin-4 for pancreatic beta cell imaging in rats. *Molecular Imaging and Biology* 2014; 16: 255–263.

III Yim C-B, Mikkola K, Fagerholm V, Rajander J, Elomaa VV, Ishizu T, Schlesinger J, Roivainen A, Nuutila P & Solin O Synthesis and preclinical characterization of [^{64}Cu]NODAGA-MAL-exendin-4 with a *N*$^{\varepsilon}$-maleoyl-L-lysyl-glycine linkage. *Nuclear Medicine and Biology* 2013; 40: 1006–1012.

IV Mikkola K, Yim C-B, Lehtiniemi P, Kauhanen S, Tarkia M, Tolvanen T, Nuutila P & Solin O Low kidney uptake of GLP-1R-targeting, beta cell-specific PET tracer, ^{18}F-labeled [Nle^{14},Lys^{40}]exendin-4 analog, shows promise for clinical imaging. *European Journal of Nuclear Medicine and Molecular Imaging Research* 2016; 6:91.

* Equal contribution

Additional results that are previously unpublished are also presented. The original publications have been reproduced with the permission of the copyright holders.

1. INTRODUCTION

Despite the large number of affected people worldwide, diabetes mellitus is yet without a cure. Diabetes can be roughly classified into two main types: type 1 (T1D) and type 2 (T2D). T1D develops due to autoimmune beta cell destruction, usually leading to absolute insulin deficiency. T2D develops due to a progressive loss of beta cell insulin secretion frequently on the background of insulin resistance (American Diabetes Association, 2017). Hyperglycemia is a late marker of the disease progression both in T1D and T2D. Even though some of the beta cells are unable to function or become destroyed over the course of the disease, the rest of the cells are initially able to compensate by increasing their insulin production until a critical point is reached and frank diabetes develops. Due to this plasticity in insulin production it is difficult to determine the functional beta cell mass.

The development of sensitive, non-invasive methods for the characterization and quantification of beta cell mass would greatly enhance our means for gaining understanding of the pathophysiology of diabetes and allow the development of novel therapies to prevent, halt and reverse the disease. Furthermore, the ongoing development of novel therapeutic approaches to diabetes, whether based on pharmacology or cell replacement, also calls for the rapid development of methods for longitudinal *in vivo* assessment of beta cell mass and function.

Studies with positron emission tomography (PET) suggest that pancreatic islets can be visualized using radioactive ligands that target insulin-producing beta cells (Medarova and Moore, 2008; Malaisse et al., 2009). However, there is an unmet need to develop a PET agent with the potential to enter clinical trials. Studies with laboratory animals are necessary to test the suitability of new radioactive tracers for studies conducted in humans. Preclinical evaluation of radiolabeled tracer candidates is needed to investigate their target specificity, biodistribution, metabolism and kinetic behavior.

In this thesis, the VMAT2 receptor targeting molecule DTBZ labeled with ^{11}C, and GLP-1R targeting exendin-based peptides labeled with ^{64}Cu, ^{18}F and ^{68}Ga were evaluated using preclinical methods, and their potential use in clinical imaging is discussed.

2. REVIEW OF THE LITERATURE

2.1 Islet physiology and regulation

The pancreas is located deep in the abdominal cavity where it is demarcated by the spleen, stomach and duodenum (Figure 1). In humans, the pancreas is a clearly defined and solid organ whereas in rodents the structure is more diffuse. Anatomically it is divided into three compartments: head (*caput*), body (*corpus*) and tail (*cauda*). The pancreas has two distinct functions: 1) the exocrine part produces digestive enzymes to be excreted into the duodenum *via* the pancreatic duct, and 2) the endocrine part which secretes hormones into the blood circulation.

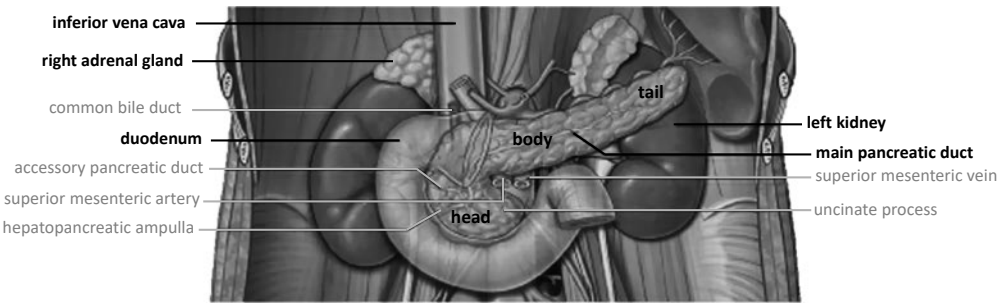

Figure 1. Location of the human pancreas in abdominal cavity. (Modified from Ellis, 2013).

The endocrine pancreas consists of small clusters of cells called islets of Langerhans which are distributed throughout the exocrine pancreas, constituting only 1–2 % of the total mass of the pancreas (Weir and Bonner-Weir, 2013). Islets consist of several different cell types: alfa, beta, delta, PP and ghrelin cells, and these produce glucagon, insulin, somatostatin, pancreatic polypeptide and ghrelin, respectively. Islets are densely innervated by sympathetic, parasympathetic and sensory nerves (Bockman, 2007). The autonomic nervous system synchronizes the function of the islets and enables the fluctuations in hormone production and optimal hormone secretion during metabolic stress, e.g. hypo- or hyperglycemia. Islets are highly vascularized with a network of fenestrated capillaries within the islet. Studies have shown islet blood flow (BF) to be 5–20 % of the total pancreatic BF and to be regulated independently of the BF in exocrine pancreas (Jansson et al., 2016). Islet BF is related to insulin release from the islets and is enhanced during hyperglycemia. Disturbed islet BF has been observed in impaired glucose tolerance (IGT) and T2D.

Blood glucose homeostasis

Glucose is the most important energy source for cell respiration and for the synthesis of organic compounds. The maintenance of glucose homeostasis is tightly regulated by the integration of hepatic glucose production, glucose uptake and utilization by peripheral tissues (muscle, liver and adipose tissue), and islet hormone secretion. The normal fasting blood glucose level in human is 4–6 mmol/l. Insulin and glucagon are the fundamental hormones for maintaining blood glucose homeostasis. Glucose metabolism is insulin-independent only in nervous tissue and blood cells. Insulin is secreted primarily in response to elevated blood glucose levels. In addition to glucose, it is secreted in a less potent manner in response to amino acids and free fatty acids (FFAs). Glucose is actively taken up from the blood into beta cells *via* specific glucose transporter molecules (Thorens, 1996; Fu et al., 2013). In beta cells, glucose is metabolized *via* glycolysis, and simultaneously ATP (adenosine triphosphate) is generated, which acts as a signal to insulin exocytosis. Insulin is secreted in a pulsatile manner (frequency/cycle 6–10 min) and in an oscillatory pattern (11–15/24 h) (Polonsky et al., 1988; Ahren, 2000). Increased pulse amplitude has been observed in conditions such as insulin resistance in obesity where the demand of insulin secretion is increased (Radetti et al., 1998; Zarkovic et al., 1999). Insulin lowers blood glucose levels by promoting glucose uptake in target organs and by inhibiting the glycogenolysis and gluconeogenesis, and the excretion of glucagon. Glucagon has opposite effects by stimulating glucose release into the blood circulation *via* glycogenolysis (liver, muscle) and gluconeogenesis (liver, kidney, intestine).

2.2 Diabetes – disease of the pancreas

The International Diabetes Federation has recently announced that 415 million people worldwide have diabetes at present and the incidence is estimated to rise to 642 million by 2040 (International Diabetes Atlas, 2015). Diabetes is a heterogeneous group of diseases characterized by hyperglycemia. It is roughly divided into type 1 (T1D) and type 2 diabetes (T2D). Other diagnosed diabetes subtypes are gestational diabetes, LADA (latent autoimmune diabetes in adults), MODY (maturity onset diabetes of the young), NDM (neonatal diabetes mellitus) and mitochondrial diabetes with deafness (MIDD) and other rare monogenic forms. Besides diabetes, other diseases of the pancreas, including pancreatitis, pancreatic insufficiency, Cushing's syndrome, hemochromatosis, pheochromocytoma and acromegaly, may also disturb blood glucose homeostasis, causing so called secondary diabetes. (American Diabetes Association, 2017.)

Type 1 diabetes (T1D)

Both genetic and environmental factors play an essential role in the pathogenesis of T1D (Figure 2). Human leukocyte antigen (HLA) genes were the first genes to be associated with genetic susceptibility of the disease, and several other loci have since then been identified (Atkinson, 2012). In most of the cases, beta cells are destroyed and T1D develops *via* T cell-mediated autoimmune attack and multiple antibodies against islet antigens are detected at disease onset (Bingley, 2010; Lampasona and Liberati, 2016). However, in 5.9 % of the cases where T1D was diagnosed, children did not express autoantibodies specific for T1D (Ziegler et al., 2013). Autoimmune attack is believed to be triggered by an environmental factor, e.g. diet, vitamin D deficiency, changes in normal gut microflora or after enterovirus infection, in genetically susceptible subjects (Atkinson, 2012). Development and onset of the disease is a long process where the asymptomatic non-diagnosed phase can last from months to years (Atkinson et al., 2014). The majority of the patients are diagnosed before 30 years of age (Maahs et al., 2010). The most common symptoms of hyperglycemia are polyuria, weight loss and exhaustion and ketoacidosis (Atkinson and Eisenbarth, 2001; Elding Larsson et al., 2014). Subjects are diagnosed to have T1D based on the autoantibodies, hyperglycemia at fast or during oral glucose tolerance test (OGTT) together with reduced C-peptide levels (Atkinson & Eisenbarth 2001, Elding Larsson 2014). Clinically diagnosed disease represents the end of the process when the majority of the beta cells are already destroyed (Eisenbarth, 1986). The speed of the beta cell destruction varies among the subjects and is highly variable during the course of the disease pathology. The rate of disease progression might be affected by several factors, e.g. genetic predisposition, age and metabolic control (Palmer, 2009). Insulin is required as a treatment to return normal blood glucose levels. Insulin therapy can be short- or long-acting compounds and administered *via* injections or specific pumps. Insulin treatment helps to balance blood glucose levels but may not completely prevent the long-term effects of diabetes such as eye, kidney, nervous and cardiac diseases. Maintaining the metabolic control in the body requires a major input from the patient. (Atkinson et al., 2014.)

Promising research results to restore the insulin secretion capacity have been obtained by immunotherapy and islet transplantation (Souza et al., 2006a). Although successful results have been achieved using the Edmonton protocol (Shapiro et al., 2000), transplantation of islets has not become a routine procedure in clinical practice because of the shortage of available islet donors, challenges in engraftment and side effects of the immunosuppressive medication needed to prevent the immune

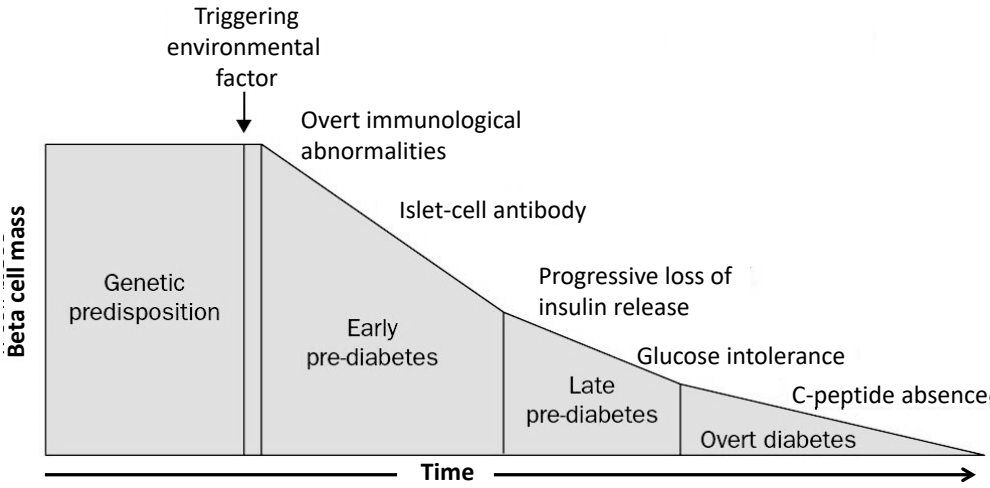

Figure 2. Model of the pathogenesis and the natural history of T1D. Both genetic and environmental factors play a role in the development of T1D. Insulin-producing beta cells are gradually destroyed *via* autoimmune attack leading to hyperglycemia. Clinically diagnosed disease represents the end of the disease pathophysiology. (Modified from Atkinson and Eisenbarth, 2001).

system from rejecting the islets (Bruni et al., 2014). Transplantation of differentiated embryonic stem cells and induced pluripotent stem cells (iPSC) may help overcome some of the present limitations (Balboa and Otonkoski, 2015). Genome-editing technology, CRISPR/Cas9, holds promise for clarifying the relevance of gene variants causing T1D and T2D, providing understanding of the pathophysiology of the disease and potential therapy (Teo et al., 2015). As an alternative to external cell replacement, reprogramming of the cell populations in the exocrine pancreas into functional beta cells could offer an autologous source for functional beta cells (De Groef et al., 2016). Biomarkers of proliferative beta cells could be utilized in the development of drugs for regenerative therapy in diabetes. One approach to restore functional beta cell mass is to develop strategies to inhibit beta cell apoptosis and dysfunction. (Benthuysen et al., 2016.) Clinically many of these approaches are still at an early stage of development.

Type 2 diabetes

T2D develops as a synergism of genetic susceptibility and environmental factors. The risk to develop T2D increases over time but it can also evolve in adolescents. Metabolic defects underlying T2D are insulin resistance, non-autoimmune beta cell dysfunction and increased hepatic glucose production. Insulin resistance (IR) is a pathological condition where glucose-utilizing tissues, e.g. skeletal muscle, liver and adipose tissue, fail to respond normally to insulin and do not promote glucose uptake

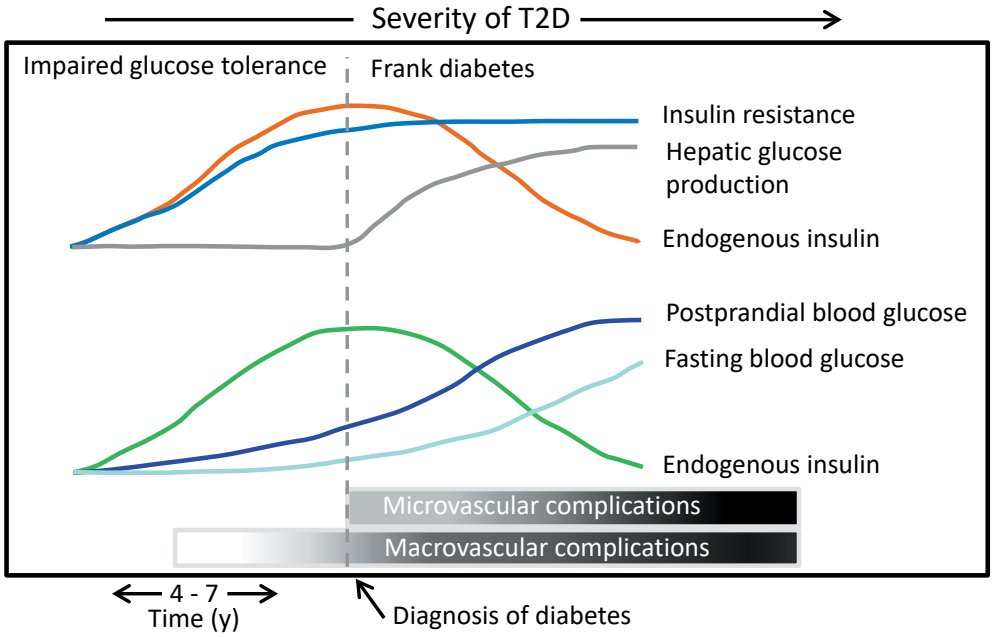

Figure 3. Model of the pathogenesis and the natural history of T2D.The disease is characterized by insulin resistance, impaired glucose tolerance and beta cell dysfunction leading to hyperglycemia and frank diabetes. Clinical symptoms are late markers of the disease process. (Modified from Ramlo-Halsted and Edelman, 2000).

into the cells (Figure 3). The effect of IR is most prominent in skeletal muscle which uses approximately 75 % of the circulating blood glucose (Nuutila et al., 1992). As a consequence, blood glucose levels remain high, and the beta cells continue to produce insulin, leading to hyperinsulinemia. Hyperinsulinemia keeps the blood glucose levels normal for a variable period of time. Eventually, beta cells are no longer able to produce enough insulin to compensate for IR and for the glucose over-production from the liver. (Souza et al., 2006a.) This will result in a state of impaired glucose tolerance (IGT) and hyperglycemia. As the IR proceeds and insulin levels fall, hepatic glucose production increases, leading to impaired fasting glucose (IFG). Over time, beta cells become refractory to glucose, beta cell function decreases and insulin production declines, leading to development of frank T2D. Clinical symptoms are a late marker of the disease; in the beginning the disease is asymptomatic or only minor symptoms are observed. An early indication of the disease is the disruption of the pulsatile secretion of insulin. (Satin et al., 2015.) IFG and IGT serve as markers for a clinical diagnosis of T2D.

Healthy diet, exercise and weight loss can prevent or at least postpone the onset of the disease (Tuomilehto et al., 2001). The treatment of T2D is based on lifestyle changes

(diet, physical activity) and medication. For morbidly obese subjects (BMI≥35 kg/m^2) bariatric surgery can be used as a tool to achieve remission. Early intervention reduces the incidence of micro- and macrovascular diseases and slows down the progression of the disease itself (Fowler, 2008). Different kinds of antidiabetic drugs appear to be effective at different stage of the disease to achieve glycemic control. Metformin is the first-line medication as it decreases weight and hepatic glucose production. Insulin secretion is increased by sulfonylureas (e.g. glibenclamide) but has a risk of hypoglycemia. Drugs either prolonging the half-life of naturally produced GLP-1 intestine by inhibition of DPP-4 enzyme came on the market 10 years ago. Thereafter, GLP-1 receptor agonists (e.g. exenatide, liraglutide) have been shown to be more potent by stimulating insulin production, decreasing glucagon production and delaying gastric emptying. SGLT2 inhibitors, the newest class of antidiabetic drugs, act by preventing glucose reabsorption to blood in kidneys. Instead, the excess glucose is excreted into urine. In the later stage of T2D, insulin often becomes mandatory in the treatment because insulin production in the beta cells is significantly decreased and glycemic control is disrupted. Challenges in insulin treatment are weight gain and hypoglycemia. (Ramlo-Halsted and Edelman, 2000.)

2.3 Beta cell mass and functional plasticity

Currently available methods for the diagnosis of diabetes only describe the function of the beta cells and not the mass of the cells. Due to the functional plasticity of beta cells, e.g. their ability to increase insulin production in response to increasing demands, the correlation between beta cell mass and function is poor. Also, a viable cell may have decreased insulin-secreting activity.

The architecture of the islet of Langerhans varies across the species. The shape of an islet is rather spherical in rodents, whereas in humans it is less regular with a size of 40–300 μm (Bosco et al., 2010). The amount of cells, the cell types in the islet and the size of the islets varies between different parts of the pancreas, within the species during different metabolic conditions, e.g. pregnancy, and between different species (Steiner et al., 2010; Roscioni et al., 2016). Studies with rats have shown the islet size to be smaller towards the upper duodenal part of the organ (*caput*) and larger towards the splenic part (*cauda*). The organization of the cells in the islets varies among species and has been associated with species difference in islet function. (Elayat et al., 1995.) It has been reported that in rodents beta cells form the core of the islet and are surrounded by the rest of the cell types (Figure 4) (Brissova et al., 2005). Instead, in primates, different cell types are distributed throughout the islet. In human islets,

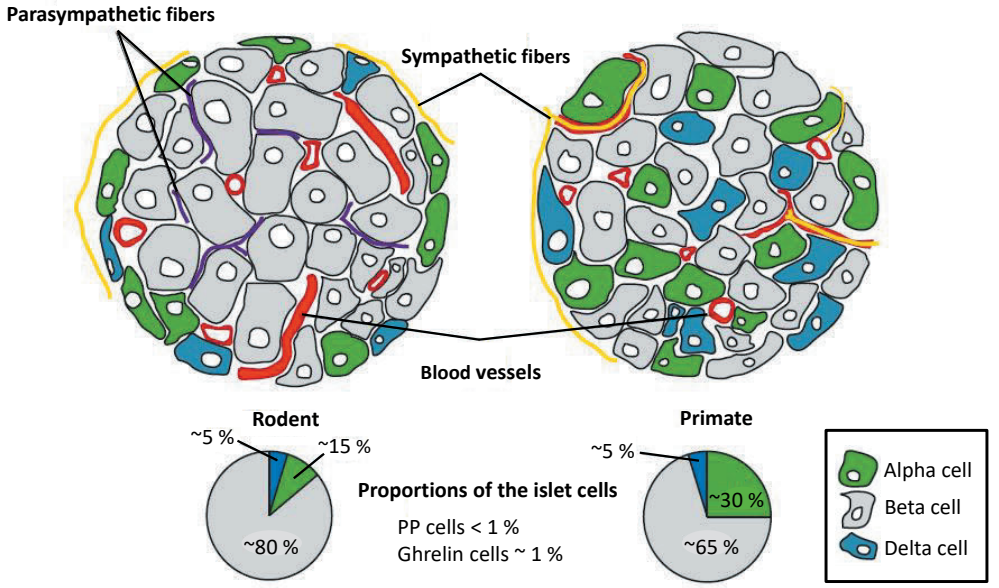

Figure 4. Islet cell architecture in rodent (A) and in human (B) is different. In rodents, beta cells are located in the core of the islet and are surrounded by the other islet cell types. In humans, different cell types are heterogeneously distributed in the islet. In diabetes the structure is disrupted and the ratio of islet cells is changed. (Modified from Arrojo e Drigo et al., 2015).

beta cells are thought to constitute ~65 % of the islet cell mass, whereas in rodents, the number is ~80 % (Cabrera et al., 2006; Arrojo e Drigo et al., 2015). More than 90 % of the endocrine cell mass is in the islets. Some isolated endocrine cells are found in ductal epithelium and as small cell clusters in proximity of ducts or scattered within the exocrine tissue (Bouwens and Pipeleers, 1998).

Despite the small size of the endocrine pancreas it has great functional capacity (Ferrannini, 2010). In metabolically healthy condition, blood glucose levels are maintained within a narrow range despite the wide fluctuations in glucose entry (e.g. meals) or clearance (e.g. exercise), mainly by the action of insulin. Sustained blood glucose level requires an adequate mass of beta cells that respond to circulating blood glucose concentration. The beta cell's capacity to produce appropriate amounts of insulin in response to fluctuating blood glucose levels is referred as beta cell function. (Matveyenko and Butler, 2008.) Studies have shown that the threshold for glucose-induced insulin release and biosynthesis varies between the beta cells (Salomon and Meda, 1986; Schuit et al., 1988). Due to this capacity and flexibility, islets can respond rapidly to changing blood glucose levels.

Studies with rodents have shown that beta cells exhibit a notable plasticity to adapt in response to altered insulin demand, starting at embryogenesis and continuing over

the whole lifespan (Bonner-Weir, 2001; Mezza and Kulkarni, 2014). In humans, high proliferation of beta cells occurs during embryogenesis and decreases postnatally (Meier et al., 2010; Gregg et al., 2012). Under normal metabolic conditions, beta cell mass remains relatively constant during adulthood (from 20 to 100 years old) because of the low levels of proliferation and apoptosis. In adulthood, beta cells are sensitive to IAPP (aggregates of islet amyloid polypeptide, IAPP), cell cycle perturbations, ER (endoplasmic reticulum) stress and oxidative stress affecting beta cell function and survival. (Mezza and Kulkarni, 2014.) The rate of beta cell apoptosis has been reported to be increased both in obese and lean T2D subjects compared with the lean and non-diabetic ones. This has been explained by the fact that the amount of islet amyloid plaques are increased in obese compared to non-diabetic subjects. (Butler et al., 2003.) Islet morphology is changed and islet amyloid deposits have been found in up to 90 % of T2D individuals after autopsy (Kahn et al., 1999).

Beta cells can cope with a wide range of body mass (Ferrannini, 2010). Autopsy studies have shown that obese non-diabetic individuals have extended beta cell mass and volume (Butler et al., 2003; Rahier et al., 2008). There is a significant reduction in beta cell mass when insulin dependent-diabetes develops (Weir et al., 1990). However, it is unclear how many beta cells are needed to maintain glucose homeostasis. Only minor deterioration in maintaining normal blood glucose levels is seen after 50 % pancreatectomy in humans and in experimental animals. Insulin resistance related to obesity is an important factor leading to hyperglycemia and yet diabetes is found only in a minority of obese people. (Ferrannini, 2010.)

The necessary amount of functional beta cell mass varies among individuals and is affected by the body weight and the level of insulin resistance and metabolic stress. Autopsy samples have shown beta cell mass to be ~60 % of normal in T2D, and the decrease in beta cell mass correlates with the duration of the clinical disease (Rahier et al. 2008). Although, such a mass of beta cells could be considered sufficient for diabetes prevention, it has been noted that the arginine and glucose stimulated insulin secretion capacity is reduced to 15 % of normal (Weir et al., 1990). Beta cells can be present after long-standing (> 5 y) T1D (Coppieters et al., 2012) and it has been shown that beta cells may persist with some T1D subjects never reaching zero (Meier et al., 2005). Even after 50 y of insulin-dependent T1D, residual beta cell mass and insulin secretion capacity have been reported (Keenan et al., 2010). Significant changes are observed in the size of the pancreas already before clinical diagnosis of T1D, indicating changes in exocrine pancreas in the course of the disease (Williams et al., 2012). At the moment it is not possible to connect this loss of function to the mass of beta cells.

2.4 The rationale of beta cell imaging and its applications

There is an unmet need for a reliable method to non-invasively characterize beta cell loss and dysfunction. Human pancreatic samples are currently available only at autopsy, surgery and material received from organ donors. Because of the location in the abdominal cavity, enzymatic composition of the organ and therefore risk of complications, pancreas is an organ hard to biopsy (Krogvold et al., 2014). With the currently clinically available methods, one can not distinguish loss of beta cell mass from the loss of beta cell function, or distinguish beta cell regeneration from functional recovery during drug therapy (Eriksson et al., 2016). Current therapeutic approaches for T1D and T2D are aimed at to preserving and/or replenishing the functional beta cell mass, enhancing *in vivo* regeneration and proliferation of existing beta cells. New therapies are needed to halt the beta cell apoptosis, to promote the function of remaining beta cells and regenerate functional beta cells (Mezza and Kulkarni, 2014). Understanding the concept of mass *vs.* function may be an area of particular interest in future diabetes research. Studies have revealed inter-individual variations in beta cell mass (Rahier et al., 2008). Increased knowledge of the pathophysiology of the disease will promote the development of more personalized care and therapy for the patient. Clinical imaging of beta cells will play a central role in the development towards personalized diabetes therapy and prevention. Such methods are expected to provide means for more precise treatment planning, such as deciding for a T2D patient whether or not it is beneficial to switch to insulin replacement therapy, or in order to learn if a T1D patient has a reserve capacity of non-functional beta cells that could restore endogenous insulin release (Faustman, 2014; Gotthardt et al., 2014).

Imaging beta cell derived tumors

Besides promoting the drug development and helping to distinguish between beta cell mass and function, beta cell specific tracers could be utilized in clinics as tools to image tumors and transplanted islets. The treatment strategy of congenital hyperinsulinism of infancy (CHI) and adult hyperinsulinemic hypoglycemia (AHH) relies mainly on the surgical removal of the tumor. Preoperative localization of the tumor is critical to minimize surgical intervention. CHI is a disease caused by gene mutations and is characterized by severe hypoglycemia due to beta cell hyperplasia and dysregulated insulin secretion. Although having a similar clinical presentation, the pathology of the disease can be either diffuse or focal, making clinical diagnosis and surgery difficult. [^{18}F]DOPA (fluorine-18 L-3,4-dihydroxyphenylalanine) PET was successfully used to detect the focal form of CHI and is currently recommended when genetic changes suggest the focal form of the lesion (Otonkoski et al., 2006; Minn et al., 2009). In

contrast to CHI, the use of [^{18}F]DOPA for AHH is not completely characterized (Kauhanen et al., 2007; Kauhanen et al., 2010; Tessonnier et al., 2010). Peptide-based tracers such as [^{68}Ga]DOTA-Tyr^{3}-octreotate (DOTATATE), [^{68}Ga]DOTA-1-Nal^{3}-octreotide (DOTANOC) and [^{68}Ga]DOTA-Tyr^{3}-octreotide (DOTATOC) that target somatostatin receptors (sst), have been used for imaging insulinomas in adults (Johnbeck et al., 2014). Unfortunately, the expression of somatostatin receptors, especially sst_2, is limited in many insulinomas, leading to false negative results (Reubi and Waser, 2003). Instead, the GLP-1R has a promising expression profile for suitable imaging of insulinomas and other neuroendocrine tumors (Hubalewska-Dydejczyk et al., 2015). The GLP-1R targeting tracers [^{111}In]DOTA-exendin-4 ([Lys^{40}(Ahx-DOTA-^{111}In)NH_2]exendin-4) (Christ et al., 2009), [^{68}Ga]NOTA-exendin-4 (^{68}Ga-NOTA-MAL-Cys^{40}-exendin-4) (Luo et al., 2016a), [^{68}Ga]DOTA-exendin-4 ([Nle^{14},Lys^{40}(Ahx-DOTA-^{68}Ga)NH_2]exendin-4) (Antwi et al., 2015) tracers were more sensitive than conventional imaging methods (CT, MRI) for detecting tumors.

Imaging islet transplantation

For T1D, pancreatic islet transplantation is a promising but still experimental treatment. Although the hepatic portal vein is the standard grafting site in clinical islet transplantation it is not without potential procedural risks such as portal thrombosis and bleeding (Bruni et al., 2014). Also, the function of the graft has been reported to decline over time. Five years after transplantation, 10–20 % maintained insulin independence (Ryan et al., 2005; Low et al., 2010). Further improvement of graft survival and function is required. Development of new implantation sites and new tools for *in vivo* detection of islet graft is needed to improve the transplantation outcomes. Pattou et al. 2010 successfully performed autologous forearm intramuscular islet engraftment and follow-up imaging with [^{111}In]DTPA-exendin-4 ([Lys^{40}(Ahx-DTPA-^{111}In)NH_2]exendin-4) one year after transplantation (Pattou et al., 2010). Recent studies with mice and rats showed linear correlation between the number of islets and radiolabeled exendin accumulation, when muscle was used as an engraftment site (Espes et al., 2016; van der Kroon et al., 2016).

2.5 Clinical imaging methods for beta cells

2.5.1 Non-invasive in vivo nuclear medicine imaging methods

Positron emission tomography (PET) is a functional and quantitative imaging method used widely to image various processes in the body. It is a sensitive method and can

be used to detect very low concentration of radiotracer in the tissue. However, the resolution is limited to 1–2 mm in animal and 4–6 mm in human PET scanners (Spanoudaki and Ziegler, 2008; Tai et al., 2005). It utilizes molecules that are labeled with short-lived positron-emitting radionuclides e.g. ^{11}C, ^{18}F (Table 1). A wide variety of biological molecules can be labeled with radionuclides and used to image various biological processes in the body, e.g. glucose metabolism or receptor-ligand interaction. Once a radiolabeled molecule is injected into the blood circulation, the radionuclide decays by emitting a positron (β^+). The positron annihilates upon interaction with an electron (e^-) and as a consequence two annihilation photons (511 keV each) are emitted simultaneously in opposite directions (Figure 5A). In a PET scanner, these photons are recognized in coincidence in a ring of detectors. Sinograms and cross-sectional images are formed after mathematical corrections, e.g. for tissue attenuation, dead-time and random events, and finally reconstructed PET images are formed. (Turkington, 2001; Rahmim et al., 2007; Rahmim and Zaidi, 2008; Spanoudaki and Ziegler, 2008.)

Table 1. Physical properties of positron emitters used in PET.

Radio-nuclide	Half-life [min]	β^+ fraction [%]	Positron max energy [keV]	Max range [mm]*	Production method
^{18}F	109.8	96.7	634	2.4	cyclotron
^{11}C	20.4	99.8	960	4.1	cyclotron
^{64}Cu	762	17.6	653	2.5	cyclotron
^{68}Ga	68.3	87.7	1899	8.9	cyclotron/generator

National Nuclear Data Center (www.nndc.bnl.gov/ 1.3.2015)
* In water

Single photon emission computed tomography (SPECT) is a method utilizing long-lived radionuclides that emit gamma radiation, e.g. ^{111}In and ^{99m}Tc. Singly emitted gamma rays are detected directly by a gamma camera rotating around the object (Figure 5B). This method of radioactivity detection has low sensitivity, meaning that a lower percentage of emitted events is detected compared to PET. Depending on the design of the collimators, higher spatial resolution, (animal SPECT scanner < 1 mm, human SPECT scanner 1–2 cm) can be achieved with dedicated small animal SPECT scanners compared to PET (Rahmim and Zaidi, 2008; Spanoudaki and Ziegler, 2008). However, increased resolution is a trade-off with decreased sensitivity. In addition to spatial resolution, temporal resolution is an important feature (dynamic imaging). As a more sensitive method, PET allows superior temporal resolution over SPECT. In SPECT, image quality is compromised by several factors including photon

attenuation, photon scatter, the partial volume effect, and motion artefacts (Ritt et al., 2011; Rahmim and Zaidi, 2008). These variables also confound the capacity of SPECT to quantify the concentration of radioactivity within given volumes of interest in absolute units (Bq/ml). In PET, options to correct for these confounding variables have been validated owing to the technical advantages offered by positron decay and coincidence detection. In SPECT, lacking the quantitative ability, such technical development has been notably slower. However, considerable technical advancement has been achieved in SPECT image reconstruction to improve the quality of data. (Ritt et al., 2011.)

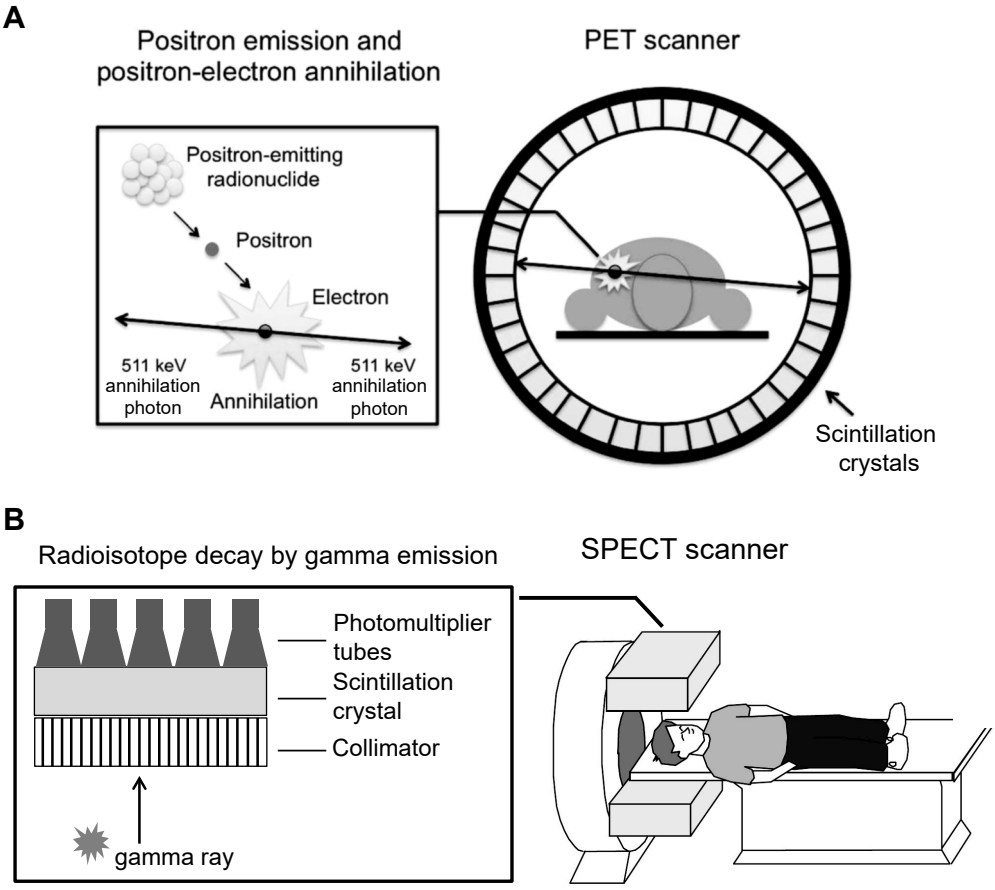

Figure 5. Physics of PET (A) and SPECT (B). A radioactively labeled compound is administered into the body. PET imaging utilizes positron emitting radionuclides. In radioactive decay, positron is emitted, it annihilates with an electron and as a consequence two opposing annihilation photons are emitted. These photons are detected in coincidence in a ring of detectors. SPECT imaging utilizes gamma ray emitting radionuclides. These singly emitted gamma rays are registered directly by detectors rotating around the object. (Modified from Cherry and Gambhir, 2001; Zeng et al., 2004).

2.5.2 Structural imaging methods – magnetic resonance imaging (MRI)

Compared to PET and SPECT, magnetic resonance imaging (MRI) does not involve radionuclides and can be used for repeated and long-term imaging. It has high spatial resolution, it is not limited by tissue penetration, and it provides excellent soft tissue contrast. However, it is less sensitive than nuclear medicine techniques. To improve the target to background signal, MRI involves the use of contrast agents such as manganese (Mn^{2+}) and gadolinium (Gd^{3+}). The use of contrast agents needs to be carefully planned to avoid the possible side effects such as allergic reactions, acute adverse reactions or nephrotoxicity. (Khalil et al., 2011; Beckett et al., 2015.)

2.6 Non-invasive imaging of pancreatic beta cells

Various kinds of potential beta cell targeting molecules and targets have been investigated (Figure 6). From a clinical perspective, the most promising results have been obtained with PET, SPECT and MRI methods. Peptides (exendin), neurotransmitter precursors such as L-dihydroxyphenylalanine (L-DOPA) and 5-hydroxytryptophan (5-HTP), antibodies for IC2 receptors or channels (repanglinide, glibenclamide) on the surface of the beta cell or inside the cell, or metabolic pathways (FDG) have been explored. Currently, molecules under clinical evaluation are radioactively labeled exendin, 5-HTP and DTBZ (dihydrotetrabenazine). Recent results have shown progress with G protein-coupled receptor 40 (GPR-40, also known as free fatty acid receptor FFAR1) and G protein-coupled receptor 44 (GPR-44, also known as prostaglandin D2 receptor PTGDR2) imaged with tritiated TAK875 and AZD 3825, respectively (Bertrand et al., 2016; Hellstrom-Lindahl et al., 2016). GPR-44 showed high beta cell specificity and has potential for good islet-to-exocrine tissue ratio. Novel biomarker FXYD2γa, a regulatory subunit of the Na^+–K^+-ATPase, was identified as beta cell specific membrane protein and its production was observed to decrease in parallel with the beta cell loss in T1D (Flamez et al., 2010). In addition, many other non-clinical methods are used for beta cell imaging purposes, for example, different optical imaging modalities such as intravital confocal microscopy (Reiner et al., 2011), optical projection tomography (Eter et al., 2016) and extended focus optical coherence tomography (Villiger et al., 2009).

MRI. Mn^{2+} is a contrast agent used in MRI. Mn^{2+} enters the beta cell in a glucose-dependent manner *via* Ca^{2+} channels. Besides beta cells, Ca^{2+} channels are present in the alpha cells of the islets. Thus, only functional cells with proper glucose metabolism will take up high levels of Mn^{2+}. The Mn^{2+} accumulation in pancreas of normal and streptozotocin (STZ) induced diabetic mice under glucose stimulation

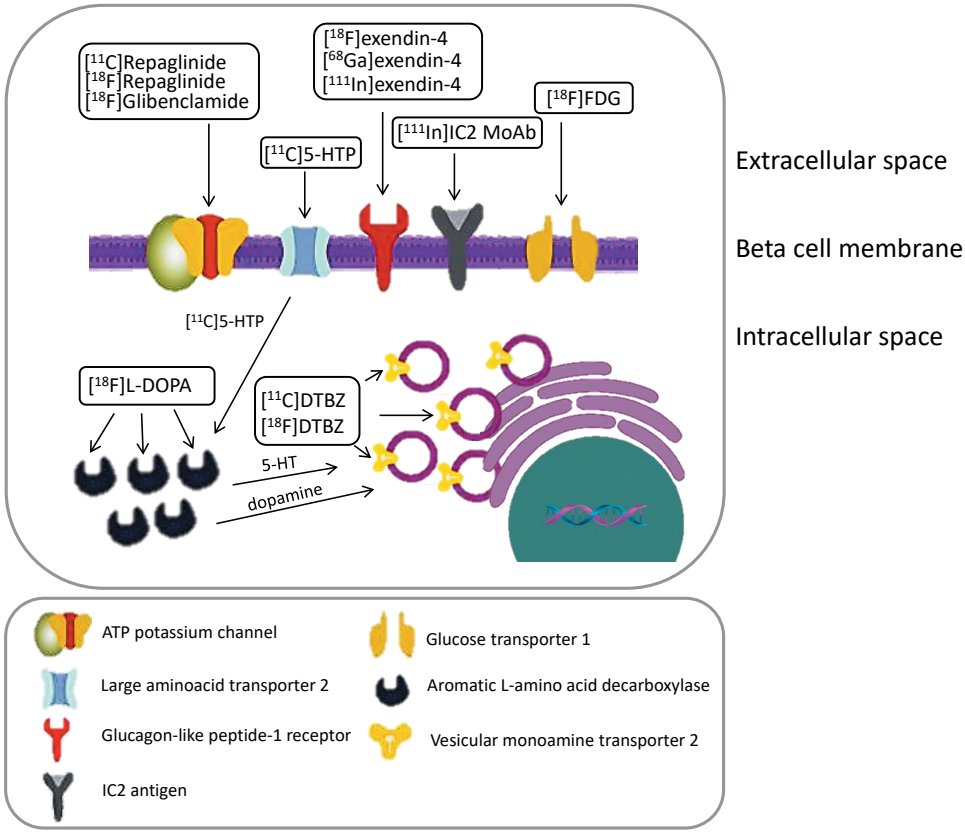

Figure 6. Schematic overview of targets and radioligands for pancreatic beta cell imaging. (Modified from Di Gialleonardo et al., 2012a).

were investigated (Antkowiak et al., 2009). In normal mice, glucose stimulation induced a 51 % increase in signal within the pancreas compared to the control (saline) group. In contrast, mice that were administered with a low dose of STZ gave a higher signal compared to mice administered with a high dose of STZ, indicating that Mn^{2+} enhanced MRI could be used to image beta cell function under glucose stimulation. However, the usefulness of Mn^{2+} is limited because Ca^{2+} channels are present in the alpha cells of the islets (lack of specificity) and because of possible cytotoxic effects of Mn^{2+}. MRI was successfully used for beta cell imaging when exendin-4 was conjugated with magnetic iron oxide-based nanoparticle probe (MN-Ex10-Cy5.5) (Wang et al., 2014). A significant decrease of probe accumulation in pancreas was observed in diabetic NOD mice compared to pre-diabetic ones, indicating the beta cell loss.

Monoclonal antibodies, such as [^{111}In]DTPA-IC2 (Moore et al., 2001), have been considered promising probes for beta cell imaging. Its accumulation in the pancreas of healthy mice was higher than in mice with STZ induced diabetes. However, because

of the large size of immunoglobulins, its clearance from blood and therefore its kinetics is slow, which limits its use in clinical applications. To overcome this problem, single-chain antibodies and antibody fragments have been developed (Ueberberg et al., 2009).

5-HTP is a serotonin precursor and [^{11}C]5-HTP was originally developed for neuroimaging. As the beta cell shares many features with neurons, 5-HTP was investigated for beta cell imaging. 5-HTP is taken up into beta cells *via* L-type amino acid receptor (LAT). Di Gialleonardo and colleagues observed [^{11}C]5-HTP uptake in rat beta cells during inhibition of 5-HTP using MAO-A (monoamine oxidase A). Without enzyme inhibition, no signal was detected. Furthermore, it was shown that by inhibiting MAO-A in the STZ-induced T1D rat model, [^{11}C]5-HTP uptake in pancreas was decreased as compared to control rats. (Di Gialleonardo et al., 2012.) Clinical studies showed a 66 % decrease of [^{11}C]5-HTP uptake in pancreas of long-standing T1D subjects compared to healthy volunteers. Besides beta cells, [^{11}C]5-HTP also targets alpha cells in the islets, thus complicating the interpretation of the results, as a loss of beta cells can be expected to only partly reduce the signal. (Eriksson et al., 2014.)

2.6.1 VMAT2 receptor and DTBZ tracers

Vesicular monoamine transporter 2 (VMAT2) is a transmembrane protein located in the monoamine-storing vesicles in beta cells (Zheng et al., 2006; Adam et al., 2008). It transports monoamines such as serotonin, dopamine and adrenaline from the cytoplasm into the vesicles (Erickson et al., 1992; Peter et al., 1994). In the islets, VMAT2 is expressed in rodent and human beta cells, but also in the PP cells (Maffei et al., 2004; Saisho et al., 2008; Freeby et al., 2012). Besides islets, VMAT2 is known to be expressed in the neuroendocrine system (chromaffin cells of the adrenal medulla), enterochromaffin and enterochromaffin-like cells of the gastrointestinal tract cells, the central and peripheral nervous system and the hematopoietic system (Weihe et al., 1994; Peter et al., 1995; Weihe and Eiden, 2000).

Originally targeted for imaging Parkinson's disease and other neurodegenerative diseases (Efange, 2000), DTBZ binds specifically to VMAT2 and has high affinity for the receptor ((+)-α-DTBZ, K_i 2 nM) (Kilbourn, 1997). Studies have shown [^{11}C]DTBZ to accumulate in the healthy pancreas of control rats and decline in the STZ-induced diabetic rats (Simpson et al., 2006). A similar observation was made with BB-DP rats (biobreeding diabetes prone, spontaneously developing T1D) compared to healthy controls (Souza et al., 2006b). In addition, the uptake in pancreas was lower with

long-standing T1D subjects compared to healthy volunteers (Goland et al., 2009). Nevertheless, residual uptake in the pancreas was observed and it prompted the question concerning tracer specificity and binding to other cells than beta cells. This residual uptake might be partly explained by the uptake in PP cells or sympathetic nerve endings innervating the pancreas, or by non-specific binding (Mei et al., 2002; Saisho et al., 2008; Eriksson et al., 2010). PP cells constitute approximately ~0.81 % of the human pancreas total volume and are also found in the pancreas of humans with long-standing T1D (Freeby et al., 2012). Studies with the T1D rat model (BB-DP) have shown nerve endings innervating the islets to degrade during the onset of T1D, while the nerve endings innervating the exocrine pancreas remain intact (Mei et al., 2002). Since VMAT2 in the pancreas is not solely expressed in beta cells of the islets, it challenges the interpretation of the *in vivo* imaging of results.

Fluorine-18 labeled DTBZ ([^{18}F]-FP-(+)-DTBZ, [^{18}F]-FE-(+)-DTBZ) was developed to overcome the short half-life of carbon-11 and improve the affinity (FP-(+)-DTBZ, K_i 0.10 ± 0.04 nM) for the target receptor (Kung et al., 2007; Kung et al., 2008b). Animal studies with [^{18}F]-FP-DTBZ showed high uptake in the pancreas and lower uptake in the non-target tissues, especially in the liver and decreased uptake in the pancreas of the T1D animal model (Kung et al., 2008a; Kung et al., 2008b; Singhal et al., 2010). Despite active research, tracer development, and promising *in vivo* results with different animal models and clinical imaging, the results of DTBZ localization selectively to pancreatic islets are controversial and have not yet been confirmed. More research is needed to understand which fraction of the radioactive signal is derived from beta cells, PP cells, exocrine pancreas or non-specific binding.

2.6.2 GLP-1, GLP-1 receptor and exendin tracers

Glucagon like peptide-1 (GLP-1) (plasma half-life < 2 min) is an incretin hormone secreted from the intestinal L-cells in response to ingestion of food. Increasing evidence show GLP-1 secretion also from the alpha cells of the pancreatic islets (Fava et al., 2016). GLP-1 contains an alanine residue in position two and is thus rapidly catabolized by dipeptidyl peptidase IV (DPP-IV). By binding to the 7-transmembrane G-protein coupled glucagon-like peptide-1 receptor (GLP-1R) on the surface of the pancreatic beta cells, GLP-1 stimulates insulin secretion in a glucose-dependent manner. GLP-1 also lowers blood glucose levels *via* inhibition of gastric emptying and inhibition of glucagon secretion from the alpha cells. (Drucker, 1998; Nadkarni et al., 2014; Fava et al., 2016.) The mechanism of GLP-1 induced inhibition of glucagon secretion is not fully understood (Holst et al., 2011). The GLP-1R expression pattern

is rather similar in rat and in human (Körner et al., 2007). The GLP-1R is expressed in pancreatic beta cells with little to no expression found on other pancreatic islet cell types (Körner et al., 2007; Tornehave et al., 2008; Brom et al., 2015).

Originally, the 39-amino acid, long-acting GLP-1R agonist exendin-4 (1-39), was purified from the venom of the *Heloderma suspectum* lizard and subsequently found to elicit biological effects that mimic the physiological actions of GLP-1. In contrast to GLP-1, exendin-4 contains a glycine residue in position two and is therefore not a substrate for DPP-IV-mediated catabolism. Exendin-4 shares 53 % homology with mammalian GLP-1 and has 10-times higher GLP-1R affinity. Exendin-3 (9-39) is a stable antagonist of GLP1-R. (Göke et al., 1993; Rylova et al., 2016.) The primary site of GLP-1 clearance appears to be through the kidney *via* mechanisms that includes glomerular filtration and tubular catabolism (Simonsen et al., 2006).

The GLP-1R has become an important target for imaging due to its abundant expression in pancreatic beta cells, the cardiovascular system, and in many tumors such as insulinoma, gastrinoma, pheochromocytoma and medullary thyroid cancer (Körner et al., 2007; Hubalewska-Dydejczyk et al., 2015). Several exendin-based tracers labeled with ^{111}In or ^{99m}Tc for SPECT (Gotthardt et al., 2006; Wild et al., 2006) and ^{68}Ga, ^{18}F, for PET (Brom et al., 2010b; Gao et al., 2011; Wu et al., 2011; Connolly et al., 2012; Kiesewetter et al., 2012b) have been intensively explored. Whether performed in animal models (Brom et al., 2010b; Wild et al., 2010) or clinical trials (Wild et al., 2008; Christ et al., 2009; Wild et al., 2011), many of the studies focused on imaging insulinomas, tumors that over-express the target receptor. [^{111}In]DTPA-exendin-4 showed high uptake in tumor-bearing transgenic Rip1Tag2 mice (Wild et al., 2006). A study by Christ and colleagues reported proof of the concept that [^{111}In]DOTA-exendin-4 SPECT is a tool to preoperatively detect intra- and extra-pancreatic insulinomas in humans (Christ et al., 2009). Tracer accumulation in tumors after *in vivo* SPECT correlated with the GLP-1R expression confirmed with *in vitro* receptor autoradiography of tumor samples. [^{111}In]DTPA-exendin-4 SPECT and [^{68}Ga]DOTATE PET *in vivo* imaging combined with *in vitro* receptor autoradiography showed that malignant insulinomas do not necessarily express GLP-1R (Wild et al., 2011; Sowa-Staszczak et al., 2016). These tumors more frequently expressed sst2 receptor than GLP-1R. Negative scan results using exendin analogs, may potentially indicate tumor malignancy (Sowa-Staszczak et al., 2016; Luo et al., 2016b). In a principle of proof study, [^{64}Cu]DO3A-VS-Cys^{40}-exendin-4 detected human islet cells transplanted into mouse liver (Wu et al., 2011). Pattou and colleagues reported detection of transplanted autologous islets in the

human forearm muscle with [^{111}In]DTPA-exendin-4 SPECT scanning one year after the transplantation (Pattou et al., 2010).

Biodistribution studies with [^{111}In]DTPA-exendin-4 using organ-derived gamma counting showed tracer uptake in whole pancreas of healthy rats and mice (Gotthardt et al., 2006). Brom and colleagues revealed that pancreatic uptake of [^{111}In]DTPA-exendin-3, as determined by *ex vivo* measurements and by *in vivo* SPECT imaging, correlated linearly with beta cell mass in rats with alloxan-induced loss of beta cells, indicating specific GLP-1R mediated uptake (Brom et al., 2010a). In addition, the uptake was shown to correlate negatively with the alpha cell mass in a rodent model of diabetes, indicating a negligible effect of the alpha cells on tracer uptake in the pancreas (Brom et al., 2015). *Ex vivo* autoradiography studies of rat pancreas showed promising results of [^{64}Cu]-Lys^{40}-Ahx-DOTA-exendin-4 labeling the islets of a healthy rat. No binding was observed in ZDF (zucker diabetic fatty) rats or healthy rats pre-treated with unlabeled exendin (Connolly et al., 2012).

Metal-labeled (^{68}Ga, ^{111}In) and chelated (NOTA, DOTA) exendin-based tracers have been successful in specific uptake in the islets and GLP-1R-expressing tumors, but the obstacle with these has been high radioactivity retention in the kidneys (Brom et al., 2014; Vegt et al., 2008; Bauman et al., 2015). Since the kidney is an organ sensitive to radiation, the radiation dose might become unacceptably high especially with long-lived isotopes (Wessels et al., 2008). In addition, high radioactivity levels compromise tissue, e.g. pancreas, visualization in the vicinity of the kidneys, thus limiting diagnostic accuracy and quantitative imaging. Peptides are excreted *via* the kidneys but persistent retention is typical for radiometal-labeled exendin derivatives. Although the details still remain be clarified, it has been suggested that the binding of peptide to megalin receptor during glomerular filtration might lead to internalization and entrapment of radioactive metabolites into the lysosomes (Vegt et al., 2010; Vegt et al., 2011). Efforts to reduce kidney uptake with co-administration of amifostine, albumin derivatives, poly-glutamic acid or Gelofusine have had promising results (Gotthardt et al., 2007; Wild et al., 2010; Melis et al., 2012). Another approach is to introduce a cleavable linker before the radioactive moiety of the peptide. This linker serves as a site for the enzymes (e.g. carboxypeptidase) in the kidney brush border membrane to cleave the radioactive moiety and, as a result, the small radiometabolite fragment can be excreted into the urine (Nakamoto et al., 1999; Fujioka et al., 2001; Fujioka et al., 2005). An N$^{\varepsilon}$-maleoyl-L-lysine linker has been successfully used to reduce kidney retention of antibody fragments in mice while maintaining radioactivity uptake in the target site. More research is needed to

resolve the applicability of cleavable linkers for exendin and to ensure the safe use of radiometal-labeled exendin analogs.

In contrast to radiometal-labeled derivatives, animal studies with fluorine-18 labeled exendin showed reduced radioactivity retention in the kidneys, and high and sustained uptake in INS-1 human tumor cell line and xenograft models. Importantly, after initial localization of high radioactivity levels in the kidneys, the clearance from kidneys was rapid as compared to radiometal-labeled analogues (Gao et al., 2011; Kiesewetter et al., 2012b; Yue et al., 2014). [^{18}F]TTCO-Cys^{40}-Exendin-4 showed specific uptake in transplanted islets in NOD/SCID mice and limited kidney retention (Wu et al., 2013b). However, the usefulness of fluorine-18 labeled exendin-4 for imaging beta cells in human pancreatic islets remains to be determined.

2.7 Development of a putative imaging agent: from preclinical evaluation to clinical use

Properties of an optimal radioactive tracer and requirements for in vivo imaging

New targets and probes for beta cell imaging can be identified using bioinformatic approaches and public access databases (Bouckenooghe et al., 2010; Lindskog et al., 2012). Proteomic and transcriptomic analyses can be used to screen unique beta cell targets (Maffei et al., 2004). A quantitative biomarker must exhibit sufficient sensitivity, reproducibility, specificity and accuracy to represent the intended biological phenomenon. Several molecules, such as antibodies, antibody fragments, peptides and small molecules for *in vivo* targeting of beta cells have been explored. Evaluation of a candidate molecule starts with *in vitro* studies using cells and tissue sections (Figure 7). If the requirements are fulfilled, the research of a candidate molecule will continue with *in vivo* studies performed in living animals. Finally, the molecule will enter clinical trials and validation in humans.

Of all imaging agents under development, 42 % are PET-based (Chopra et al., 2012). Good contrast, i.e. a high signal-to-background ratio, is of paramount importance for PET imaging and target visualization. Thus, the selected ligand should target the beta cell with high specificity and high affinity, and not bind to the other cells in the islet, the exocrine pancreas or organs close to the pancreas. Furthermore, the expression level of the target should be unaltered by metabolic stress such as hyperglycemia or inflammation. Simultaneously, the compound should have low non-specific binding and fast clearance from the blood and non-target tissues. Only then, will the radioactivity measured with PET mirror the beta cell mass.

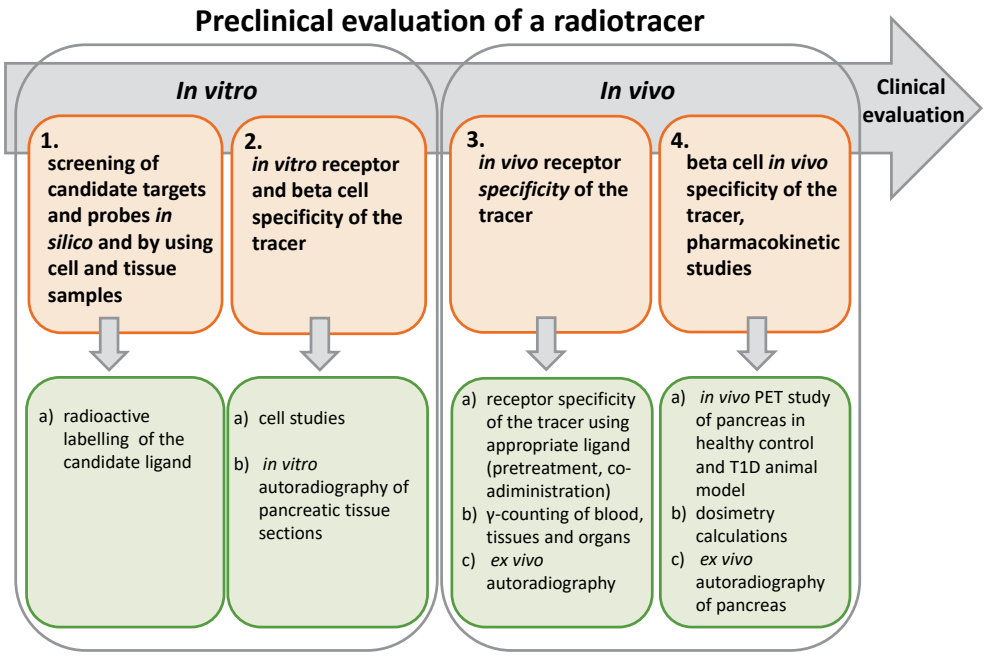

Figure 7. Basic stages of the preclinical evaluation of a given radiotracer candidate. Prospective scheme for the screening and evaluation process of novel beta cell imaging agents. After identification of a promising biomarker, a candidate ligand is radiolabeled. The *in vitro* specificity of the radioligand is tested with cell and tissue studies. Thereafter *in vivo* receptor specificity in healthy animals is investigated using appropriate unlabeled compounds. Finally, *in vivo* studies using T1D animal model and radiation dosimetry calculations are performed. After preclinical *in vitro* and *in vivo* assessment, radiotracer development continues with clinical trials. (Modified from Eriksson et al. 2016).

When imaging beta cells, the amount of target receptor may be much lower than in tumors, e.g. insulinomas in the case of GLP-1R. When imaging targets (e.g. receptors) of low expression levels, high specific activity (MBq/nmol, radioactivity/concentration) of the radiotracer is needed in order to obtain high quality quantitative (PET) images and to avoid receptor saturation with the unlabeled, non-radioactive, compound. Potential pharmacological and toxic effects of the compound are avoided only when a low amount of mass is injected. A metabolically stable tracer allows specific accumulation into the target tissue. The time the tracer circulates in the blood is determined by its degradation and excretion speed. Small molecules and peptides are usually excreted faster than large antibodies. Depending on their lipophilicity, compounds are excreted *via* two main routs: hydrophilic *via* kidneys and lipophilic *via* liver. In pancreas, hydrophobic tracers may accumulate in the fat in the exocrine pancreas and impair the target-to-background signal. When no metabolic excretion pathway exists, a tracer may also be internalized and metabolically trapped in cells.

Candidate tracers may fail for many reasons: insufficient uptake in the target tissue, low binding affinity, rapid catabolism or degradation relative to the process investigated, high hydrophilicity (low lipophilicity), inability to cross the blood-brain barrier (BBB), undesirable diffusion out of the target cells, low synthesis yield or low specific activity of the radiotracer. Also, species differences, e.g. in receptor expression or affinity between the experimental animals used for tracer evaluation and humans should be carefully considered. Many of these properties can be recognized before the animal studies or at the early phase of preclinical evaluation. However, a candidate molecule showing promising results *in vitro* may still fail in *in vivo* studies and in clinical trials. (Eriksson et al., 2016.)

3. AIMS OF THE STUDY

The aim of this study was to evaluate novel positron emitting radiotracers for imaging pancreatic islet beta cells with PET.

The following objectives were set:

1. To investigate whether VMAT2 PET tracer [^{11}C]DTBZ localizes in the islets of healthy and diabetic rat and healthy human pancreas (I).
   Study hypothesis: the binding of [^{11}C]DTBZ is beta cell specific in pancreas.

2. To compare the binding kinetics and islet specificity of glucagon like peptide-1 receptor (GLP-1R) targeting [^{64}Cu]exendin-4 and [^{68}Ga]exendin-4 radiotracers in healthy rat and to estimate their suitability for clinical imaging (II).
   Study hypothesis: both tracers are beta cell specific and the longer half-life of [^{64}Cu]NODAGA-exendin-4 and expected higher specific activity has benefits over [^{68}Ga]NODAGA-exendin-4 in clinical use.

3. To investigate whether the radioactivity retention in kidneys could be decreased by incorporating a biodegradable MAL-linker into chelated, metal-labeled exendin, [^{64}Cu]NODAGA-MAL-exendin-4, or by using non-chelated, non-metal radionuclide, fluorine-18 (^{18}F) to label exendin, [^{18}F]exendin-4 (III), (IV).
   Study hypothesis: the biodegradable linker and radionuclide selection reduce the radioactivity accumulation in the kidneys and are valuable assets for further development of clinical grade beta cell imaging agents.

4. MATERIALS AND METHODS

4.1 Experimental animals (I–IV)

Sprague–Dawley male rats (200–350 g), bred and housed under standard conditions at the Central Animal Laboratory, University of Turku, Turku, Finland, were used. Bovine adrenal gland was obtained from a local slaughterhouse (Paimion Teurastamo Paimio, Finland). Finnish landrace pigs (N=3, 33 ± 3 kg) were obtained from a local farmer. All animal experiments were approved by the Regional State Administrative Agency for Southern Finland (permission ESLH-2009-05275/Ym-23, ESAVI/3899/04.10.07/2013, ESAVI/823/04.10.07/2013, ESAVI/4660/04.10.07/2016), and the animal care complied with the guidelines of the International Council of Laboratory Animal Science (ICLAS).

4.2 Induction of diabetes in rats (I)

On day 1, 2 weight-matched groups of rats, were fasted for 4 h. The rats were anesthetized with isoflurane, and either streptozotocin (65 mg/kg) (Sigma Aldrich) dissolved in 0.1 M citrate buffer (pH 4.6) (N=8) or citrate buffer alone (N=6) was intravenously administered. Blood glucose levels and body weights were monitored regularly. The control rats remained euglycemic (7.0 ± 0.7 mM on day 8), and their body weights increased (from 332 ± 19 g on day 0, to 346 ± 16 g on day 8). Two of the rats in the streptozotocin groups were excluded from the study because they showed only moderate elevations in blood glucose levels, and their body weights increased. The rest of the rats in the streptozotocin group (N=6) exhibited elevated blood glucose levels (exceeding 22 mM from day 3 onward), and decreasing body weights (from 329 ± 21 g on day 1 to 283 ± 22 g on day 7). On day 7 (streptozotocin group) or day 8 (control group), the rats were sacrificed, and the pancreata were dissected and frozen. Pancreatic sections were sliced on a cryostat and stored frozen until used.

4.3 Human tissue samples (I, IV)

Human pancreatic tissue was obtained from a total of 5 non-diabetic subjects that underwent pancreatic resection at Turku University Hospital (Turku, Finland). In

study I, tissue from 4 subjects (3 women and 1 man, 59 ± 12 y old) with pancreatic cystadenoma or pancreatic cystadenocarcinoma was used. In study IV, pancreatic tissue was obtained from 1 subject (woman, 36 y old) with pancreatic mucinous neoplasm. Approval for the use of human pancreatic tissue was obtained from the Ethics Committee of the Hospital District of Southwest Finland (ETMK 42/180/2008). All subjects provided written informed consent before participating in the study.

4.4 Production of positron emitting radionuclides and synthesis of radiotracers

4.4.1 [^{11}C]DTBZ (I)

(+)-α-[^{11}C]DTBZ (^{11}C-dihydrotetrabenazine) was synthesized by ^{11}C-methylation of (+)-9-*O*-desmethyl-α-DTBZ with [^{11}C]methyl triflate prepared from cyclotron-produced [^{11}C]methane *via* [^{11}C]methyl iodide using a previously described method (Chan et al., 1999), with minor modifications. ^{11}C was prepared by the ^{14}N(p,α)^{11}C nuclear reaction and obtained as [^{11}C]methane. [^{11}C]Methyl iodide was synthesized from [^{11}C]methane and iodine in gas phase reaction at 720 °C (Larsen, 1997). [^{11}C]Methyl triflate was prepared online by passing [^{11}C]methyl iodide through a silver triflate/graphitized carbon column at 200 °C and bubbled into the reaction solution containing the precursor in acetone in the presence of sodium hydroxide (NaOH). The reaction mixture was purified with semi-preparative HPLC. After removal of the mobile phase by evaporation, [^{11}C]DTBZ was formulated in propylene glycol / ethanol / 0.1 M sterile phosphate buffer (5/2/93, v/v/v).

4.4.2 [^{11}C]Methionine (II)

[^{11}C]Methionine, which was used to verify the spatial location of the rat pancreas in the PET imaging studies, was prepared using a previously reported method (Någren and Halldin, 1998).

4.4.3 Peptides (II, III, IV)

In study II, the peptide sequence of NODAGA-exendin-4 (Nle^{14},Lys^{40}(Ahx-NODAGA)NH_2-exendin-4(1–39)) was HGEGTFTSDLSKQBEEEAVRLFIEWL KNGGPSSGAPPPSK(X-NODAGA)NH_2, where B=norleucine and X=hexanoyl spacer (Peptide Specialty Laboratories, Heidelberg, Germany). In study III, NODAGA-MAL-exendin-4 (Met^{14},Cys^{40}(MAL-NODAGA)NH_2-exendin-4(1-39)) was

synthesized from a thiol-maleimide addition between N^{ε}-Maleoyl-L-lysyl-glycyl-NODAGA and the peptide sequence HGEGTFTSDLSKQMEEEAVRLFIEWLKNG GPSSGAPPPSC-NH_2 (GenScript USA Inc., Piscataway, NJ, USA). In study IV, the peptide sequence of azido-exendin-4 ([Nle^{14},Lys^{40}(N_3)NH_2]exendin-4(1-39)) was HGEGTFTSDLSKQBEEEAVRLFIEWLKNGGPSSGAPPPSZ, where B=norleucine and Z=azido-lysine-amide (Peptide Specialty Laboratories).

4.4.4 [^{64}Cu]NODAGA-exendin-4 (II) and [^{64}Cu]NODAGA-MAL-exendin-4 (III)

^{64}Cu in the form of [^{64}Cu]$CuCl_2$ was produced *via* the ^{64}Ni(p,n)^{64}Cu nuclear reaction, as previously described (Avila-Rodriguez et al., 2007; Elomaa et al., 2014).

[^{64}Cu]NODAGA-exendin-4 (^{64}Cu-labeled [Nle^{14},Lys^{40}(Ahx-NODAGA)NH_2] exendin-4) and [^{64}Cu]NODAGA-MAL-exendin-4 (^{64}Cu-labeled [$Met^{14}Cys^{40}$(MAL-NODAGA)NH_2]exendin-4 were prepared by incubating [^{64}Cu]$CuCl_2$ (500 MBq) and peptide (5 nmol) in ammonium acetate solution (500 µl, 0.5 M, pH 6) at 90 °C for 15 min (II) and at 60 °C for 30 min (III). Quality control was performed using reversed-phase radio-HPLC (high performance liquid chromatography) with a Proteo C_{12} column (Phenomex). The specific activity was calculated as the ratio of the added radioactivity to the total mass of added peptide, and corrected for radiochemical yield and decay.

4.4.5 [^{68}Ga]NODAGA-exendin-4 (II)

^{68}Ga was obtained as [^{68}Ga]$GaCl_3$ from a ^{68}Ge/^{68}Ga generator (IGG100 1850 MBq, Eckert & Ziegler) by elution with 0.1 M HCl.

[^{68}Ga]NODAGA-exendin-4 (^{68}Ga-labeled [Nle^{14},Lys^{40}(Ahx-NODAGA)NH_2]exendin-4) was prepared by mixing sodium acetate (18 mg, Merck) with 500 µl of [^{68}Ga]$GaCl_3$ (268 ± 62 MBq, range=198–399 MBq) and the pH was adjusted to approximately 3.5 with HCl. Subsequently, NODAGA-exendin-4 (5 nmol) was added and the reaction mixture was incubated at 95°C for 15 min. The radiochemical purity was determined by radio-HPLC (C18 column, Phenomenex).

4.4.6 [^{18}F]exendin-4 (IV)

Aqueous [^{18}F]fluoride was produced by proton bombardment of ^{18}O-enriched water using the MGC-20 cyclotron from Efremov (St. Petersburg, Russia), as reported previously (Solin et al., 1988).

The synthesis was started by allowing tosylate to react with a [^{18}F]fluoride-Kryptofix complex in anhydrous DMSO. After purification by HPLC, the collected fraction was concentrated on an Oasis HLB cartridge (Waters, Milford, MA, USA). The obtained [^{18}F]fluoro-propargyl-triethylene glycol (FPTG) was allowed to react with exendin-4-azide in the presence of pre-activated copper sulfate/sodium ascorbate to produce radiofluorinated exendin-4. After purification by HPLC, the collected fraction was retained on a Sep-Pak C8 cartridge (Waters), and formulated in ethanol/saline. Radiochemical analysis of [Nle^{14},Lys^{40}([^{18}F]FTTG)NH_2]exendin-4 ([^{18}F]exendin-4) was performed with HPLC and thin layer chromatography (TLC). The specific activity was determined from concentration series of azido-exendin.

4.5 Synthesis of [^{nat}Cu]- and [^{nat}Ga]NODAGA-exendin-4 (II)

NODAGA-exendin-4 (10.1 mg) in ammonium acetate buffer (pH 5.4, 0.5 M, 500 µl) and an aliquot of an aqueous solution of $^{nat}CuCl_2 \times 2H_2O$ (6.7 µl, 0.3 M) was allowed to react at room temperature for 3.5 h. The complex formation was checked by analytical HPLC. [Nle^{14},Lys^{40}(Ahx-NODAGA-^{nat}Cu)NH_2]-exendin-4 ([^{nat}Cu]NODAGA-exendin-4) was purified by preparative HPLC and 3.3 mg was isolated.

A mixture of NODAGA-exendin-4 (13.5 mg) in sodium acetate buffer (pH 4.0, 0.2 M, 1 ml) and an aliquot of an aqueous solution of $^{nat}Ga(NO_3)_3 \times H_2O$ (24 µl, 0.3 M) was heated at 95 °C for 10 min. Complex formation was checked by analytical HPLC. A total of 2.4 mg of [Nle^{14},Lys^{40}(Ahx-NODAGA-^{nat}Ga)NH_2]-exendin-4 ([^{nat}Ga]NODAGA-exendin-4) complex was isolated after preparative HPLC.

4.6 Characterization of binding affinity of [^{nat}Cu]- and [^{nat}Ga]NODAGA-exendin-4 for GLP-1R (II)

The binding affinities of the two exendin analogues and GLP-1 as a control were evaluated in competition binding experiments performed *in vitro* in GLP-1R-expressing human insulinomas using autoradiography, as reported previously (Reubi and Waser, 2003; Körner et al., 2007). For each of the tested compounds, complete competition binding experiments with [^{125}I]GLP-1(7-36) amide (74 GBq/µmol, Anawa) and increasing concentrations of the unlabeled peptides (range 0.1–1000 nM) were performed in triplicate. IC_{50} values were calculated as described previously (Körner et al., 2007).

4.7 Stability and lipophilicity of the radiotracers *in vitro* (II, III)

The *in vitro* stability of [^{64}Cu]NODAGA-exendin-4, [^{68}Ga]NODAGA-exendin-4 and [^{64}Cu]NODAGA-MAL-exendin-4 was tested in human serum and in phosphate-buffered saline (PBS, pH 7.4) at 37°C. At selected time-points, aliquots were treated with acetonitrile to precipitate the serum proteins. After centrifugation, the supernatant was analyzed using radio-HPLC (C_{12} column, Phenomex).

The octanol/water distribution coefficients of the peptides were measured by vortex-mixing equal amount of 1-octanol and PBS (pH 7.4) (500 µl) with approximately 0.1 MBq of radiolabeled peptide (for 2–3 min). Following centrifugation (at 16,000×g for 8 min), samples from the organic and aqueous phases were analyzed using a γ-counter (1480 Wizard 3″ Gamma Counter, PerkinElmer). Log(D)octanol/water was calculated as log([radioactivity]$_{octanol}$/[radioactivity]$_{water}$).

4.8 Tracer biodistribution studies

Details of the animals and methods are summarized in Table 2.

4.8.1 Ex vivo organ biodistribution (I–IV)

Rats were briefly anesthetized with CO_2:O_2 gas or with isoflurane/O_2 and injected *via* a tail vein with the tracer (Table 3). Animals were sacrificed at various time-points (15 min – 40 h) either with CO_2 gas or isoflurane, and blood was collected by cardiac puncture. Plasma, tissues, and organs were weighed, and their radioactivities were measured using a γ-counter. The biodistribution of the radioactivity, corrected for radionuclide decay, was reported as percentage of the injected dose per gram of tissue (%ID/g). The GLP-1R specificity of the radiopeptides (II, IV) in rats was assessed at 1 h post injection (*p.i.*) in separate groups of animals by intravenous injection (*i.v.*) of an excess of unlabeled exendin-3, administered immediately before the radiopeptide injection.

Table 2. Details of the animals and methods used in the studies.

Study	Animal model	Radiotracer	Animal weight [g]	N	PET imaging [min]	Sacrifice time *p.i.*	γ-counting	Metabolites	*ex vivo* ARG	*in vitro* ARG	Insulin IHC
I	SD rat	[^{11}C]DTBZ	269 ± 45	14	-	10min, 1h	x	x	x	x	x
	STZ vehicle	[^{3}H]DTBZ	329 ± 21 332 ± 19	6 6	- -	- -	- -	- -	- -	x x	x x
II	SD rat	[^{64}Cu]NODAGA-exendin-4	290 ± 28	31	0-60, 0-120	5min, 1h, 18h, 40h	x	x	x	-	x
		[^{68}Ga]NODAGA-exendin-4	296 ± 31	10	0-60	1h	x	-	x	-	x
		[^{11}C]Methionine	275 ± 16	3	0-30, 0-40	-	-	-	-	-	-
III	SD rat	[^{64}Cu]NODAGA-exendin-4	303 ± 39	15	0-60, 30*	1h, 24h	x	x	x	-	x
		[^{64}Cu]MAL-exendin-4	284 ± 40	17	0-60, 30*	1h, 24h	x	x	x	-	x
IV	SD rat, pig	[^{18}F]exendin-4	285 ± 30 33 ± 3^	43 3	0-60, 30*	15min, 30min, 1h, 4h, 6h	x	x	x	x	x

* static imaging, ^ weight in kg, ARG: autoradiography, IHC: immunohistochemistry

Table 3. Characteristics of PET tracers for beta cell imaging used in the thesis (mean ± SD).

Study	Radiotracer	Injected radioactivity [MBq/kg]	Injected specific radioactivity [MBq/nmol]	Injected mass [μg/kg]	N
I	[^{11}C]DTBZ	170 ± 105	155 ± 93	0.7 ± 0.7	14
II	[^{64}Cu]NODAGA-exendin-4	94 ± 35	80 ± 42	9 ± 8	31
	[^{68}Ga]NODAGA-exendin-4	121 ± 34	13 ± 2	46 ± 12	10
III	[^{64}Cu]NODAGA-exendin-4	117 ± 53	76 ± 42	12 ± 12	12
	[^{64}Cu]NODAGA-MAL-exendin-4	114 ± 53	52 ± 22	14 ± 11	14
IV	[^{18}F]exendin-4				
	SD rat	23 ± 5	66 ± 31	2 ± 1	43
	pig	1.2 ± 0.2	40 ± 12	0.14 ± 0.04	3

4.8.2 Organ regional distribution of radioactivity

The pancreata (I–IV) and brains (I, IV) were frozen by immersion in isopentane chilled with dry ice and sectioned (20 μm) on a cryostat. The sections were dried under a fan and apposed to imaging plates (Fuji BAS-TR2025; Fuji Photo Film Co., Tokyo, Japan) for approximately two radionuclide half-lives. In study II, the gastrointestinal channel was emptied and the stomach and the caecum were unfolded. The gastrointestinal channel was covered with cling film and apposed to an imaging plate for autoradiography as described above. Digital images were obtained by scanning the imaging plates with a BAS-5000 scanner (Fuji Photo Film Co.) at a 25 μm resolution or with an FLA-5100 scanner (Fuji Photo Film Co.) at 10 μm resolution. Images were analyzed with an image analysis software (Aida 4 and 4.5, Raytest, Isotopenmessgeräte, Straubenhardt, Germany), and the results were reported as photostimulated luminescence per square millimeter (PSL/mm^2). Three sections per rat were evaluated. In study I, the pancreatic head-to-tail binding ratio was determined for each rat, and the results were statistically analyzed by comparing the head-to-tail ratios to the hypothetical value 1. In studies II-IV, PSL/mm^2 for ten prominently labeled islets and of the exocrine tissue was determined and corrected for background noise. Finally, the islet-to-exocrine tissue ratio was calculated. Islet localization was verified by insulin immunohistochemistry (see 4.12 Immunohistochemistry of human and rat pancreas). The radioactivity in the gastrointestinal region was analyzed similarly by outlining regions of interest and calculating regional signal ratios.

4.9 Radiometabolite assay (I–IV)

The presence of radioactive metabolites in rat plasma, urine and selected organs at several radionuclide-dependent time-points after tracer injection was determined either with HPTLC or radio-HPLC. Tracer added to rat plasma or pig plasma (IV) was used as a standard to allow identification of the parent (intact) compound. Plasma and urine (500 µl) proteins were precipitated by adding 1:1 volume of acetonitrile and removed by centrifugation (2 x 5 min, 12,000 g). The tissue samples were homogenized, treated with acetonitrile, and the radioactive material was purified in two centrifugation steps. Supernatants (10 µl) were applied to an HPTLC Silica Gel 60 plate (105547; Merck) (I) or analyzed with radio-HPLC (C12 column, Phenomex, (250 × 10 mm) (II, III, IV). Chloroform:methanol (85:15) was used as the mobile phase with HPTLC. The HPTLC plate was subsequently apposed to an imaging plate as previously described (see 4.8.2 Organ regional distribution of radioactivity). The HPLC conditions were as follows: flow rate=1 ml/min, buffer A=0.1 % trifluoroacetic acid (TFA) in water, buffer B=0.1 % TFA in acetonitrile. The linear gradient was 18 % to 60 % of buffer B in buffer A over 5 min.

In addition, the stability of [^{18}F]exendin-4 was determined in pig plasma (IV). Prior to blood sampling, the pigs were anesthetized (midazolam 1 mg/kg, xylazine 4 mg/kg intra muscular), connected to a respirator, and ventilated mechanically. Anesthesia was maintained with an *i.v.* infusion of propofol (10–20 mg/kg/h) and fentanyl (4–8 µg/kg/h). Vital signs were monitored throughout the study. Pigs were injected *i.v.* with [^{18}F]exendin-4 (radioactivity: 1.2 ± 0.2 MBq/kg, mass: 0.14 ± 0.04 µg/kg), and blood was sampled at 5, 15, 30, 60, and 180 min *p.i.* (N=3 samples/time-point). Plasma was treated and analyzed as described above.

4.10 Small animal PET imaging (II, III, IV)

Whole-body distribution kinetics of radiotracers in rats was evaluated using an Inveon Multimodality PET/CT (Siemens Medical Solutions, Knoxville, TN, USA). Rats were anaesthetized with isoflurane/O_2 and kept warm on a heating pad during the imaging procedure. Animals were injected *i.v.* with the radiotracer and a dynamic PET scan started at the time of injection. Attenuation correction was obtained by a CT scan performed prior to the PET scan. PET data were acquired in 3D list mode with an energy window of 350–650 keV. The data were reconstructed using the ordered-subset expectation maximization OSEM2D algorithm. The details of the PET studies are presented in Table 2.

In study II, the pancreas was visualized using [^{11}C]Methionine. In addition, animals were imaged with [^{64}Cu]NODAGA-exendin-4 using two different study protocols. Dynamic [^{11}C]Methionine data were collected either for 30 min immediately prior to a [^{64}Cu]NODAGA-exendin-4 120 min PET scan (N=1) or dynamic 40 min [^{11}C]Methionine data were collected the day before a [^{64}Cu]NODAGA-exendin-4 60-min PET scan (N=2).

After the PET scan, the rats were deeply anaesthetized with isoflurane, blood was collected by cardiac puncture and tissues of interest were collected and measured, and the results were reported as described above (see 4.8.1 *Ex vivo* organ biodistribution).

4.10.1 Analysis of PET images

Quantitative analyses were performed using Inveon Research Workplace 3 software (Siemens Medical Solutions, USA Inc.) by defining the volumes of interest (VOIs) on selected tissues (heart, kidney, liver, lung, muscle, stomach wall). In study II, The VOIs for the pancreas were defined in the [^{11}C]Methionine images and copied onto the corresponding [^{64}Cu]NODAGA-exendin-4 images. The radioactivity uptake, corrected for radionuclide decay to the time of injection, was expressed as %ID/g or standardized uptake value (SUV). SUV_{bw} was calculated as the ratio of tissue radioactivity concentration at time (t), c(t) and the injected radioactivity dose at the time of injection divided by body weight: SUV_{bw}=c(t)/(injected dose/body weight).

4.11 Tracer *in vitro* studies

4.11.1 Pharmacological characterization of [^{3}H]DTBZ binding (I)

α-2-[^{3}H]DTBZ ([^{3}H]DTBZ) (0.74 MBq/nmol, American Radiolabeled Chemicals) saturation and competition binding assays were performed by incubating duplicate sections of rat pancreas, rat brain, and bovine adrenal gland with [^{3}H]DTBZ and various unlabeled compounds (chlorpromazine, haloperidol, ketanserin, lobeline, reserpine, tetrabenazine) in 50 mM potassium phosphate buffer for 2 h at room temperature. In the saturation binding experiment, sections from rat and bull were incubated with various concentrations of [^{3}H]DTBZ (range 0.38–47.3 nM). Adjacent sections were incubated in the presence of an excess of a VMAT2 antagonist (100 mM ketanserin) to determine non-specific binding. The competition binding experiment was performed with 1.8 nM [^{3}H]DTBZ and several concentrations (range 0–0.1 mM) of unlabeled VMAT2 specific compounds (chlorpromazine, haloperidol, ketanserin,

lobeline, reserpine, tetrabenazine, Sigma-Aldrich Co.). Rat pancreas, brain, and adrenal glands of cow and bull were used in the competition binding experiment. Because similar results were obtained from the cow and the bull, their corresponding binding values were averaged.

After the incubations, the sections were washed for 20 min in ice-cold buffer, rapidly rinsed in ice-cold distilled water, and dried under a fan. Sections were apposed to imaging plates (Fuji BAS-TR2025) for 10 d. Tritium standards (ART-123; American Radiolabeled Chemicals) were co-exposed with the sections to allow comparisons of the results from separate experiments. [^{3}H]DTBZ binding levels in the rat pancreas, rat striatum and bovine adrenal medulla were measured. Equilibrium dissociation (K_d) and inhibition (K_i) constants were determined by least squares non-linear regression analysis of the binding results with GraphPad Prism 5 (GraphPad Software). The saturation binding results were analyzed with simultaneous fitting of total and non-specific binding. K_d values obtained from the saturation binding experiment were used to calculate K_i values for the unlabeled compounds applied in the competition binding experiment; for this purpose, we used the Cheng–Prusoff equation (Cheng and Prusoff, 1973): K_i 5 IC_{50}/(1 + [radioligand]/K_d), where IC_{50} is the 50 % inhibitory concentration.

4.11.2 Tracer binding in sections of human pancreas (I, IV)

In order to study the binding of [^{3}H]DTBZ (I) and [^{18}F]exendin-4 (IV) in human beta cells, sections of fresh frozen human pancreas were incubated with the tracer. To determine the specificity of tracer binding, an excess of competing compound (ketanserin or exendin-3 as indicated) was used. In study I, duplicate sections of pancreas were incubated at room temperature with 5.4 nM [^{3}H]DTBZ in 50 mM potassium phosphate buffered saline for 30 min in the absence or presence of an excess of ketanserin. Sections of rat brain and bovine adrenal medulla were included as controls. The sections were washed in buffer for 20 min, rinsed in ice-cold distilled water, dried, and exposed to imaging plates for 14 d. In study IV, the sections were incubated for 30 min with 1 % bovine serum albumin/PBS prior to incubation with [^{18}F]exendin-4. Thereafter, the sections were incubated for an hour with various concentrations of [^{18}F]exendin-4 (range 2.5–20 nM) in the presence or absence of an excess of unlabeled exendin-3. Sections of rat pancreas were included as controls. The sections were washed and dried as described above and exposed to imaging plates for approximately 4 h. Digital images were obtained as described in 4.8.2 Organ regional distribution of radioactivity.

4.12 Immunohistochemistry of human and rat pancreas

To verify the islet localization, human and rat pancreatic sections that had been processed for autoradiography were stained with hematoxylin and eosin or with insulin antibody. A polyclonal guinea pig primary antibody raised against human insulin (Abcam), diluted 1:500, and then a biotinylated goat anti–guinea pig secondary antibody (Jackson ImmunoResearch), diluted 1:500 or MACH-1 (Biocare) detected with DAB (3,3′diaminobenzidine), were used. In addition, fluorescence labeled antibodies against insulin (1' rabbit-anti-insulin 1/200, Euro-Diagnostica; 2' Alexa 488 goat-anti-rabbit 1/500, Invitrogen) and VMAT2 (guinea pig-anti-VMAT2 1/500, Euro-Diagnostica; 2' Alexa 568 goat-anti-rabbit 1/500, Invitrogen) were used. The results were documented by taking a high-magnification mosaic image of a stained section on a Zeiss Axiovert 200 M microscope (Carl Zeiss Inc.) or by using the Slide Scanner (Pannoramic 250F, 3DHistech, Hungary) of a confocal microscope (Melles Griot, Carlsbad, CA, Yhdysvallat). Pancreatic islets were identified and manually outlined on the digital images, and the outlines were combined with the autoradiographic images using Photoshop CS3 (Adobe Systems Inc.) or Corel-DRAW X3 (Corel Corp.).

4.13 Estimation of radiation doses for humans (II, IV)

Absorbed radiation doses were calculated with the OLINDA/EXM1.0 software (Howell et al., 1999; Stabin et al., 2005) which includes radionuclide information and a selection of human body phantoms. Rat *ex vivo* biodistribution results and PET imaging results were integrated as area under the time-activity curves. The obtained residence times were converted into corresponding human values by multiplication with organ-specific factors to scale organ and body weights: $(W_{TB,rat}/W_{Organ,rat})\times(W_{Organ,human}/W_{TB,human})$, where $W_{TB,rat}$ and $W_{TB,human}$ are the body weights of rat and human (70-kg male), respectively, and $W_{Organ,rat}$ and $W_{Organ,human}$ are the organ weights of rat and human (70-kg male), respectively.

4.14 Statistics

Statistical analyses were performed using GraphPad Prism 4 and 5 (GraphPad Software) and results were reported as mean ± SD. Two-tailed, unpaired Student's *t* test and one-way or two-way ANOVA were used for the analyses of statistical differences between groups. In further pairwise comparisons Bonferroni's multiple comparison test was used. Differences between ratios and 1 were analyzed with a 2-tailed 1-sample t test (I). Values of $P<0.05$ were considered statistically significant.

5. RESULTS

5.1 DTBZ (I)

5.1.1 Radiochemistry

The radiopharmaceutical [^{11}C]DTBZ was obtained at a radiochemical yield of 1360 ± 260 MBq, using a 40 min target irradiation with 17 MeV protons. The specific activity measured by analytical HPLC was 420 ± 220 GBq/μmol at the end of a 35–40 min synthesis. The radiochemical purity exceeded 98 % in all syntheses.

5.1.2 Regional distribution of [^{11}C]DTBZ in rat pancreas and brain

The highest accumulation of [^{11}C]DTBZ radioactivity in the organs studied was found in the pancreas, with similar levels at 10 and 60 min *p.i.*, 3.03 ± 0.62 %ID/g (N=7) and 2.74 ± 0.59 %ID/g (N=7), respectively (Figure 8). In addition, the striatum exhibited high uptake of radioactivity 10 min *p.i.* 2.92 ± 0.97 %ID/g (N=6), but at the 60 min time point, radioactivity in the striatum was significantly reduced, 1.17 ± 0.43 %ID/g (N=5). These results suggest different kinetics for [^{11}C]DTBZ binding in the pancreas and the VMAT2-rich striatum. Autoradiography results

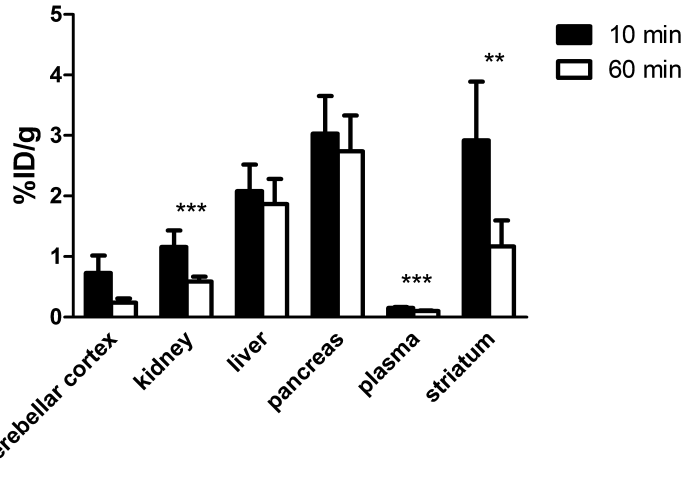

Figure 8. [^{11}C]DTBZ biodistribution in rat 10 and 60 minutes after tracer injection measured by *ex vivo* gamma counting (N=3–7). Results are expressed as mean ± SD percentage injected dose per gram of tissue. (Data based on study I).

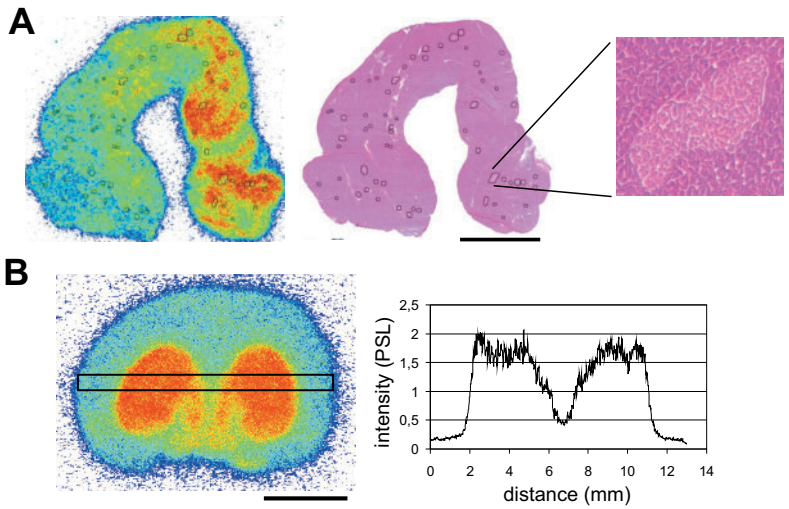

Figure 9. Distribution of [^{11}C]DTBZ radioactivity in rat pancreas (A) and brain (B) 10 min after tracer injection. A) Same pancreatic section used for autoradiography was stained with hematoxylin and eosin. ^{11}C-radioactivity did not co-localize with the islets (black circles). Distribution of radioactivity was heterogeneous with higher levels toward the head of the pancreas (B) High [^{11}C]DTBZ uptake in the striatum, VMAT2-rich area in the brain. Scale bars 5000 µm. (A Data modified from study I, B Data based on study I).

showed heterogeneous distribution of radioactivity in the pancreas; the levels in the head of the pancreas were 70 % higher compared to those in the pancreatic tail (*P* 0.046 N=6) 10 min *p.i.* (Figure 9). At the 60 min time point, this gradient was no longer observed. At neither time point, did [^{11}C]DTBZ radioactivity accumulate specifically in pancreatic islets. In brain, [^{11}C]DTBZ binding corresponded to the known distribution of VMAT2.

5.1.3 Analysis of [^{11}C]DTBZ metabolites

The amount of intact tracer 10 min *p.i.* was 94 % in plasma, 85 % in urine, 83 % in liver, 98 % in the head of the pancreas (*caput*), 99 % in the mid pancreas (*corpus*) and 98 % in the tail of the pancreas (*cauda*). Two to three radioactive metabolites were distinguished. The Rf (retardation factor) values of the metabolites were lower than the corresponding value of [^{11}C]DTBZ, which indicates that the metabolites were more polar than the parent compound.

5.1.4 In vitro binding of [^{11}C]DTBZ in pancreatic sections of control and STZ induced diabetic rats

Analysis of autoradiograms revealed lower [^{11}C]DTBZ binding in the pancreas of diabetic rats compared to controls, supporting previous findings obtained by *in vivo*

PET imaging (Simpson et al., 2006; Souza et al., 2006b; Goland et al., 2009). The decrease in [^{11}C]DTBZ binding was observed throughout the pancreas, indicating that it was not directly associated with a decrease in beta cell mass.

5.1.5 *Pharmacological characterization of [^{3}H]DTBZ binding in rat pancreas in vitro*

Pancreatic islets could not be visualized when sections of rat pancreas were incubated with [^{3}H]DTBZ. Only homogenous binding was observed. In the pancreas, the [^{3}H]DTBZ binding increased in a concentration-dependent, non-saturable manner. In contrast, saturable [^{3}H]DTBZ binding was observed in the rat striatum (K_d 1.3 nM) and bovine adrenal medulla (K_d 3.3 nM). In the rat striatum and bovine adrenal medulla, VMAT2 antagonists competed for [^{3}H]DTBZ binding (rank order of potency: tetrabenazine > ketanserin > reserpine > haloperidol > lobeline ≈ chlorpromazine) corresponding to the pharmacological profile of VMAT2 (Scherman et al., 1983; Darchen et al., 1988; Teng et al., 1998). In the rat pancreas, a non-VMAT2 competition binding profile was observed (rank order of potency: lobeline ≈ ketanserin > haloperidol ≈ chlorpromazine > tetrabenazine ≈ reserpine) and a reliable 50 % inhibitory concentration could not be determined. In the pancreas, [^{3}H]DTBZ (1.8 nM) binding was poorly displaced by unlabeled compounds. The *in vitro* binding results indicate that [^{3}H]DTBZ binding in the rat pancreas, in contrast to binding in the rat striatum and bovine adrenal medulla, is non-specific.

5.1.6 *[^{3}H]DTBZ binding in human pancreatic tissue sections*

Binding of [^{3}H]DTBZ was low and in most islets of human pancreas did not exceed the binding in the exocrine pancreas (Figure 10). Only some intermediate to larger islets were faintly visible. Insulin staining of pancreatic islets was detected in all samples of human pancreas. Ketanserin (100 μM) inhibited islet-specific binding of [^{3}H]DTBZ, suggesting specific ligand binding to VMAT2 receptor. Labeling intensity in the islets (ligand concentration 5.4 nM) was less than two times higher when compared to exocrine pancreas. In contrast, the labeling intensity was seven times higher in rat striatum and bovine adrenal medulla compared to rat cerebral cortex and bovine adrenal cortex.

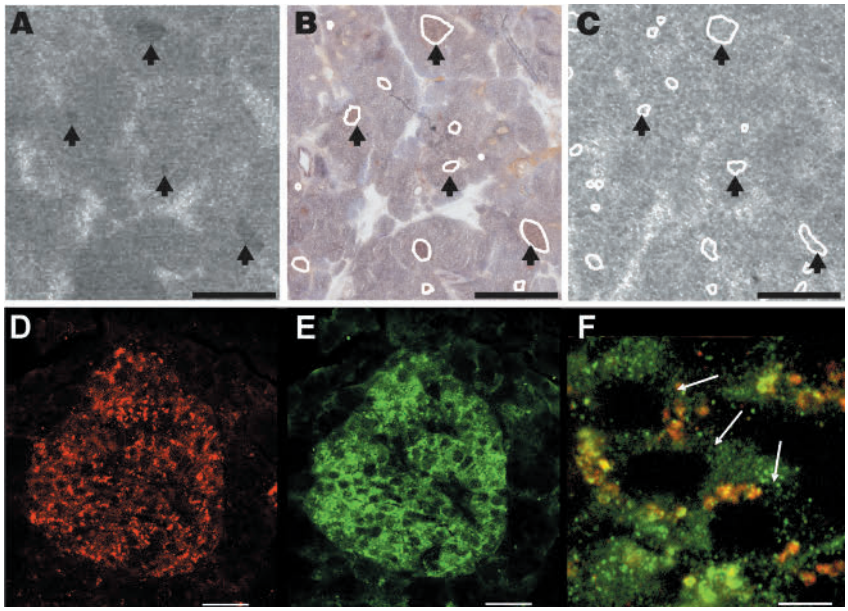

Figure 10. [^{3}H]DTBZ binding (A–C) and insulin-VMAT2 stainig (D–F) in human pancreas. Binding of [^{3}H]DTBZ in human pancreatic islets (arrows) was weak (A). Islets were identified and outlined (white circles) after insulin staining of the same section (B).Adjacent section was incubated with [^{3}H]DTBZ and 100 µM ketanserin (C). Absence of [^{3}H]DTBZ binding in islets indicated VMAT-2 specific labelling in A. Fluorescence insulin (D) and VMAT2 (E) staining of an islet in human pancreas and co-localization in the separate cells (white arrows) (F). Scale bars correspond to 1000 µm (A–C), 30 µm (D–E), 5 µm (F). (A–C published in study I, D–F unpublished data).

5.2 Exendin-based tracers (II, III, IV)

5.2.1 Radiochemistry

The specific activity of [^{64}Cu]NODAGA-exendin-4 was 90 ± 10 GBq/µmol at the end of synthesis, with a radiochemical purity of 93 ± 4 % (II). The corresponding values for [^{68}Ga]NODAGA-exendin-4 were 20 ± 5 GBq/µmol and 98.0 ± 0.3 % (II).

The specific activity of [^{64}Cu]NODAGA-MAL-exendin-4 and its reference [^{64}Cu]NODAGA-exendin-4 was 58 ± 33 MBq/nmol (N=4) and 106 ± 32 MBq/nmol (N=6), respectively, at the end of the synthesis, with a radiochemical purity of at least 91 % (III).

The specific activity for [^{18}F]exendin-4 was 12–323 MBq/nmol at the end of the synthesis, with a radiochemical purity exceeding 90 % (IV).

5.2.2 *In vitro stability and lipophilicity of metal-labeled exendin tracers*

The stability of [^{64}Cu]NODAGA-exendin-4 (II), [^{64}Cu]NODAGA-MAL-exendin-4 (III) and [^{68}Ga]NODAGA-exendin-4 (II) was tested in human serum and in PBS. After a 3 h incubation, the stability of [^{64}Cu]NODAGA-exendin-4 and [^{68}Ga]NODAGA-exendin-4 exceeded 91 %. After 24 h, the amount of intact tracer was more than 82 % with copper-64 labeled tracers. Similar results obtained for [^{64}Cu]NODAGA-exendin-4 and [^{64}Cu]NODAGA-MAL-exendin-4 indicated that glycyl-lysine sequence did not affect the *in vitro* stability of [^{64}Cu]NODAGA-MAL-exendin-4. The Log(D) value for [^{64}Cu]NODAGA-exendin-4 was −0.92 ± 0.37, for [^{64}Cu]NODAGA-MAL-exendin-4 −1.38 ± 0.16, and for [^{68}Ga]NODAGA-exendin-4 −2.38 ± 0.37. The difference in LogD value between [^{64}Cu]NODAGA-exendin-4 and [^{64}Cu]NODAGA-MAL-exendin-4 is probably due to the hydrophilic character of the maleimide linkage. The IC_{50} values were 1.0 ± 0.2 nM for GLP-1, 2.70 ± 0.62 nM for [^{nat}Cu]NODAGA-exendin-4, and 2.17 ± 0.42 nM for [^{nat}Ga]NODAGA-exendin-4.

5.2.3 *Ex vivo and in vivo whole-body biodistribution*

The biodistribution of [^{64}Cu]NODAGA-exendin-4 (II), [^{64}Cu]NODAGA-MAL-exendin-4 (III), [^{68}Ga]NODAGA-exendin-4 (II) and [^{18}F]exendin-4 (IV) was investigated in blood and multiple organs and tissues. With all of the investigated tracers, radioactivity was rapidly cleared from the blood circulation. The accumulated radioactivity levels in whole pancreas were low but remained elevated over the whole time span of the study (Figure 11A). The uptake of [^{18}F]exendin-4 in pancreas was significantly higher than its metal-labeled counterparts at 60 min *p.i.* (range 0.04–0.18 %ID/g). With all investigated tracers, the kidney was the organ with the highest uptake of radioactivity (Figure 11B). Kidney radioactivity at the 1 h time-point for [^{64}Cu]NODAGA-exendin-4 was 30 ± 4 %ID/g, for [^{64}Cu]NODAGA-MAL-exendin-4 was 23 ± 8 %ID/g, for [^{68}Ga]NODAGA-exendin-4 28 ± 7 %ID/g, and for [^{18}F]exendin-4 17 ± 3. As a comparison, the corresponding value for [^{111}In]DTPA-exendin-4 was 29 ± 2 (Brom et al., 2014). At 24 h *p.i.*, kidneys still retained 25 ± 1 %ID/g of the [^{64}Cu]NODAGA-MAL-exendin-4 activity, and at 40 h 9 ± 7 %ID/g of [^{64}Cu]NODAGA-exendin-4. *In vivo* imaging revealed that radioactivity accumulation of all exendin tracers was high in the kidneys soon after tracer injection. In comparison to its metal-labeled counterparts, the uptake of [^{18}F]exendin-4 in the kidney was similarly high right after the injection, but thereafter clearance was fast and the retention decreased to 1.5 ± 0.4 %ID/g at 6 h *p.i.* (Figure 11B). Accumulation of exendin-based tracer radioactivity was also rather high in lung and stomach wall which fits with the known regional expression of GLP-1R. Liver accumulation of

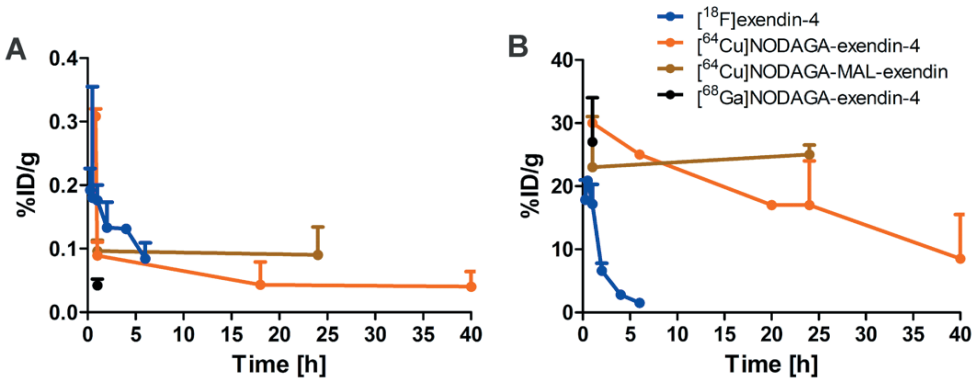

Figure 11. *Ex vivo* retention of exendin tracers in pancreas (A) and kidney (B). The uptake in whole pancreas remained low but constant over the course of the study. Compared to metal-labeled exendin tracers, the renal clearance of [^{18}F]exendin-4 (blue) was rapid. (Data based on studies II–IV).

tracers remained low over the course of the study, indicating that the tracer was not metabolized *via* the hepatic pathway. When animals were simultaneously injected with the radioactive tracer and cold exendin-3, significantly reduced uptake was observed in the pancreas, lung, and stomach wall but not in the kidney, suggesting that the observed radioactivity uptake was not GLP-1 receptor-specific in this tissue.

5.2.4 Ex vivo and in vitro autoradiography in rat

All exendin-based tracers demonstrated uptake in pancreatic islets at all investigated time-points after injection into living animals (Figure 12). At the 1 h time-point, the islet-to-exocrine tissue ratio was observed to be similar for [^{64}Cu]NODAGA-exendin-4 (II) and [^{64}Cu]NODAGA-MAL-exendin-4 (III), 106 ± 63 (N=9) and 96 ± 21 (N=11), respectively. The corresponding value for [^{68}Ga]NODAGA-exendin-4 (II) (23 ± 8, N=6) was substantially lower when compared to the copper-64 labeled counterparts. Studies with [^{18}F]exendin-4 (IV) revealed a sustained level of radioactivity in the islets and clearance from the exocrine pancreas over time. Analysis of autoradiograms

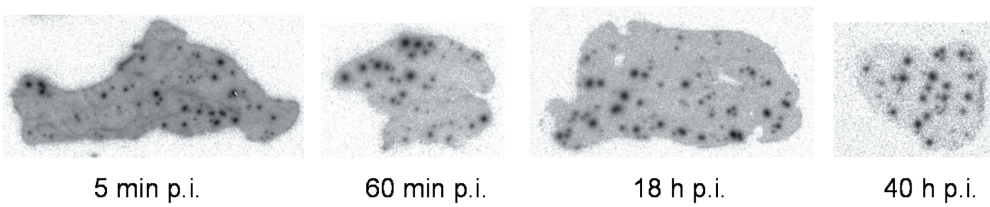

Figure 12. Labeling of islets in rat pancreatic tissue sections at several time points after [^{64}Cu]NODAGA-exendin-4 injection. (Unpublished data based on study II).

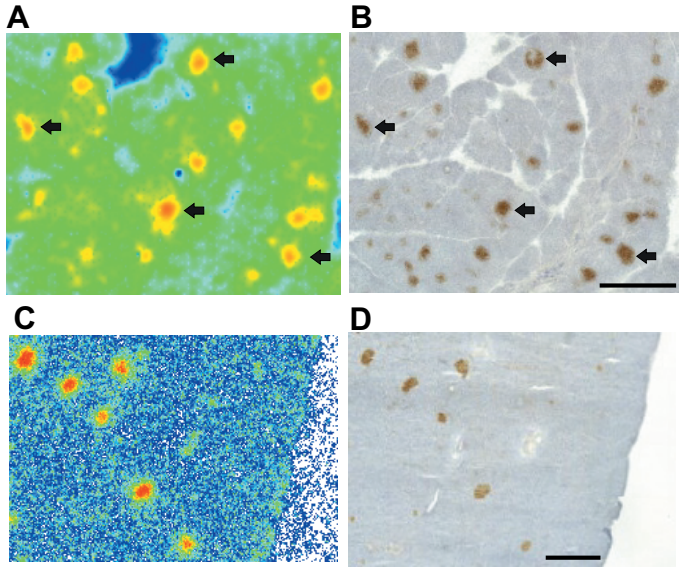

Figure 13. *In vitro* binding of [^{18}F]exendin-4 in human (A-B) and rat (C-D) pancreas. Tracer binding was clearly visible in human and rat pancreatic tissue sections and co-localization with the islets was confirmed with insulin immunohistochemistry (B–D). Scale bars correspond to 1000 µm. (A–D Data modified from study IV).

showed increased islet-to-exocrine tissue ratio towards the longer time-points (78 ± 29 1 h *p.i. vs.* 140 ± 63 6 h *p.i.*). The uptake of the tracers was not detected when the rats were co-injected with any of the radioactive exendin ligands and an excess of cold exendin-3, indicating GLP-1R specific binding in the islets. In addition to islets, autoradiography results revealed GLP-1R positive labeling in the glandular stomach and as a narrow band in the area of the pyloric sphincter at the border of the stomach and the duodenum. Binding of [^{64}Cu]NODAGA-exendin-4 and [^{68}Ga]NODAGA-exendin-4 in the remainder of the gastrointestinal region was weak and homogenous.

Similarly, islet labeling was observed after incubating rat pancreatic sections with the tracers *in vitro* (Figure 13 C–D). Islet labeling was not detected when an excess of cold exendin-3 was added. Labeling of the GLP-1R areas in the brain was clearly visible (IV).

5.2.5 Tracer binding in tissue sections of human pancreas

To investigate the tracer binding in human pancreas, sections were incubated with various concentrations of [^{18}F]exendin-4. The same section used for ligand incubations, was stained with insulin antibody to confirm the co-localization of ligand binding sites with the insulin-producing cells in the islets. *In vitro* autoradiography results combined with immunohistochemistry showed that ^{18}F radioactivity co-localized

with the human pancreatic islets expressing the GLP-1R (Figure 13 A–B). No islet-specific [^{18}F]exendin-4 binding was observed when the sections were incubated with an excess of cold exendin-3.

5.2.6 Analysis of exendin radiometabolites

In vivo radioactive metabolites were assessed using HPLC. The metal-labeled exendin molecules turned out to be more stable in rat plasma or serum than their fluorine-18 labeled counterpart. The amount of intact [^{64}Cu]NODAGA-exendin-4, [^{64}Cu]NODAGA-MAL-exendin-4 and [^{68}Ga]NODAGAexendin-4 in serum at 1 h p.i. was 55 ± 12 %, 47 ± 26 % and 70 ± 5 %, respectively. The corresponding value for [^{18}F]exendin-4 was 28 ± 2.9 %. In pancreas, 44 ± 13 % of the [^{64}Cu]NODAGA-exendin-4 radioactivity, 26 ± 14 % of the [^{64}Cu]NODAGA-MAL-exendin-4 radioactivity, 32 ± 5 % of the [^{68}Ga]NODAGA-exendin-4 and 20 ± 7 % of the [^{18}F]exendin-4 radioactivity represented intact tracer. In kidney and urine, almost all the radioactivity was observed to be in metabolized form. Additional plasma stability measurements in pig showed that 87 ± 6 % (N=3) of the radioactivity in plasma was attributable to [^{18}F]exendin-4 at 5 min *p.i.* and decreased gradually to 77 ± 3 % at 60 min after administration.

5.2.7 Dosimetry (II, IV)

For all the exendin-based tracers, the kidney was the dose-limiting organ (Table 4). Extrapolated from the rat *ex vivo* results, the mean effective dose for [^{64}Cu]NODAGA-exendin-4 was 0.074 mSv/MBq and 0.021 mSv/MBq for [^{18}F]exendin-4. Extrapolated from the PET *in vivo* results the effective dose for [^{68}Ga]NODAGA-exendin-4 was 0.012 mSv/MBq. The absorbed kidney dose was highest for [^{64}Cu]NODAGA-exendin-4 (1.48 mSv/MBq) and lowest for [^{18}F]exendin-4 (0.300 mSv/MBq).

Table 4. Radiation dosimetry of exendin-based tracers.

Radiotracer	effective dose [mSv/MBq]	absorbed kidney dose [mSv/MBq]
[^{18}F]exendin-4	0.021	0.300
[^{64}Cu]NODAGA-exendin-4	0.074	1.48
[^{68}Ga]NODAGA-exendin-4	0.012	0.523

6. DISCUSSION

6.1 Radiolabeled DTBZ as an imaging agent (I)

Imaging rat pancreas

Previous studies using DTBZ or its derivatives showed accumulation of radioactivity in the pancreas (Souza et al., 2006b; Simpson et al., 2006; Kung et al., 2008a; Kung et al., 2008b). However, in those investigations tracer accumulation in islets was not assessed directly by using autoradiography to determine the spatial distribution of radioactivity within the pancreas. In the present study, [^{11}C]DTBZ and [^{3}H]DTBZ showed that accumulation of radioactivity in rat endocrine pancreas did not exceed the binding in exocrine pancreas *in vitro* or after injection into the living animals. Similar results were reported by Tsao and colleagues when [^{18}F]-FP-DTBZ was used. [^{18}F]-FP-DTBZ showed islet labeling when investigated with healthy rat pancreatic sections and *in vitro* autoradiography, but not after tracer injection into living animals (Tsao et al., 2010). Furthermore, we observed that the distribution of [^{11}C]DTBZ radioactivity in rat pancreas was heterogeneous 10 min after tracer injection, but it did not correspond to the distribution of islets. This heterogeneous distribution might be a consequence of regional differences in blood flow or blood perfusion in the pancreas. However, [^{3}H]DTBZ and [^{11}C]DTBZ exhibited the expected binding pattern in VMAT2-rich areas in rat brain (striatum) and bovine adrenal gland (adrenal medulla).

In vitro binding profiles of [^{3}H]DTBZ further confirmed that the radioactivity did not co-localize with VMAT2 in the rat pancreas (study I). Our results showed that binding in rat pancreas was non-saturable (non-specific), whereas in brain and adrenal medulla saturable (specific) [^{3}H]DTBZ binding was observed. Competition binding studies with VMAT2 antagonists showed a pharmacological profile corresponding to VMAT2 in rat striatum and bovine adrenal medulla, but not in rat pancreas.

In the endocrine pancreas, VMAT2 has been shown to be expressed mainly in the beta cells of and, to some extent, in the PP-cells (Saisho et al., 2008). Sympathetic nerve fibers also show VMAT2-positive receptor expression (Anlauf et al., 2003). In addition, it was recently reported that, [^{18}F]-FP-DTBZ binds not only to the high affinity VMAT2 receptor, but also to the low affinity sigma receptor in rat pancreatic

islets and exocrine pancreas (Tsao et al., 2010; Tsao et al., 2011). These multiple specific binding and non-specific binding sites complicate the attempt to discern the signal derived from the beta cells *in vivo*. Our studies showed decreased binding of [^{11}C]DTBZ in pancreatic sections of STZ-induced diabetic rats compared to controls. Because the binding in control and STZ pancreatic sections was uniform, the decrease in radioactivity could not be due to a decrease in beta cell mass. The mechanism behind the reduction in non-specific (non-VMAT2) DTBZ binding in the exocrine pancreas in rats with T1D (STZ-induced or autoimmune) is still unknown. This reduction of non-specific binding instead of specific binding in beta cells may lead to misinterpretation of PET results, and can be falsely associated with beta cell loss. The studies show reduced tracer uptake in rodent models of T1D but simultaneously marked residual tracer uptake in the pancreas.

Although ^{18}F-labeled DTBZ molecules were developed to improve the tracer affinity for the receptor and therefore islet labeling, time-activity curves of a PET scan showed similar kinetics for [^{11}C]DTBZ and [^{18}F]-FP-DTBZ in healthy rat pancreas (Singhal et al., 2010). Scans showed a 30 % decrease of both tracers in STZ induced T1D diabetic rats compared to healthy controls. A 65 % decrease of pancreatic [^{11}C]DTBZ radioactivity was detected in another rat model of T1D, the BB-DP rat, when compared to controls (Souza et al., 2006b). Sympathetic nerves are gradually destroyed along with the beta cells as the disease progresses in the BB-DP model (Mei et al., 2002; Raffo et al., 2008). Instead, STZ destroys only the beta cells (Mei et al., 2002; Raffo et al., 2008). The concentration of VMAT2 is higher in sympathetic nerves than in beta cells, which might partly explain the differences of these two animal models (Anlauf et al., 2003). Taken together, these results underline the importance of the rodent model used when interpreting the results.

In vitro imaging of human pancreas

In human pancreatic tissue sections, the [^{3}H]DTBZ labeling of islets *in vitro* was weak and observed only in the larger islets (study I). In most of the islets, [^{3}H]DTBZ binding did not exceed the binding in exocrine pancreas. In another study by Eriksson et al., *in vitro* studies with isolated human islets showed specific binding of [^{18}F]-FE-DTBZ but the level of binding did not exceed the non-specific binding in exocrine pancreas (65 % non-displaceable, i.e. binding to other structures than VMAT2), resulting in a low islet-to-exocrine tissue signal ratio. Tissue autoradiography performed with human pancreatic slices revealed no difference in tracer binding between T1D or T2D and healthy control. Thus, the total tracer uptake in pancreas was not representative

of beta cell mass. (Eriksson et al., 2010.) These results are in line with our results when [^{3}H]DTBZ was used to detect the islets in healthy human pancreatic sections *in vitro* (study I). In conclusion, the results of human tissue *in vitro* studies showed poor labeling of the islets.

Clinical imaging of pancreas

A similar residual binding of radioactivity as observed in T1D animal models was reported in clinical studies. Residual binding of [^{11}C]DTBZ radioactivity was observed in long-standing T1D subjects when imaged with PET although depletion of beta cell mass is almost total in long-standing T1D (Goland et al., 2009). Pancreatic binding potential (BP_{ND}, indicative of specific binding to VMAT2) was reported to decrease by 14 % in T1D subjects compared to healthy controls. C-peptide measurements correlated with BP_{ND} in controls but not in T1D subjects. When fluorine-18 labeled DTBZ was used, the mean integrated pancreatic uptake of [^{18}F]-FP-DTBZ was decreased by 59 % (Normandin et al., 2012) and 63 % (Freeby et al., 2016) in T1D subjects compared to healthy subjects. Pancreatic [^{18}F]-FP-DTBZ binding correlated with stimulated C-peptide measurements (Normandin et al., 2012; Freeby et al., 2016). No significant difference in BP_{ND} between T2D and controls was observed (Freeby et al., 2016).

The above-mentioned ^{18}F-labeled DTBZ derivatives displayed a similar uptake profile in the pancreas as ^{11}C-labeled DTBZ. Preclinical studies with rodent models and clinical studies with healthy and T1D subjects have shown significant residual uptake of fluorine-18 and carbon-11 labeled DTBZ derivatives in the pancreas. This residual uptake can be caused by binding to the sigma receptor in endocrine and exocrine pancreas (Tsao et al., 2011), binding to the VMAT2 positive sympathetic nerve fibers innervating the pancreas (Anlauf et al., 2003; Mei et al., 2002), binding to the VMAT2 expressed in PP cells of a healthy or long-standing T1D subject (Freeby et al., 2012), VMAT2 specific binding to residual beta cell mass even with long-standing T1D (Goland et al., 2009; Normandin et al., 2012; Freeby et al., 2016) or non-specific (non-VMAT2) binding in exocrine pancreas (study I). Based on our results and those of others, the uptake of DTBZ-based PET tracers in the pancreas is not representative of beta cell mass, and the results are not promising for quantification of the mass.

6.2 Radiolabeled exendin-4 as an imaging agent (II, III, IV)

Tracer biodistribution in rat pancreas and other organs

Studies with radiolabeled exendin analogs for PET and SPECT have shown promising results and binding to GLP-1R expressing beta cells. Results have shown significantly reduced (80 %) tracer uptake in the islets of alloxan and STZ treated animals and other T1D animal models compared to healthy controls (Brom et al., 2014; Connolly et al., 2012). In this study, novel exendin-based tracers [^{64}Cu]NODAGA-exendin-4, [^{68}Ga]NODAGA-exendin4, [^{64}Cu]NODAGA-MAL-exendin-4 and [^{18}F]exendin-4 were evaluated. The tracers showed persistent and islet specific binding when incubated with tissue sections *in vitro* and after injection into the living animal *ex vivo*. Specificity studies using unlabeled exendin-3 combined with autoradiography and insulin immunohistochemistry confirmed islet-specific and GLP-1R-specific binding. Uptake of tracer-derived radioactivity in the whole pancreas determined by gamma counting remained low at all investigated time-points, which together with autoradiography, indicated low binding in the exocrine pancreas. Of the tracers studied, uptake in whole pancreas was the highest with [^{18}F]exendin-4.

Tracers were rapidly cleared from the blood after *i.v.* injection, which is an advantageous feature for the target-to-background ratio. High and persistent uptake in the islets, together with low exocrine pancreas uptake, further contributes to a high islet-to-exocrine tissue signal ratio. Theoretical estimates of the islet-to-exocrine tissue ratio for successful quantitative *in vivo* beta cell imaging vary from 100:1 to 1000:1 (Sweet et al., 2004a; Sweet et al., 2004b). [^{18}F]exendin-4 was produced with a specific activity reaching 323 MBq/nmol. By analyzing the autoradiography results, [^{18}F]exendin-4 showed the highest ratio, increasing over time (140 ± 63 at 6 h *p.i.*), indicating persistent uptake in the islets and clearance from the exocrine pancreas. These results are highly promising for the development of a clinical grade tracer.

Besides the pancreatic islets, GLP-1R-specific labeling was observed in lung, stomach wall and in a distinct narrow band in the proximal duodenum (II). A Similar kind of focal accumulation of [^{111}In]DOTA-exendin-4 radioactivity was detected in subjects with insulinoma imaged with SPECT (Christ et al., 2009). In contrast to human, GLP-1R has been reported to have high expression levels in rat lung (Körner et al., 2007). In study II, all the investigated target organs accumulated more [^{64}Cu]NODAGA-exendin-4 than [^{68}Ga]NODAGA-exendin-4. This is most likely because of the higher specific activity of [^{64}Cu]NODAGA-exendin-4 (90 ± 10 GBq/μmol) as compared to [^{68}Ga]NODAGA-exendin-4 (20 ± 5 GBq/μmol), and therefore lower injected mass

of the [^{64}Cu]NODAGA-exendin-4 tracer. Previous studies have shown moderate to substantial accumulation of ^{18}F labeled GLP-1 analogs in liver of mouse xenograft models (Gao et al., 2011; Yue et al., 2014; Kiesewetter et al., 2012a; Wu et al., 2013a; Wu et al., 2013b). The liver is the main site of insulinoma metastasis and an organ of choice for islet transplantation. In study IV, only low amounts of [^{18}F]exendin-4 radioactivity was observed in the liver, which should allow for sufficiently high tumor-to-background and transplant-to-background signal ratios.

In vivo PET imaging of rat pancreas

Studies with *in vivo* PET imaging have shown variable results in the aim to visualize beta cells in rodent pancreas. Although the renal retention of [^{18}F]exendin-4 was significantly decreased as compared to its metal-labeled counterparts, we were unable to visualize the pancreas *in vivo* by PET imaging. This was probably due to PVE (partial volume effect) and the spillover effect from the high radioactivity of the kidneys that hamper the signal from the adjacent low radioactivity pancreas. In humans the spillover signal from the kidneys is probably less severe since the distance between the organs is greater.

In rodents, the resolution of CT is not good enough to discern the pancreas from the surrounding soft tissues in the abdominal area. In humans, the pancreas can be delineated on CT images. Therefore, in study II, [^{11}C]Methionine was used to delineate the rat pancreas and derive the SUV of [^{64}Cu]NODAGA-exendin-4. While others have been able to visualize the rat pancreas *in vivo* using [^{18}F]Al-NOTA-MAL-Cys^{39}-exendin-4 (Mi et al., 2016), or [^{64}Cu]DO3A-VS-Cys^{40}-exendin-4 and [^{68}Ga]NODA-VS-Cys^{40}-exendin-4 (Bandara et al., 2016) others have failed when using [^{68}Ga]DO3A-VS-Cys^{40}-exendin-4 ([^{68}Ga]DO3A-exendin-4) (Selvaraju et al., 2013). Mi and colleagues showed a reduction in the radioactive signal from the pancreas after pre-injection of unlabeled Cys^{39}-exendin-4 and when using STZ treatment to induce T1D (Mi et al., 2016). Bandara et al. confirmed the uptake in the pancreas only by using the unlabeled peptide, exendin-9-39-amide (antagonist) and exendin-4 (agonist) (Bandara et al., 2016). These aforementioned unlabeled peptides are commonly used to demonstrate specific GLP-1R binding in the target tissue. However, as these peptides are structurally almost identical to the employed radiolabeled peptide, they can be expected to reduce also nonspecific binding, making interpreting the results of *in vivo* imaging, where individual islets cannot be identified, challenging. Besides using unlabeled exendin, the results of *in vivo* imaging could have been confirmed with a T1D animal model. Although contend to be able to visualize the pancreas in PET images, no time-activity curves (TACs) or further analyses were provided to confirm the results. In addition,

only one image plane instead of multiple ones (coronal, transaxial, sagittal) was shown (Bandara et al., 2016; Mi et al., 2016). Furthermore, no islet-to-exocrine tissue ratio was reported that would have supported the results. As shown in our study II, high and specific accumulation of [^{64}Cu]NODAGA-exendin-4 radioactivity in the GLP-1R rich area in the proximal duodenum was detected. It can be speculated whether the signal could be falsely interpreted as a signal from the pancreas of *in vivo* PET. Studies with larger animals could overcome some of these hurdles. Unfortunately, the widely used pig as an animal model before clinical studies is challenging since *i.v.* injection of radiolabeled exendin-4 caused increased heart rate in pigs soon after tracer administration as noticed by us (study IV) and others (Nalin et al., 2014; Ryden et al., 2016).

Kidney retention of radiometal-labeled exendin

Radiolabeled peptides are generally excreted *via* the kidneys into the urine. Studies with pigs showed exendin-4 to be cleared solely *via* glomerular filtration (Simonsen et al., 2006). High and persistent kidney retention of metal-labeled PET and SPECT analogs with only minor clearance has been demonstrated previously (Vegt et al., 2008; Brom et al., 2014; Bauman et al., 2015). The high radioactivity accumulation of metal-labeled exendin analogs in the kidney cortex is mediated *via* a GLP-1R independent (non-specific) mechanism (Vegt et al., 2011). Peptides may be partly reabsorbed and retained in the proximal tubular cells in the kidney cortex. Also in our study (II) autoradiography results of [^{64}Cu]- and [^{68}Ga]NODAGA-exendin-4 showed high and persistent retention in the kidney cortex. Several efforts have been made to reduce the radioactivity retention in the kidneys, e.g. introducing enzymatically cleavable functional groups that can be cleaved in the kidney and the metabolites excreted more readily into urine (Wilbur et al., 2011). Recently, cleavable linker sequences and substrates for kidney brush border enzyme meprin β were designed and investigated using indium-111 labeled exendin-4 (Jodal et al., 2015). Although the linkers were cleaved *in vitro* they failed to do so *in vivo*. In this study (III), we developed a copper-64 labeled exendin peptide with MAL linkage in order to decrease the tracer retention in the kidneys by producing radioactive catabolites that could be excreted into urine. Although [^{64}Cu]NODAGA-MAL-exendin-4 showed persistent and high labeling of rat pancreatic islets, it unfortunately demonstrated similar kinetics and kidney retention as the reference compound [^{64}Cu]NODAGA-exendin-4. This could be due to the limited exposure of the MAL linkage that would prevent enzyme access to the glycyl-lysine sequence, or due to steric interference of the exendin-4 peptide. Although these attempts were not successful in

decreasing the kidney retention, the tracer still retained its labeling efficiency towards the target, highlighting the versatility of this peptide for modifications.

The effect of radionuclide selection on kidney retention and radiation dose

Because of the persistent retention and low clearance, the half-life for the long-lived copper-64 and indium-111 labeled exendin tracers, repeated scanning and longitudinal studies of healthy controls and T1D or T2D diabetic subjects are likely to cause an unacceptably high radiation burden for the kidney. Accordingly, it has been shown that high radiation doses of [^{111}In]DTPA-exendin-4 caused nephrotoxicity in mice (Melis et al., 2010). The need to limit the maximum injected dose and thus hinder peptide-based receptor imaging and therapy (Behr et al., 1998).

^{18}F-labeled exendin-4 was developed to overcome this problem (IV). In the beginning of dynamic PET imaging (0–30 min) the kinetics of [^{18}F]exendin-4 in the kidney was similar to that of its metal-labeled counterparts (studies II and III) but, thereafter, the clearance was rapid as demonstrated also with *ex vivo* radioactivity measurements (Figure 11B). In studies II and III, the uptake of metal-labeled tracers in the kidney was similar. However, because of the longer half-life of ^{64}Cu (12.7 h) as compared to ^{68}Ga (68 min), the radiation dose of ^{64}Cu-labeled exendin was significantly higher than for ^{68}Ga-labeled exendin (II) (Table 4). In study IV, the absorbed kidney dose and effective dose of [^{18}F]exendin-4 was found to be similar to that reported for [^{68}Ga]DO3A-exendin-4, 0.276 mSv/MBq and 0.016 mSv/MBq, respectively (Selvaraju et al., 2015), and the effective dose seven-fold lower than that for [^{111}In]DTPA-exendin-4, 0.155 mSv/MBq (Wild et al., 2010). Although the dosimetry results are similar for gallium-68 and fluorine-18 labeled exendin tracers. However, the radiation properties (β^+ fraction and maximal energy, Table 1) and longer half-life of fluorine-18, enable longer study protocols and ensure high quality, high resolution PET imaging, making fluorine-18 better for beta cell imaging.

In vitro imaging of human pancreas

Quantitative PCR has shown GLP-1R to be expressed at higher levels in human islets than in rat islets (islet-to-exocrine ratio human 47, rat 13) (Brom et al., 2014). In our study (IV), *in vitro* experiments using non-diabetic human pancreas revealed specific [^{18}F]exendin-4 labeling of the islets. Recently, *in vitro* studies with healthy human pancreatic sections have shown [^{125}I]BH-exendin(9-39) binding in the islets and displacement using cold peptide (Waser and Reubi, 2014). Furthermore, stability studies of [^{18}F]exendin-4 *in vivo* in pigs revealed significantly higher recovery of

the parent compound in pig plasma compared to rat plasma. These indications are promising for further clinical studies aiming to image pancreatic beta cells.

Clinical imaging of pancreas

A clinical study with the SPECT tracer [^{111}In]DTPA-exendin-4 revealed markedly decreased tracer uptake in T1D subjects compared to healthy controls (Brom et al., 2014). However, inter-individual variation and overlap of the tracer uptake in the pancreas between the groups was observed. This variation may be caused by the natural variation in the existing beta cell mass in diabetic and healthy subjects (Ritzel et al., 2006; Rahier et al., 2008; Keenan et al., 2010). The radioactivity in the pancreas remained unchanged during the course of the study (4–48 h), as could be predicted on the basis of the results of animal studies. The mean integrated pancreatic uptake was decreased by 62 % in T1D subjects compared to healthy subjects (Eriksson et al., 2016).

In humans, the pharmacologically effective dose of exenatide is low (10 μg BID, *s.c.*), and in animal studies exendin-4 was a potent glucose-lowering agent at a dose of 0.001 to 10 μg (*i.p.*) (Young et al., 1999). [^{18}F]exendin-4 was produced with a specific activity up to 323 MBq/nmol, and therefore an injected mass as low as 2 ± 1 μg/kg. Studies have shown the plasma half-life of *s.c.* administered exendin-4 to be considerably longer compared to plasma concentrations after *i.v.* injection (Parkes et al., 2001). Properties such as high specific activity and injected mass in the light of receptor saturation and pharmacological effects should be carefully considered. With doses of 7–25 μg of [^{68}Ga]NOTA-exendin-4 (*i.v.*), some of the subjects experienced palpitation, vomiting, and nausea after tracer injection (Luo et al., 2016b): these are known possible side effects also after *s.c.* injection of exenatide.

More clinical studies are needed to further understand the variation in tracer uptake. One approach would be to image subjects expected to have different beta cell masses, e.g. obese subjects with normoglycemia or subjects with early childhood onset of the T1D. Moreover, additional research is needed to better understand the effect of metabolic conditions on the expression levels of GLP-1R. Animal studies have shown significant decrease in GLP-1R mRNA expression in hyperglycemia (Xu et al., 2007). From an imaging point of view, this could lead to false negative results when tracer uptake would probably indicate a lower beta cell mass compared to histological analysis.

6.3 Limitations and challenges of beta cell imaging

The feasibility of quantitative *in vivo* imaging of pancreatic beta cells is still an issue of debate (Andralojc et al., 2012; Blomberg et al., 2013). The limited spatial resolution of PET is associated with partial volume effect (PVE). The PVE comes into play when imaging small target tissues or targets with low expression levels of the receptor. PVE is most prominent for structures that are smaller than 2.5-times the spatial resolution of PET. Movement of the pancreas induced by respiratory motion further degrades the spatial resolution and increases the PVE. (Basu et al., 2007.) Moreover, the pancreas of T1D and T2D subjects is anthropic (approximately 30 % as determined by MRI) (Normandin et al., 2012; Williams et al., 2012). If not corrected for PVE, these issues will result in an underestimation of the true radioactivity concentration in the target, and may lead to misinterpretation of the PET result (Basu et al., 2007; Hickeson et al., 2002). Therefore, it is a challenge to reliably detect differences in radioactivity uptake between healthy controls and diabetic subjects. Because of the low resolution of the PET camera and the small size of the pancreatic islets, single islets cannot be distinguished, and instead the receptor density in unit per pancreatic tissue volume or total pancreatic receptor content (indicating beta cell mass) is measured (Kwee et al., 2011). It has been estimated that islets should retain ~100–1000 times more radioactivity than the exocrine pancreas in order to enable quantitative imaging (Sweet et al., 2004a; Sweet et al., 2004b). To overcome these hurdles, a PET tracer with high affinity, high specific activity, long retention, a high number of binding sites per cell and a high target-to-background signal ratio is needed. Moreover, because of the high and specific accumulation of the ligand, a radionuclide with optimal radiation properties and half-life is essential in order to minimize the radiation dose for beta cells. Exendin peptides (studies II–IV), and especially [^{18}F]exendin-4, showed promising results regarding many of these qualities.

Summary of clinical studies

Exendin (Brom et al., 2014) and DTBZ (Normandin et al., 2012; Freeby et al., 2016) derived ligands have shown variable pancreatic uptake in healthy controls and T1D subjects (Table 5). Uptake in the pancreas is decreased in T1D subjects but uptake levels overlap with those of healthy subjects. The mean average integrated decrease of [^{18}F]-FP-DTBZ and [^{111}In]DTPA-exendin-4 uptake in the pancreas of T1D subjects compared to healthy ones was 59–62 %. However, [^{111}In]DTPA-exendin-4 showed the highest maximal decrease in uptake (96 %) between the groups, and therefore shows promise for further studies. Studies have shown high variability in the beta cell mass of T1D and healthy subjects (Keenan et al., 2010; Coppieters et al., 2012). In addition, in

T1D, the mass of the exocrine pancreas is reduced even before the clinical diagnosis of the disease, implying disease-associated changes that are still unresolved (Williams et al., 2012). Moreover, animal studies have shown plasticity in islet cell composition in different metabolic conditions (Mezza and Kulkarni, 2014; Roscioni et al., 2016). On the basis of these considerations, variation in PET and SPECT tracer uptake can be expected and more clinical grade research is needed to further understand these results.

Table 5. Signal decrease in pancreas of subjects with T1D compared to healthy controls.

Signal decrease (%) in pancreas	**[^{18}F]-FP-DTBZ**	**[^{111}In]DTPA-exendin-4**
Mean	59–63	62
Maximal	78–79	96

Integrated values (volume of the pancreas is taken into account). In [^{18}F]-FP-DTBZ studies the number of healthy subjects is N=9–14 and T1D subjects N=7–8 (Freeby et al., 2016, Normandin et al., 2012). In [^{111}In]DTPA-exendin-4 the number of healthy subjects is N=5 and T1D subjects N=5 (Brom et al., 2014). (Modified from Eriksson et al., 2016).

7. SUMMARY AND CONCLUSIONS

In this study, five different PET tracers were investigated as tracers for the imaging of pancreatic beta cells.

In study I, the VMAT2 specific [^{11}C]DTBZ tracer was investigated as previous studies had shown high [^{11}C]DTBZ binding in the pancreas and decreased accumulation in T1D. However, our results clearly showed that [^{11}C]DTBZ was not suitable for beta cell imaging. Non-specific binding in the exocrine pancreas dominated and specific binding in beta cells was not observed in rats and was very low in humans (study I). The results suggest that the decrease of tracer binding in T1D is not related to the loss of beta cell mass. The results of our studies suggest that [^{11}C]DTBZ can not be used for the quantitative imaging of beta cell mass.

In studies II–IV, four different novel exendin-based imaging agents were developed and evaluated. In study II, the islet specificity of [^{64}Cu]NODAGA-exendin-4 and [^{68}Ga]NODAGA-exendin-4 was studied. Both tracers showed persistent islet specific labeling. Autoradiography results, together with the significantly higher tracer specific activity, showed [^{64}Cu]NODAGA-exendin-4 to be more efficient in labeling the islets, with a higher islet-to-exocrine tissue signal ratio compared to [^{68}Ga]NODAGA-exendin-4. As a result of these properties, [^{68}Ga]NODAGA-exendin-4 could be used to detect tumors that overexpress the GLP-1R. However, both tracers showed high and persistent kidney retention. The long half-life of [^{64}Cu]NODAGA-exendin-4 makes it a useful tool for preclinical research. The concomitant high radiation at the kidneys may, however, restrict the use of this tracer as a clinical imaging agent.

The high kidney retention of all the metal-labeled exendin tracers also compromises tissue visualization in the kidney region, including pancreas, and therefore limits diagnostic accuracy. In study III, a biodegradable MAL linker was developed to reduce the renal radioactivity levels. Although maintaining the islet-specific labeling, the MAL linkage in [^{64}Cu]NODAGA-MAL-exendin-4 did not reduce the tracer accumulation in the kidneys as compared to [^{64}Cu]NODAGA-exendin-4. The applicability of metabolizable linkages in the design of kidney-saving exendin-4 analogs requires further investigation.

To further investigate the possibility to reduce the kidney retention by radionuclide selection, [^{18}F]exendin-4 was developed (IV). Moreover, the radiation properties of

fluorine-18 have potential to be used as a clinical tracer. In this study, [^{18}F]exendin-4 showed specific and sustained uptake in rat pancreas *ex vivo* and islet-specific labeling of human pancreatic tissue sections *in vitro*. In contrast to the metal-labeled exendin tracers, [^{18}F]exendin-4 showed rapid renal clearance, excretion of radioactivity into the urine, and a concomitant reduced absorbed radiation dose for the kidneys. The indications are promising for the further development of clinical grade [^{18}F]exendin-4 tracer for beta cell imaging.

ACKNOWLEDGEMENTS

This study was conducted at Turku PET Centre, Institute of Clinical Medicine, Department of Clinical Physiology and Nuclear Medicine, University of Turku, Finland during the years 2010–2016. I express my appreciation to Professor Jaakko Hartiala and Adjunct Professor Jukka Kemppainen from the Department of Clinical Physiology and Nuclear Medicine and Professor Juhani Knuuti, the Director of Turku PET Centre for providing excellent facilities for research. I warmly thank Professor Sirpa Jalkanen for the possibility to carry out the scientific work at the facilities of MediCity Research Laboratory.

I am deeply grateful to my supervisors Professor Pirjo Nuutila, Professor Olof Solin and Dr Veronica Fagerholm. I want to thank Pirjo for introducing me to the world of diabetes research and for support throughout the thesis. I appreciate your ability to be strict and honest, and still allow room for personal growth and independence. I want to thank Olof for guiding me into the world of radiochemistry and development of novel radiotracers. Your passion and experience for radiochemistry and molecular imaging is truly inspiring. I want to thank Veronica for all the help and guidance provided. Thank you for teaching me the critical thinking needed for science. I have enjoyed our scientific and nonscientific discussions during the years and have learned indescribably much from all of you.

Professor Timo Otonkoski and Associate Professor Irina Velikyan are gratefully acknowledged for the review of my thesis manuscript and for their valuable comments, constructive criticism and advice. I wish to thank the Doctoral Programme of Clinical Investigation and the members of my follow-up committee, Professor Timo Otonkoski and Adjunct Professor Tiina Henttinen, for their valuable advice during the doctoral training. I warmly thank Tiina for guidance at the Biology Department during the studies and for suggesting me the PET Centre as a place to do my Master's thesis.

I wish to thank all of my co-authors for their valuable contribution. I express my sincere gratitude to Cheng-Bin Yim. I couldn't have managed this without you. I admire your enthusiasm for science, your motivation and how you get excited about new things. Team work with you has left me with unforgettable memories. I have had a privilege to work in BetaImage and BetaCure EU projects coordinated by Professor Martin Gotthardt. I would like to express my gratitude to Professor Gotthardt for giving me this unique opportunity to learn and be part of these consortiums. Eveliina

Arponen, Kjell Någren, Jörn Schlesinger, Viki-Veikko Elomaa, Johan Rajander, Jori Jurttila and Paula Lehtiniemi are acknowledged for their expertise in radiochemistry and tracer production. Professor Anne Roivainen, Professor Jean Claude Reubi, Professor Helmut Mäcke, Martin Béhé, Eleni Gourni and Tiina Saanijoki are warmly thanked for their knowledge with the [^{68}Ga]exendin studies. I am deeply grateful to Adjunct Professor Merja Haaparanta-Solin for introducing me to the fascinating world of preclinical PET imaging and teaching me so many valuable skills needed in research. Thank you for your support and warm presence over the years. Saila Kauhanen is thanked for providing the invaluable human tissue samples and long collaboration together. I want to thank Tuula Tolvanen for her expertise with the radiation dosimetry calculations and Miikka Tarkia for his know-how in pig studies. Tamiko Ishizu is thanked for her help with the preclinical work, Marko Tirri for his help with PET/CT data management and Vesa Oikonen for his know-how with PET/CT data analysis.

I express my gratitude to the personnel of the Medicity Research Laboratory. Tarja Marttila and Marko Vehmanen are acknowledged for the technical assistance and also Tarja for taking care of the project finances, Elisa Riuttala your knowhow in animal work has been essential, Aake Honkaniemi and Leena Tokoi-Eklund are thanked for their expertise at the animal PET/CT camera. The personnel of the PET laboratory is thanked, especially Sanna Suominen, for her kind and helpful presence during the pig studies. Furthermore, I wish to thank the personnel of the Accelerator Laboratory and Radiopharmaceutical Chemistry Laboratory for their help in tracer production.

I am privileged to have magnificent and skilled colleagues and friends in Turku PET Centre, especially Tove Grönroos, Rea Pihlaja, Francisco López-Picón, Jatta Takkinen, Susanne Vainio, Johanna Tuomela, Laura Lammela, Jarna Hannukainen, Jukka Koffert, Henry Karlsson, Henri Honka and all the students and post-docs over the years. Anniina Snellman and Jonna Sinkkonen, we started the journey into science together at the PET Centre when preparing our Master's theses. Your peer support and presence has been invaluable over the years, especially in the beginning when everything was so new. This project would have been much lonelier without you.

I warmly thank Turku University Hospital Research Foundation and Professor Olli Ruuskanen for giving me the opportunity to finalize my thesis manuscript at the Foundation's Research Unit. The people from Tutkari: Anna E, Anna N, Johanna O, Johanna U, Kjell, Laura, Lauri, Mari, Nora, Sari, Sirkku, Ulla and all the others along the way. Thank you for your company and support during the lunch and coffee breaks. The time at Tutkari has been memorable and one of a kind.

I am truly fortunate to have my friends in my life. Kirsi, Markus, Maria and Elsi, we met as young students at the University and our team has been close ever since. We have so many good memories to share, full of joy and laughter. Thank you for being there. I am fortunate to have such a good group of friends around me, Hanna-Mari, Martiina, Susanna, Kaisa, and all the other friends outside science, thank you all!

Finally, I warmly thank my family for their care and support. Kiitän vanhempiani Seijaa ja Raimoa sekä siskojani Marjoa ja Eliseä avusta ja läsnäolosta välimatkoista huolimatta. En voi kyllin kiittää siitä tuesta, jonka olen teiltä saanut. Kummityttöni Pinja, kiitos että olet todellinen auringonsäde ja saat meidät kaikki hymyilemään ja nauramaan. Kiitos Jani, että olet huolehtinut ja tukenut minua kaikki nämä vuodet. Kiitos!

This project was conducted within the Finnish Centre of Excellence in Cardiovascular and Metabolic Diseases supported by the Academy of Finland, the University of Turku, Turku University Hospital and Åbo Akademi University. Financial support was received from the EC 7th framework program BetaImage (FP7/2007–2013, grant agreement 222980) and BetaCure (FP7/2014–2018, grant agreement 602812), the Novo Nordisk Foundation, the Diabetes Research Foundation, the Finnish Cultural Foundation, the Maud Kuistila Memorial Foundation, University of Turku Doctoral Programme of Clinical Investigation and the State Research Funding of the Turku University Hospital.

Turku, May 2017

Kirsi Mikkola

REFERENCES

Adam, Y., Edwards, R. H. & Schuldiner, S. 2008. Expression and function of the rat vesicular monoamine transporter 2. *Am J Physiol Cell Physiol,* 294(4), pp C1004-11.

Ahren, B. 2000. Autonomic regulation of islet hormone secretion--implications for health and disease. *Diabetologia,* 43(4), pp 393-410.

American Diabetes Association 2017. 2. Classification and Diagnosis of Diabetes. *Diabetes Care,* 40(Suppl 1), pp 11-24.

Andralojc, K., Srinivas, M., Brom, M., Joosten, L., de Vries, I. J., Eizirik, D. L., Boerman, O. C., Meda, P. & Gotthardt, M. 2012. Obstacles on the way to the clinical visualisation of beta cells: looking for the Aeneas of molecular imaging to navigate between Scylla and Charybdis. *Diabetologia,* 55(5), pp 1247-57.

Anlauf, M., Eissele, R., Schäfer, M., Eiden, L., Arnold, R., Pauser, U., Klöppel, G. & Weihe, E. 2003. Expression of the two isoforms of the vesicular monoamine transporter (VMAT1 and VMAT2) in the endocrine pancreas and pancreatic endocrine tumors. *J Histochem Cytochem,* 51(8), pp 1027-40.

Antkowiak, P. F., Tersey, S. A., Carter, J. D., Vandsburger, M. H., Nadler, J. L., Epstein, F. H. & Mirmira, R. G. 2009. Noninvasive assessment of pancreatic beta-cell function in vivo with manganese-enhanced magnetic resonance imaging. *Am J Physiol Endocrinol Metab,* 296(3), pp E573-8.

Antwi, K., Fani, M., Nicolas, G., Rottenburger, C., Heye, T., Reubi, J. C., Gloor, B., Christ, E. & Wild, D. 2015. Localization of Hidden Insulinomas with ^{68}Ga-DOTA-Exendin-4 PET/CT: A Pilot Study. *J Nucl Med,* 56(7), pp 1075-8.

Arrojo e Drigo, R., Ali, Y., Diez, J., Srinivasan, D. K., Berggren, P. O. & Boehm, B. O. 2015. New insights into the architecture of the islet of Langerhans: a focused cross-species assessment. *Diabetologia,* 58(10), pp 2218-28.

Atkinson, M. A. 2012. The pathogenesis and natural history of type 1 diabetes. *Cold Spring Harb Perspect Med,* 2(11), pp 1-18.

Atkinson, M. A. & Eisenbarth, G. S. 2001. Type 1 diabetes: new perspectives on disease pathogenesis and treatment. *Lancet,* 358(9277), pp 221-9.

Atkinson, M. A., Eisenbarth, G. S. & Michels, A. W. 2014. Type 1 diabetes. *Lancet,* 383(9911), pp 69-82.

Avila-Rodriguez, M. A., Nye, J. A. & Nickles, R. J. 2007. Simultaneous production of high specific activity ^{64}Cu and ^{61}Co with 11.4 MeV protons on enriched ^{64}Ni nuclei. *Appl Radiat Isot,* 65(10), pp 1115-20.

Balboa, D. & Otonkoski, T. 2015. Human pluripotent stem cell based islet models for diabetes research. *Best Pract Res Clin Endocrinol Metab,* 29(6), pp 899-909.

Bandara, N., Zheleznyak, A., Cherukuri, K., Griffith, D. A., Limberakis, C., Tess, D. A., Jianqing, C., Waterhouse, R. & Lapi, S. E. 2016. Evaluation of Cu-64 and Ga-68 Radiolabeled Glucagon-Like Peptide-1 Receptor Agonists as PET Tracers for Pancreatic beta cell Imaging. *Mol Imaging Biol,* 18(1), pp 90-8.

Basu, S., Zaidi, H., Houseni, M., Bural, G., Udupa, J., Acton, P., Torigian, D. A. & Alavi, A. 2007. Novel quantitative techniques for assessing regional and global function and structure based on modern imaging modalities: implications for normal variation, aging and diseased states. *Semin Nucl Med,* 37(3), pp 223-39.

Bauman, A., Valverde, I. E., Fischer, C. A., Vomstein, S. & Mindt, T. L. 2015. Development of ^{68}Ga- and ^{89}Zr-Labeled Exendin-4 as Potential Radiotracers for the Imaging of Insulinomas by PET. *J Nucl Med,* 56(10), pp 1569-74.

Beckett, K. R., Moriarity, A. K. & Langer, J. M. 2015. Safe Use of Contrast Media: What the Radiologist Needs to Know. *Radiographics,* 35(6), pp 1738-50.

Behr, T. M., Goldenberg, D. M. & Becker, W. 1998. Reducing the renal uptake of radiolabeled antibody fragments and peptides for diagnosis and therapy: present status, future prospects and limitations. *Eur J Nucl Med,* 25(2), pp 201-12.

Benthuysen, J. R., Carrano, A. C. & Sander, M. 2016. Advances in beta cell replacement and regeneration strategies for treating diabetes. *J Clin Invest,* 126(10), pp 3651-3660.

Bertrand, R., Hamp, I., Bronstrup, M., Weck, R., Lukacevic, M., Polyak, A., Ross, T. L., Gotthardt, M., Plettenburg, O. & Derdau, V. 2016. Synthesis of GPR40 targeting ^{3}H- and ^{18}F-probes towards selective beta cell imaging. *J Labelled Comp Radiopharm,* 59(14), pp 604-610.

Bingley, P. J. 2010. Clinical applications of diabetes antibody testing. *J Clin Endocrinol Metab,* 95(1), pp 25-33.

Blomberg, B. A., Eriksson, O., Saboury, B. & Alavi, A. 2013. beta-Cell mass imaging with DTBZ

positron emission tomography: is it possible? *Mol Imaging Biol,* 15(1), pp 1-2.

Bockman, D. E. 2007. Nerves in the pancreas: what are they for? 194(4), pp 61–64.

Bonner-Weir, S. 2001. Beta-cell turnover: its assessment and implications. *Diabetes,* 50(Suppl 1), pp 20-4.

Bosco, D., Armanet, M., Morel, P., Nicklauss, N., Sgroi, A., Muller, A. D., Giovannoni, L., Parnaud, G. & Berney, T. 2010. Unique arrangement of alpha- and beta-cells in human islets of Langerhans. *Diabetes,* 50(5), pp 1202-1210.

Bouckenooghe, T., Flamez, D., Ortis, F., Goldman, S. & Eizirik, D. 2010. Identification of new pancreatic beta cell targets for in vivo imaging by a systems biology approach. *Curr Pharm Des,* 16(14), pp 1609-18.

Bouwens, L. & Pipeleers, D. G. 1998. Extra-insular beta cells associated with ductules are frequent in adult human pancreas. *Diabetologia,* 41(6), pp 629-33.

Brissova, M., Fowler, M. J., Nicholson, W. E., Chu, A., Hirshberg, B., Harlan, D. M. & Powers, A. C. 2005. Assessment of human pancreatic islet architecture and composition by laser scanning confocal microscopy. *J Histochem Cytochem,* 53(9), pp 1087-97.

Brom, M., Andrałojć, K., Oyen, W., Boerman, O. & Gotthardt, M. 2010a. Development of radiotracers for the determination of the beta-cell mass in vivo. *Curr Pharm Des,* 16(14), pp 1561-7.

Brom, M., Joosten, L., Frielink, C., Boerman, O. & Gotthardt, M. 2015. ^{111}In-exendin uptake in the pancreas correlates with the β-cell mass and not with the α-cell mass. *Diabetes,* 64(4), pp 1324-8.

Brom, M., Oyen, W., Joosten, L., Gotthardt, M. & Boerman, O. 2010b. ^{68}Ga-labelled exendin-3, a new agent for the detection of insulinomas with PET. *Eur J Nucl Med Mol Imaging,* 37(7), pp 1345-55.

Brom, M., Woliner-van der Weg, W., Joosten, L., Frielink, C., Bouckenooghe, T., Rijken, P., Andralojc, K., Goke, B. J., de Jong, M., Eizirik, D. L., Behe, M., Lahoutte, T., Oyen, W. J., Tack, C. J., Janssen, M., Boerman, O. C. & Gotthardt, M. 2014. Non-invasive quantification of the beta cell mass by SPECT with ^{111}In-labelled exendin. *Diabetologia,* 57(5), pp 950-9.

Bruni, A., Gala-Lopez, B., Pepper, A. R., Abualhassan, N. S. & Shapiro, A. J. 2014. Islet cell transplantation for the treatment of type 1 diabetes: recent advances and future challenges. *Diabetes Metab Syndr Obes,* 7(211-23.

Butler, A. E., Janson, J., Bonner-Weir, S., Ritzel, R., Rizza, R. A. & Butler, P. C. 2003. Beta-cell deficit and increased beta-cell apoptosis in humans with type 2 diabetes. *Diabetes,* 52(1), pp 102-10.

Cabrera, O., Berman, D. M., Kenyon, N. S., Ricordi, C., Berggren, P. O. & Caicedo, A. 2006. The unique cytoarchitecture of human pancreatic islets has implications for islet cell function. *Proc Natl Acad Sci U S A,* 103(7), pp 2334-9.

Chan, G. L., Holden, J. E., Stoessl, A. J., Samii, A., Doudet, D. J., Dobko, T., Morrison, K. S., Adam, M., Schulzer, M., Calne, D. B. & Ruth, T. J. 1999. Reproducibility studies with ^{11}C-DTBZ, a monoamine vesicular transporter inhibitor in healthy human subjects. *J Nucl Med,* 40(2), pp 283-9.

Cheng, Y. & Prusoff, W. H. 1973. Relationship between the inhibition constant (K1) and the concentration of inhibitor which causes 50 per cent inhibition (I50) of an enzymatic reaction. *Biochem Pharmacol,* 22(23), pp 3099-108.

Cherry, S. R. & Gambhir, S. S. 2001. Use of positron emission tomography in animal research. *Ilar j,* 42(3), pp 219-32.

Chopra, A., Shan, L., Eckelman, W. C., Leung, K., Latterner, M., Bryant, S. H. & Menkens, A. 2012. Molecular Imaging and Contrast Agent Database (MICAD): evolution and progress. *Mol Imaging Biol,* 14(1), pp 4-13.

Christ, E., Wild, D., Forrer, F., Brändle, M., Sahli, R., Clerici, T., Gloor, B., Martius, F., Maecke, H. & Reubi, J. 2009. Glucagon-like peptide-1 receptor imaging for localization of insulinomas. *J Clin Endocrinol Metab,* 94(11), pp 4398-405.

Connolly, B. M., Vanko, A., McQuade, P., Guenther, I., Meng, X., Rubins, D., Waterhouse, R., Hargreaves, R., Sur, C. & Hostetler, E. 2012. Ex vivo imaging of pancreatic beta cells using a radiolabeled GLP-1 receptor agonist. *Mol Imaging Biol,* 14(1), pp 79-87.

Coppieters, K. T., Dotta, F., Amirian, N., Campbell, P. D., Kay, T. W., Atkinson, M. A., Roep, B. O. & von Herrath, M. G. 2012. Demonstration of islet-autoreactive CD8 T cells in insulitic lesions from recent onset and long-term type 1 diabetes patients. *J Exp Med,* 209(1), pp 51-60.

Darchen, F., Scherman, D., Laduron, P. M. & Henry, J. P. 1988. Ketanserin binds to the monoamine transporter of chromaffin granules and of synaptic vesicles. *Mol Pharmacol,* 33(6), pp 672-7.

De Groef, S., Staels, W., Van Gassen, N., Lemper, M., Yuchi, Y., Sojoodi, M., Bussche, L., Heremans, Y., Leuckx, G., De Leu, N., Van de Casteele, M., Baeyens, L. & Heimberg, H. 2016. Sources of beta cells inside the pancreas. *Diabetologia,* 59(9), pp 1834-7.

Di Gialleonardo, V., Signore, A., Scheerstra, E. A., Visser, A. K., van Waarde, A., Dierckx, R. A. & de Vries, E. F. 2012. 11C-hydroxytryptophan uptake and metabolism in endocrine and exocrine pancreas. *J Nucl Med,* 53(11), pp 1755-63.

Drucker, D. J. 1998. Glucagon-like peptides. *Diabetes,* 47(2), pp 159-69.

Efange, S. M. 2000. In vivo imaging of the vesicular acetylcholine transporter and the vesicular monoamine transporter. *Faseb j,* 14(15), pp 2401-13.

Eisenbarth, G. S. 1986. Type I diabetes mellitus. A chronic autoimmune disease. *N Engl J Med,* 314(21), pp 1360-8.

Elayat, A. A., el-Naggar, M. M. & Tahir, M. 1995. An immunocytochemical and morphometric study of the rat pancreatic islets. *J Anat,* 186(629-37.

Elding Larsson, H., Vehik, K., Gesualdo, P., Akolkar, B., Hagopian, W., Krischer, J., Lernmark, A., Rewers, M., Simell, O., She, J. X., Ziegler, A. & Haller, M. J. 2014. Children followed in the TEDDY study are diagnosed with type 1 diabetes at an early stage of disease. *Pediatr Diabetes,* 15(2), pp 118-26.

Ellis, H. 2013. Anatomy of the pancreas and the spleen. 31(6), pp 263–266.

Elomaa, V. V., Jurttila, J., Rajander, J. & Solin, O. 2014. Automation of ^{64}Cu production at Turku PET Centre. *Applied Radiation and Isotopes,* 89(74-78.

Erickson, J. D., Eiden, L. E. & Hoffman, B. J. 1992. Expression cloning of a reserpine-sensitive vesicular monoamine transporter. *Proc Natl Acad Sci U S A,* 89(22), pp 10993-7.

Eriksson, O., Espes, D., Selvaraju, R. K., Jansson, E., Antoni, G., Sorensen, J., Lubberink, M., Biglarnia, A. R., Eriksson, J. W., Sundin, A., Ahlstrom, H., Eriksson, B., Johansson, L., Carlsson, P. O. & Korsgren, O. 2014. Positron emission tomography ligand [11C]5-hydroxy-tryptophan can be used as a surrogate marker for the human endocrine pancreas. *Diabetes,* 63(10), pp 3428-37.

Eriksson, O., Jahan, M., Johnström, P., Korsgren, O., Sundin, A., Halldin, C. & Johansson, L. 2010. In vivo and in vitro characterization of [^{18}F]-FE-(+)-DTBZ as a tracer for beta-cell mass. *Nucl Med Biol,* 37(3), pp 357-63.

Eriksson, O., Laughlin, M., Brom, M., Nuutila, P., Roden, M., Hwa, A., Bonadonna, R. & Gotthardt, M. 2016. In vivo imaging of beta cells with radiotracers: state of the art, prospects and recommendations for development and use. *Diabetologia,* 59(7), pp 1340-1349.

Espes, D., Selvaraju, R., Velikyan, I., Krajcovic, M., Carlsson, P. O. & Eriksson, O. 2016. Quantification of beta-Cell Mass in Intramuscular Islet Grafts Using Radiolabeled Exendin-4. *Transplant Direct,* 2(8), pp e93.

Eter, W. A., Parween, S., Joosten, L., Frielink, C., Eriksson, M., Brom, M., Ahlgren, U. & Gotthardt, M. 2016. SPECT-OPT multimodal imaging enables accurate evaluation of radiotracers for beta-cell mass assessments. *Sci Rep,* 6(1-6.

Faustman, D. L. 2014. Why were we wrong for so long? The pancreas of type 1 diabetic patients commonly functions for decades. *Diabetologia,* 57(1), pp 1-3.

Fava, G. E., Dong, E. W. & Wu, H. 2016. Intra-islet glucagon-like peptide 1. *J Diabetes Complications,* 30(8), pp 1651-1658.

Ferrannini, E. 2010. The stunned beta cell: a brief history. *Cell Metab,* 11(5), pp 349-52.

Flamez, D., Roland, I., Berton, A., Kutlu, B., Dufrane, D., Beckers, M. C., De Waele, E., Rooman, I., Bouwens, L., Clark, A., Lonneux, M., Jamar, J. F., Goldman, S., Marechal, D., Goodman, N., Gianello, P., Van Huffel, C., Salmon, I. & Eizirik, D. L. 2010. A genomic-based approach identifies FXYD domain containing ion transport regulator 2 (FXYD2)gammaa as a pancreatic beta cell-specific biomarker. *Diabetologia,* 53(7), pp 1372-83.

Fowler, M. J. 2008. Microvascular and Macrovascular Complications of Diabetes. *Clinical Diabetes,* 26(2), pp 77-82.

Freeby, M., Ichise, M. & Harris, P. E. 2012. Vesicular monoamine transporter, type 2 (VMAT2) expression as it compares to insulin and pancreatic polypeptide in the head, body and tail of the human pancreas. *Islets,* 4(6), pp 393-7.

Freeby, M. J., Kringas, P., Goland, R. S., Leibel, R. L., Maffei, A., Divgi, C., Ichise, M. & Harris, P. E. 2016. Cross-sectional and Test-Retest Characterization of PET with [18F]FP-(+)-DTBZ for beta Cell Mass Estimates in Diabetes. *Mol Imaging Biol,* 18(2), pp 292-301.

Fu, Z., Gilbert, E. R. & Liu, D. 2013. Regulation of insulin synthesis and secretion and pancreatic Beta-cell dysfunction in diabetes. *Curr Diabetes Rev,* 9(1), pp 25-53.

Fujioka, Y., Arano, Y., Ono, M., Uehara, T., Ogawa, K., Namba, S., Saga, T., Nakamoto, Y., Mukai, T., Konishi, J. & Saji, H. 2001. Renal metabolism of 3'-iodohippuryl N$^{\varepsilon}$-maleoyl-L-lysine (HML)-conjugated Fab fragments. *Bioconjug Chem,* 12(2), pp 178-85.

Fujioka, Y., Satake, S., Uehara, T., Mukai, T., Akizawa, H., Ogawa, K., Saji, H., Endo, K. & Arano, Y. 2005. In vitro system to estimate renal brush border enzyme-mediated cleavage of Peptide linkages for designing radiolabeled antibody fragments of low renal radioactivity levels. *Bioconjug Chem,* 16(6), pp 1610-6.

Gao, H., Niu, G., Yang, M., Quan, Q., Ma, Y., Murage, E. N., Ahn, J. M., Kiesewetter, D. O. & Chen, X. 2011. PET of insulinoma using ^{18}F-FBEM-EM3106B, a new GLP-1 analogue. *Mol Pharm,* 8(5), pp 1775-82.

Goland, R., Freeby, M., Parsey, R., Saisho, Y., Kumar, D., Simpson, N., Hirsch, J., Prince, M., Maffei, A., Mann, J. J., Butler, P. C., Van Heertum, R., Leibel, R. L., Ichise, M. & Harris, P. E. 2009. 11C-dihydrotetrabenazine PET of the pancreas in subjects with long-standing type 1 diabetes and in healthy controls. *J Nucl Med,* 50(3), pp 382-9.

Gotthardt, M., Eizirik, D. L., Cnop, M. & Brom, M. 2014. Beta cell imaging - a key tool in optimized diabetes prevention and treatment. *Trends Endocrinol Metab,* 25(8), pp 375-7.

Gotthardt, M., Lalyko, G., van Eerd-Vismale, J., Keil, B., Schurrat, T., Hower, M., Laverman, P., Behr, T., Boerman, O., Göke, B. & Béhé, M. 2006. A new technique for in vivo imaging of specific GLP-1 binding sites: first results in small rodents. *Regul Pept,* 137(3), pp 162-7.

Gotthardt, M., van Eerd-Vismale, J., Oyen, W., de Jong, M., Zhang, H., Rolleman, E., Maecke, H., Béhé, M. & Boerman, O. 2007. Indication for different mechanisms of kidney uptake of radiolabeled peptides. *J Nucl Med,* 48(4), pp 596-601.

Gregg, B. E., Moore, P. C., Demozay, D., Hall, B. A., Li, M., Husain, A., Wright, A. J., Atkinson, M. A. & Rhodes, C. J. 2012. Formation of a human beta-cell population within pancreatic islets is set early in life. *J Clin Endocrinol Metab,* 97(9), pp 3197-206.

Göke, R., Fehmann, H. C., Linn, T., Schmidt, H., Krause, M., Eng, J. & Goke, B. 1993. Exendin-4 is a high potency agonist and truncated exendin-(9-39)-amide an antagonist at the glucagon-like peptide 1-(7-36)-amide receptor of insulin-secreting beta-cells. *J Biol Chem,* 268(26), pp 19650-5.

Hellstrom-Lindahl, E., Danielsson, A., Ponten, F., Czernichow, P., Korsgren, O., Johansson, L. & Eriksson, O. 2016. GPR44 is a pancreatic protein restricted to the human beta cell. *Acta Diabetol,* 53(3), pp 413-21.

Hickeson, M., Yun, M., Matthies, A., Zhuang, H., Adam, L. E., Lacorte, L. & Alavi, A. 2002. Use of a corrected standardized uptake value based on the lesion size on CT permits accurate characterization of lung nodules on FDG-PET. *Eur J Nucl Med Mol Imaging,* 29(12), pp 1639-47.

Holst, J. J., Christensen, M., Lund, A., de Heer, J., Svendsen, B., Kielgast, U. & Knop, F. K. 2011. Regulation of glucagon secretion by incretins. *Diabetes Obes Metab,* 13 Suppl 1(89-94.

Howell, R. W., Wessels, B. W., Loevinger, R., Watson, E. E., Bolch, W. E., Brill, A. B., Charkes, N. D., Fisher, D. R., Hays, M. T., Robertson, J. S., Siegel, J. A. & Thomas, S. R. 1999. The MIRD perspective 1999. Medical Internal Radiation Dose Committee. *J Nucl Med,* 40(1), pp 3-10.

Hubalewska-Dydejczyk, A., Sowa-Staszczak, A., Tomaszuk, M. & Stefanska, A. 2015. GLP-1 and exendin-4 for imaging endocrine pancreas. A review. Labelled glucagon-like peptide-1 analogues: past, present and future. *Q J Nucl Med Mol Imaging,* 59(2), pp 152-60.

International Diabetes Atlas. 2015. *International Diabetes Federation. IDF Diabetes Atlas.* [Online]. Brussels, Belgium: International Diabetes Federation, 2015. Available: http://www.diabetesatlas.org/.

Jansson, L., Barbu, A., Bodin, B., Drott, C. J., Espes, D., Gao, X., Grapensparr, L., Kallskog, O., Lau, J., Liljeback, H., Palm, F., Quach, M., Sandberg, M., Stromberg, V., Ullsten, S. & Carlsson, P. O. 2016. Pancreatic islet blood flow and its measurement. *Ups J Med Sci,* 121(2), pp 81-95.

Jodal, A., Pape, F., Becker-Pauly, C., Maas, O., Schibli, R. & Behe, M. 2015. Evaluation of ^{111}In-labelled exendin-4 derivatives containing different meprin beta-specific cleavable linkers. *PLoS One,* 10(4), pp e0123443.

Johnbeck, C. B., Knigge, U. & Kjaer, A. 2014. PET tracers for somatostatin receptor imaging of neuroendocrine tumors: current status and review of the literature. *Future Oncol,* 10(14), pp 2259-77.

Kahn, S. E., Andrikopoulos, S. & Verchere, C. B. 1999. Islet amyloid: a long-recognized but underappreciated pathological feature of type 2 diabetes. *Diabetes,* 48(2), pp 241-53.

Kauhanen, S., Seppanen, M., Minn, H., Gullichsen, R., Salonen, A., Alanen, K., Parkkola, R., Solin, O., Bergman, J., Sane, T., Salmi, J., Valimaki, M. & Nuutila, P. 2007. Fluorine-18-L-dihydroxyphenylalanine (^{18}F-DOPA) positron emission tomography as a tool to localize an insulinoma or beta-cell hyperplasia in adult patients. *J Clin Endocrinol Metab,* 92(4), pp 1237-44.

Kauhanen, S., Seppänen, M., Minn, H. & Nuutila, P. 2010. Clinical PET imaging of insulinoma and beta-cell hyperplasia. *Curr Pharm Des,* 16(14), pp 1550-60.

Keenan, H. A., Sun, J. K., Levine, J., Doria, A., Aiello, L. P., Eisenbarth, G., Bonner-Weir, S. & King, G. L. 2010. Residual insulin production and pancreatic ss-cell turnover after 50 years of diabetes: Joslin Medalist Study. *Diabetes,* 59(11), pp 2846-53.

Khalil, M. M., Tremoleda, J. L., Bayomy, T. B. & Gsell, W. 2011. Molecular SPECT Imaging: An Overview. *Int J Mol Imaging,* 2011(1-15.

Kiesewetter, D. O., Gao, H., Ma, Y., Niu, G., Quan, Q., Guo, N. & Chen, X. 2012a. ^{18}F-radiolabeled analogs of exendin-4 for PET imaging of GLP-1 in insulinoma. *Eur J Nucl Med Mol Imaging,* 39(3), pp 463-73.

Kiesewetter, D. O., Guo, N., Guo, J., Gao, H., Zhu, L., Ma, Y., Niu, G. & Chen, X. 2012b. Evaluation of an [^{18}F]AlF-NOTA Analog of Exendin-4 for Imaging of GLP-1 Receptor in Insulinoma. *Theranostics,* 2(10), pp 999-1009.

Kilbourn, M. R. 1997. In vivo radiotracers for vesicular neurotransmitter transporters. *Nucl Med Biol,* 24(7), pp 615-9.

Krogvold, L., Edwin, B., Buanes, T., Ludvigsson, J., Korsgren, O., Hyoty, H., Frisk, G., Hanssen, K. F. & Dahl-Jorgensen, K. 2014. Pancreatic biopsy by minimal tail resection in live adult patients at the onset of type 1 diabetes: experiences from the DiViD study. *Diabetologia,* 57(4), pp 841-3.

Kung, H., Lieberman, B., Zhuang, Z., Oya, S., Kung, M., Choi, S., Poessl, K., Blankemeyer, E., Hou, C., Skovronsky, D. & Kilbourn, M. 2008a. In vivo imaging of vesicular monoamine transporter 2 in pancreas using an ^{18}F epoxide derivative of tetrabenazine. *Nucl Med Biol,* 35(8), pp 825-37.

Kung, M., Hou, C., Goswami, R., Ponde, D., Kilbourn, M. & Kung, H. 2007. Characterization of optically resolved 9-fluoropropyl-dihydrotetrabenazine as a potential PET imaging agent targeting vesicular monoamine transporters. *Nucl Med Biol,* 34(3), pp 239-46.

Kung, M., Hou, C., Lieberman, B., Oya, S., Ponde, D., Blankemeyer, E., Skovronsky, D., Kilbourn, M. & Kung, H. 2008b. In vivo imaging of beta-cell mass in rats using ^{18}F-FP-(+)-DTBZ: a potential PET ligand for studying diabetes mellitus. *J Nucl Med,* 49(7), pp 1171-6.

Kwee, T. C., Basu, S., Saboury, B., Torigian, D. A., Naji, A. & Alavi, A. 2011. Beta-cell imaging: opportunities and limitations. *J Nucl Med,* 52(3), pp 493-5.

Körner, M., Stöckli, M., Waser, B. & Reubi, J. 2007. GLP-1 receptor expression in human tumors and human normal tissues: potential for in vivo targeting. *J Nucl Med,* 48(5), pp 736-43.

Lampasona, V. & Liberati, D. 2016. Islet Autoantibodies. *Curr Diab Rep,* 16(6), pp 1-10.

Larsen, P. U. J., Dahlstrom, K. & Jensen, M. 1997. Synthesis of [^{11}C]iodomethane by iodination of [^{11}C]methane. *Appl. Radiat. Isot.,* 48(2), pp 153-157.

Lindskog, C., Korsgren, O., Ponten, F., Eriksson, J. W., Johansson, L. & Danielsson, A. 2012. Novel pancreatic beta cell-specific proteins: antibody-based proteomics for identification of new biomarker candidates. *J Proteomics,* 75(9), pp 2611-20.

Low, G., Hussein, N., Owen, R. J., Toso, C., Patel, V. H., Bhargava, R. & Shapiro, A. M. 2010. Role of imaging in clinical islet transplantation. *Radiographics,* 30(2), pp 353-66.

Luo, Y., Li, N., Kiesewetter, D. O., Chen, X. & Li, F. 2016a. ^{68}Ga-NOTA-Exendin-4 PET/CT in Localization of an Occult Insulinoma and Appearance of Coexisting Esophageal Carcinoma. *Clin Nucl Med,* 41(4), pp 341-3.

Luo, Y., Pan, Q., Shao, Y., Yu, M., Wu, W., Xue, H., Kiesewetter, D. O., Zhu, Z., Li, F., Zhao, Y. & Chen, X. 2016b. Glucagon-like Peptide-1 Receptor PET/CT with ^{68}Ga-NOTA-exendin-4 for Detecting Localized Insulinoma: a Prospective Cohort Study. *J Nucl Med,* 57(5), pp 715-720.

Maahs, D. M., West, N. A., Lawrence, J. M. & Mayer-Davis, E. J. 2010. Chapter 1: Epidemiology of Type 1 Diabetes. *Endocrinol Metab Clin North Am,* 39(3), pp 481-97.

Maffei, A., Liu, Z., Witkowski, P., Moschella, F., Del Pozzo, G., Liu, E., Herold, K., Winchester, R., Hardy, M. & Harris, P. 2004. Identification of tissue-restricted transcripts in human islets. *Endocrinology,* 145(10), pp 4513-21.

Malaisse, W., Louchami, K. & Sener, A. 2009. Noninvasive imaging of pancreatic beta cells. *Nat Rev Endocrinol,* 5(7), pp 394-400.

Matveyenko, A. V. & Butler, P. 2008. Relationship between beta-cell mass and diabetes onset. *Diabetes Obes Metab,* 10(Suppl 4), pp 23-31.

Medarova, Z. & Moore, A. 2008. Non-invasive detection of transplanted pancreatic islets. *Diabetes Obes Metab,* 10(Suppl 4), pp 88-97.

Mei, Q., Mundinger, T. O., Lernmark, A. & Taborsky, G. J., Jr. 2002. Early, selective, and marked loss of sympathetic nerves from the islets of BioBreeder diabetic rats. *Diabetes,* 51(10), pp 2997-3002.

Meier, J. J., Bhushan, A., Butler, A. E., Rizza, R. A. & Butler, P. C. 2005. Sustained beta cell apoptosis in patients with long-standing type 1 diabetes: indirect evidence for islet regeneration? *Diabetologia,* 48(11), pp 2221-8.

Meier, J. J., Kohler, C. U., Alkhatib, B., Sergi, C., Junker, T., Klein, H. H., Schmidt, W. E. & Fritsch, H. 2010. Beta-cell development and turnover during prenatal life in humans. *Eur J Endocrinol,* 162(3), pp 559-68.

Melis, M., Valkema, R., Krenning, E. P. & de Jong, M. 2012. Reduction of renal uptake of radiolabeled octreotate by amifostine coadministration. *J Nucl Med,* 53(5), pp 749-53.

Melis, M., Vegt, E., Konijnenberg, M. W., de Visser, M., Bijster, M., Vermeij, M., Krenning, E. P., Boerman, O. C. & de Jong, M. 2010. Nephrotoxicity in mice after repeated imaging using ^{111}In-labeled peptides. *J Nucl Med,* 51(6), pp 973-7.

Mezza, T. & Kulkarni, R. N. 2014. The regulation of pre- and post-maturational plasticity of mammalian islet cell mass. *Diabetologia,* 57(7), pp 1291-303.

Mi, B., Xu, Y., Pan, D., Wang, L., Yang, R., Yu, C., Wan, W., Wu, Y. & Yang, M. 2016. Non-invasive glucagon-like peptide-1 receptor imaging in pancreas with 18F-Al labeled Cys39-exendin-4. *Biochem Biophys Res Commun,* 471(1), pp 47-51.

Minn, H., Kauhanen, S., Seppanen, M. & Nuutila, P. 2009. ^{18}F-FDOPA: a multiple-target molecule. *J Nucl Med,* 50(12), pp 1915-8.

Moore, A., Bonner-Weir, S. & Weissleder, R. 2001. Noninvasive in vivo measurement of beta-cell mass in mouse model of diabetes. *Diabetes,* 50(10), pp 2231-6.

Nadkarni, P., Chepurny, O. G. & Holz, G. G. 2014. Regulation of glucose homeostasis by GLP-1. *Prog Mol Biol Transl Sci,* 121, pp 23-65.

Nakamoto, Y., Sakahara, H., Saga, T., Sato, N., Zhao, S., Arano, Y., Fujioka, Y., Saji, H. & Konishi, J. 1999. A novel immunoscintigraphy technique using metabolizable linker with angiotensin II treatment. *Br J Cancer,* 79(11-12), pp 1794-9.

Nalin, L., Selvaraju, R. K., Velikyan, I., Berglund, M., Andreasson, S., Wikstrand, A., Ryden, A., Lubberink, M., Kandeel, F., Nyman, G., Korsgren, O., Eriksson, O. & Jensen-Waern, M. 2014. Positron emission tomography imaging of the glucagon-like peptide-1 receptor in healthy and streptozotocin-induced diabetic pigs. *Eur J Nucl Med Mol Imaging,* 41(9), pp 1800-10.

Normandin, M. D., Petersen, K. F., Ding, Y. S., Lin, S. F., Naik, S., Fowles, K., Skovronsky, D. M., Herold, K. C., McCarthy, T. J., Calle, R. A., Carson, R. E., Treadway, J. L. & Cline, G. W. 2012. In vivo imaging of endogenous pancreatic beta-cell mass in healthy and type 1 diabetic subjects using 18F-fluoropropyl-dihydrotetrabenazine and PET. *J Nucl Med,* 53(6), pp 908-16.

Nuutila, P., Koivisto, V. A., Knuuti, J., Ruotsalainen, U., Teras, M., Haaparanta, M., Bergman, J., Solin, O., Voipio-Pulkki, L. M., Wegelius, U. & et al. 1992. Glucose-free fatty acid cycle operates in human heart and skeletal muscle in vivo. *J Clin Invest,* 89(6), pp 1767-74.

Någren, K. & Halldin, C. 1998. Methylation of amide and thiol functions with [^{11}C]methyl triflate, as exemplified by [^{11}C]NMSP, [^{11}C]flumazenil and [^{11}C]methionine. *J Labelled Comp Radiopharm,* 41(9), pp 831-841.

Otonkoski, T., Nanto-Salonen, K., Seppanen, M., Veijola, R., Huopio, H., Hussain, K., Tapanainen, P., Eskola, O., Parkkola, R., Ekstrom, K., Guiot, Y., Rahier, J., Laakso, M., Rintala, R., Nuutila, P. & Minn, H. 2006. Noninvasive diagnosis of focal hyperinsulinism of infancy with [^{18}F]-DOPA positron emission tomography. *Diabetes,* 55(1), pp 13-8.

Palmer, J. P. 2009. C-peptide in the natural history of type 1 diabetes. *Diabetes Metab Res Rev,* 25(4), pp 325-8.

Parkes, D., Jodka, C., Smith, P., Nayak, S., Rinehart, L., Gingerich, R., Chen, K. & Young, A. 2001. Pharmacokinetic actions of exendin-4 in the rat: Comparison with glucagon-like peptide-1. *Drug Dev Res,* 53(4), pp 260-267.

Pattou, F., Kerr-Conte, J. & Wild, D. 2010. GLP-1-receptor scanning for imaging of human beta cells transplanted in muscle. *N Engl J Med,* 363(13), pp 1289-90.

Peter, D., Jimenez, J., Liu, Y., Kim, J. & Edwards, R. H. 1994. The chromaffin granule and synaptic vesicle amine transporters differ in substrate recognition and sensitivity to inhibitors. *J Biol Chem,* 269(10), pp 7231-7.

Peter, D., Liu, Y., Sternini, C., de Giorgio, R., Brecha, N. & Edwards, R. H. 1995. Differential expression of two vesicular monoamine transporters. *J Neurosci,* 15(9), pp 6179-88.

Polonsky, K. S., Given, B. D. & Van Cauter, E. 1988. Twenty-four-hour profiles and pulsatile patterns of insulin secretion in normal and obese subjects. *J Clin Invest,* 81(2), pp 442-8.

Radetti, G., Ghizzoni, L., Paganini, C., Iughetti, L., Caselli, G. & Bernasconi, S. 1998. Insulin pulsatility in obese and normal prepubertal children. *Horm Res,* 50(2), pp 78-82.

Raffo, A., Hancock, K., Polito, T., Xie, Y., Andan, G., Witkowski, P., Hardy, M., Barba, P., Ferrara, C., Maffei, A., Freeby, M., Goland, R., Leibel, R. L., Sweet, I. R. & Harris, P. E. 2008. Role of vesicular monoamine transporter type 2 in rodent insulin secretion and glucose metabolism revealed by its specific antagonist tetrabenazine. *J Endocrinol,* 198(1), pp 41-9.

Rahier, J., Guiot, Y., Goebbels, R. M., Sempoux, C. & Henquin, J. C. 2008. Pancreatic beta-cell mass in European subjects with type 2 diabetes. *Diabetes Obes Metab,* 10(Suppl 4), pp 32-42.

Rahmim, A., Rousset, O. & Zaidi, H. 2007. Strategies for Motion Tracking and Correction in PET. *PET Clin,* 2(2), pp 251-66.

Rahmim, A. & Zaidi, H. 2008. PET versus SPECT: strengths, limitations and challenges. *Nucl Med Commun,* 29(3), pp 193-207.

Ramlo-Halsted, B. A. & Edelman, S. V. 2000. The Natural History of Type 2 Diabetes: Practical Points to Consider in Developing Prevention and Treatment Strategies. *Clinical Diabetes,* 18(2), pp 80-84.

Reiner, T., Thurber, G., Gaglia, J., Vinegoni, C., Liew, C. W., Upadhyay, R., Kohler, R. H., Li, L., Kulkarni, R. N., Benoist, C., Mathis, D. & Weissleder, R. 2011. Accurate measurement of pancreatic islet beta-cell mass using a second-generation fluorescent exendin-4 analog. *Proc Natl Acad Sci U S A,* 108(31), pp 12815-20.

Reubi, J. C. & Waser, B. 2003. Concomitant expression of several peptide receptors in

neuroendocrine tumours: molecular basis for in vivo multireceptor tumour targeting. *Eur J Nucl Med Mol Imaging,* 30(5), pp 781-93.

Ritt, P., Vija, H., Hornegger, J. & Kuwert, T. 2011. Absolute quantification in SPECT. *Eur J Nucl Med Mol Imaging,* 38(Suppl 1), pp 69-77.

Ritzel, R. A., Butler, A. E., Rizza, R. A., Veldhuis, J. D. & Butler, P. C. 2006. Relationship between beta-cell mass and fasting blood glucose concentration in humans. *Diabetes Care,* 29(3), pp 717-8.

Roscioni, S. S., Migliorini, A., Gegg, M. & Lickert, H. 2016. Impact of islet architecture on beta-cell heterogeneity, plasticity and function. *Nat Rev Endocrinol*.

Ryan, E. A., Paty, B. W., Senior, P. A., Bigam, D., Alfadhli, E., Kneteman, N. M., Lakey, J. R. & Shapiro, A. M. 2005. Five-year follow-up after clinical islet transplantation. *Diabetes,* 54(7), pp 2060-9.

Ryden, A., Nyman, G., Nalin, L., Andreasson, S., Korsgren, O., Eriksson, O. & Jensen-Waern, M. 2016. Cardiovascular side-effects and insulin secretion after intravenous administration of radiolabeled Exendin-4 in pigs. *Nucl Med Biol,* 43(7), pp 397-402.

Rylova, S. N., Waser, B., Del Pozzo, L., Tonnesmann, R., Mansi, R., Meyer, P. T., Reubi, J. C. & Maecke, H. R. 2016. Approaches to improve the pharmacokinetics of radiolabeled GLP-1 receptor ligands using antagonistic tracers. *J Nucl Med*.

Saisho, Y., Harris, P., Butler, A., Galasso, R., Gurlo, T., Rizza, R. & Butler, P. 2008. Relationship between pancreatic vesicular monoamine transporter 2 (VMAT2) and insulin expression in human pancreas. *J Mol Histol,* 39(5), pp 543-51.

Salomon, D. & Meda, P. 1986. Heterogeneity and contact-dependent regulation of hormone secretion by individual B cells. *Exp Cell Res,* 162(2), pp 507-20.

Satin, L. S., Butler, P. C., Ha, J. & Sherman, A. S. 2015. Pulsatile insulin secretion, impaired glucose tolerance and type 2 diabetes. *Mol Aspects Med,* 42(61-77.

Scherman, D., Jaudon, P. & Henry, J. P. 1983. Characterization of the monoamine carrier of chromaffin granule membrane by binding of [2-^{3}H]dihydrotetrabenazine. *Proc Natl Acad Sci U S A,* 80(2), pp 584-8.

Schuit, F. C., In't Veld, P. A. & Pipeleers, D. G. 1988. Glucose stimulates proinsulin biosynthesis by a dose-dependent recruitment of pancreatic beta cells. *Proc Natl Acad Sci U S A,* 85(11), pp 3865-9.

Selvaraju, R. K., Bulenga, T. N., Espes, D., Lubberink, M., Sorensen, J., Eriksson, B., Estrada, S., Velikyan, I. & Eriksson, O. 2015. Dosimetry of [^{68}Ga]Ga-DO3A-VS-Cys^{40}-Exendin-4 in rodents, pigs, non-human primates and human - repeated scanning in human is possible. *Am J Nucl Med Mol Imaging,* 5(3), pp 259-69.

Selvaraju, R. K., Velikyan, I., Johansson, L., Wu, Z., Todorov, I., Shively, J., Kandeel, F., Korsgren, O. & Eriksson, O. 2013. In vivo imaging of the glucagonlike peptide 1 receptor in the pancreas with ^{68}Ga-labeled DO3A-exendin-4. *J Nucl Med,* 54(8), pp 1458-63.

Shapiro, A. M., Lakey, J. R., Ryan, E. A., Korbutt, G. S., Toth, E., Warnock, G. L., Kneteman, N. M. & Rajotte, R. V. 2000. Islet transplantation in seven patients with type 1 diabetes mellitus using a glucocorticoid-free immunosuppressive regimen. *N Engl J Med,* 343(4), pp 230-8.

Simonsen, L., Holst, J. J. & Deacon, C. F. 2006. Exendin-4, but not glucagon-like peptide-1, is cleared exclusively by glomerular filtration in anaesthetised pigs. *Diabetologia,* 49(4), pp 706-12.

Simpson, N., Souza, F., Witkowski, P., Maffei, A., Raffo, A., Herron, A., Kilbourn, M., Jurewicz, A., Herold, K., Liu, E., Hardy, M., Van Heertum, R. & Harris, P. 2006. Visualizing pancreatic beta-cell mass with [11C]DTBZ. *Nucl Med Biol,* 33(7), pp 855-64.

Singhal, T., Ding, Y., Weinzimmer, D., Normandin, M., Labaree, D., Ropchan, J., Nabulsi, N., Lin, S., Skaddan, M., Soeller, W., Huang, Y., Carson, R., Treadway, J. & Cline, G. 2010. Pancreatic Beta Cell Mass PET Imaging and Quantification with [11C]DTBZ and [18F]FP-(+)-DTBZ in Rodent Models of Diabetes. *Mol Imaging Biol,* 13(5), pp 973-984.

Solin, O., Bergman, J., Haaparanta, M. & Reissell, A. 1988. Production of ^{18}F from water targets. Specific radioactivity and anionic contaminants. *Appl Radiat Isot.,* 39(10), pp 1065-1071.

Souza, F., Freeby, M., Hultman, K., Simpson, N., Herron, A., Witkowsky, P., Liu, E., Maffei, A. & Harris, P. E. 2006a. Current progress in non-invasive imaging of beta cell mass of the endocrine pancreas. *Curr Med Chem,* 13(23), pp 2761-73.

Souza, F., Simpson, N., Raffo, A., Saxena, C., Maffei, A., Hardy, M., Kilbourn, M., Goland, R., Leibel, R., Mann, J., Van Heertum, R. & Harris, P. 2006b. Longitudinal noninvasive PET-based beta cell mass estimates in a spontaneous diabetes rat model. *J Clin Invest,* 116(6), pp 1506-13.

Sowa-Staszczak, A., Trofimiuk-Muldner, M., Stefanska, A., Tomaszuk, M., Buziak-Bereza, M., Gilis-Januszewska, A., Jabrocka-Hybel, A., Glowa, B., Malecki, M., Bednarczuk, T., Kaminski, G., Kowalska, A., Mikolajczak, R., Janota, B. & Hubalewska-Dydejczyk, A. 2016. 99mTc Labeled Glucagon-Like Peptide-1-Analogue (99mTc-GLP1) Scintigraphy in the Management of Patients with Occult Insulinoma. *PLoS One,* 11(8), pp e0160714.

Spanoudaki, V. C. & Ziegler, S. I. 2008. Handbook of Experimental Pharmacology, Molecular Imaging I. *In:* Semmler, W. & Schwaiger, M. (eds.) *PET & SPECT instrumentation.* 2008, Springer.

Stabin, M. G., Sparks, R. B. & Crowe, E. 2005. OLINDA/EXM: the second-generation personal computer software for internal dose assessment in nuclear medicine. *J Nucl Med,* 46(6), pp 1023-7.

Steiner, D. J., Kim, A., Miller, K. & Hara, M. 2010. Pancreatic islet plasticity: interspecies comparison of islet architecture and composition. *Islets,* 2(3), pp 135-45.

Sweet, I., Cook, D., Lernmark, A., Greenbaum, C. & Krohn, K. 2004a. Non-invasive imaging of beta cell mass: a quantitative analysis. *Diabetes Technol Ther,* 6(5), pp 652-9.

Sweet, I., Cook, D., Lernmark, A., Greenbaum, C., Wallen, A., Marcum, E., Stekhova, S. & Krohn, K. 2004b. Systematic screening of potential beta-cell imaging agents. *Biochem Biophys Res Commun,* 314(4), pp 976-83.

Tai, Y. C., Ruangma, A., Rowland, D., Siegel, S., Newport, D. F., Chow, P. L. & Laforest, R. 2005. Performance evaluation of the microPET focus: a third-generation microPET scanner dedicated to animal imaging. *J Nucl Med,* 46(3), pp 455-63.

Teng, L., Crooks, P. A. & Dwoskin, L. P. 1998. Lobeline displaces [^{3}H]dihydrotetrabenazine binding and releases [^{3}H]dopamine from rat striatal synaptic vesicles: comparison with d-amphetamine. *J Neurochem,* 71(1), pp 258-65.

Teo, A. K., Gupta, M. K., Doria, A. & Kulkarni, R. N. 2015. Dissecting diabetes/metabolic disease mechanisms using pluripotent stem cells and genome editing tools. *Mol Metab,* 4(9), pp 593-604.

Tessonnier, L., Sebag, F., Ghander, C., De Micco, C., Reynaud, R., Palazzo, F. F., Conte-Devolx, B., Henry, J. F., Mundler, O. & Taieb, D. 2010. Limited value of 18F-F-DOPA PET to localize pancreatic insulin-secreting tumors in adults with hyperinsulinemic hypoglycemia. *J Clin Endocrinol Metab,* 95(1), pp 303-7.

Thorens, B. 1996. Glucose transporters in the regulation of intestinal, renal, and liver glucose fluxes. *Am J Physiol,* 270(4 Pt 1), pp G541-53.

Tornehave, D., Kristensen, P., Rømer, J., Knudsen, L. & Heller, R. 2008. Expression of the GLP-1 receptor in mouse, rat, and human pancreas. *J Histochem Cytochem,* 56(9), pp 841-51.

Tsao, H. H., Lin, K. J., Juang, J. H., Skovronsky, D. M., Yen, T. C., Wey, S. P. & Kung, M. P. 2010. Binding characteristics of 9-fluoropropyl-(+)-dihydrotetrabenzazine (AV-133) to the vesicular monoamine transporter type 2 in rats. *Nucl Med Biol,* 37(4), pp 413-9.

Tsao, H. H., Skovronsky, D. M., Lin, K. J., Yen, T. C., Wey, S. P. & Kung, M. P. 2011. Sigma receptor binding of tetrabenazine series tracers targeting VMAT2 in rat pancreas. *Nucl Med Biol,* 38(7), pp 1029-34.

Tuomilehto, J., Lindstrom, J., Eriksson, J. G., Valle, T. T., Hamalainen, H., Ilanne-Parikka, P., Keinanen-Kiukaanniemi, S., Laakso, M., Louheranta, A., Rastas, M., Salminen, V. & Uusitupa, M. 2001. Prevention of type 2 diabetes mellitus by changes in lifestyle among subjects with impaired glucose tolerance. *N Engl J Med,* 344(18), pp 1343-50.

Turkington, T. G. 2001. Introduction to PET instrumentation. *J Nucl Med Technol,* 29(1), pp 4-11.

Ueberberg, S., Meier, J. J., Waengler, C., Schechinger, W., Dietrich, J. W., Tannapfel, A., Schmitz, I., Schirrmacher, R., Koller, M., Klein, H. H. & Schneider, S. 2009. Generation of novel single-chain antibodies by phage-display technology to direct imaging agents highly selective to pancreatic beta- or alpha-cells in vivo. *Diabetes,* 58(10), pp 2324-34.

van der Kroon, I., Andralojc, K., Willekens, S. M., Bos, D., Joosten, L., Boerman, O. C., Brom, M. & Gotthardt, M. 2016. Noninvasive Imaging of Islet Transplants with ^{111}In-Exendin-3 SPECT/CT. *J Nucl Med,* 57(5), pp 799-804.

Vegt, E., de Jong, M., Wetzels, J., Masereeuw, R., Melis, M., Oyen, W., Gotthardt, M. & Boerman, O. 2010. Renal toxicity of radiolabeled peptides and antibody fragments: mechanisms, impact on radionuclide therapy, and strategies for prevention. *J Nucl Med,* 51(7), pp 1049-58.

Vegt, E., Melis, M., Eek, A., de Visser, M., Brom, M., Oyen, W. J., Gotthardt, M., de Jong, M. & Boerman, O. C. 2011. Renal uptake of different radiolabelled peptides is mediated by megalin: SPECT and biodistribution studies in megalin-deficient mice. *Eur J Nucl Med Mol Imaging,* 38(4), pp 623-32.

Vegt, E., van Eerd, J. E., Eek, A., Oyen, W. J., Wetzels, J. F., de Jong, M., Russel, F. G., Masereeuw, R., Gotthardt, M. & Boerman, O. C. 2008. Reducing renal uptake of radiolabeled peptides using albumin fragments. *J Nucl Med,* 49(9), pp 1506-11.

Villiger, M., Goulley, J., Friedrich, M., Grapin-Botton, A., Meda, P., Lasser, T. & Leitgeb, R. A. 2009. In vivo imaging of murine endocrine islets of Langerhans with extended-focus optical coherence microscopy. *Diabetologia,* 52(8), pp 1599-607.

Wang, P., Yoo, B., Yang, J., Zhang, X., Ross, A., Pantazopoulos, P., Dai, G. & Moore, A. 2014. GLP-1R-targeting magnetic nanoparticles for pancreatic islet imaging. *Diabetes,* 63(5), pp 1465-74.

Waser, B. & Reubi, J. C. 2014. Radiolabelled GLP-1 receptor antagonist binds to GLP-1 receptor-

expressing human tissues. *Eur J Nucl Med Mol Imaging,* 41(6), pp 1166-71.

Weihe, E. & Eiden, L. E. 2000. Chemical neuroanatomy of the vesicular amine transporters. *Faseb j,* 14(15), pp 2435-49.

Weihe, E., Schafer, M. K., Erickson, J. D. & Eiden, L. E. 1994. Localization of vesicular monoamine transporter isoforms (VMAT1 and VMAT2) to endocrine cells and neurons in rat. *J Mol Neurosci,* 5(3), pp 149-64.

Weir, G. C. & Bonner-Weir, S. 2013. Islet beta cell mass in diabetes and how it relates to function, birth, and death. *Ann N Y Acad Sci,* 1281, pp 92-105.

Weir, G. C., Bonner-Weir, S. & Leahy, J. L. 1990. Islet mass and function in diabetes and transplantation. *Diabetes,* 39(4), pp 401-5.

Wessels, B. W., Konijnenberg, M. W., Dale, R. G., Breitz, H. B., Cremonesi, M., Meredith, R. F., Green, A. J., Bouchet, L. G., Brill, A. B., Bolch, W. E., Sgouros, G. & Thomas, S. R. 2008. MIRD pamphlet No. 20: the effect of model assumptions on kidney dosimetry and response--implications for radionuclide therapy. *J Nucl Med,* 49(11), pp 1884-99.

Wilbur, D. S., Chyan, M. K., Hamlin, D. K., Nguyen, H. & Vessella, R. L. 2011. Reagents for astatination of biomolecules. 5. Evaluation of hydrazone linkers in ^{211}At- and ^{125}I-labeled closo-decaborate(2-) conjugates of Fab' as a means of decreasing kidney retention. *Bioconjug Chem,* 22(6), pp 1089-102.

Wild, D., Béhé, M., Wicki, A., Storch, D., Waser, B., Gotthardt, M., Keil, B., Christofori, G., Reubi, J. & Mäcke, H. 2006. [Lys^{40}(Ahx-DTPA-^{111}In)NH$_2$] exendin-4, a very promising ligand for glucagon-like peptide-1 (GLP-1) receptor targeting. *J Nucl Med,* 47(12), pp 2025-33.

Wild, D., Christ, E., Caplin, M. E., Kurzawinski, T. R., Forrer, F., Brandle, M., Seufert, J., Weber, W. A., Bomanji, J., Perren, A., Ell, P. J. & Reubi, J. C. 2011. Glucagon-like peptide-1 versus somatostatin receptor targeting reveals 2 distinct forms of malignant insulinomas. *J Nucl Med,* 52(7), pp 1073-8.

Wild, D., Macke, H., Christ, E., Gloor, B. & Reubi, J. C. 2008. Glucagon-like peptide 1-receptor scans to localize occult insulinomas. *N Engl J Med,* 359(7), pp 766-8.

Wild, D., Wicki, A., Mansi, R., Béhé, M., Keil, B., Bernhardt, P., Christofori, G., Ell, P. & Mäcke, H. 2010. Exendin-4-based radiopharmaceuticals for glucagonlike peptide-1 receptor PET/CT and SPECT/CT. *J Nucl Med,* 51(7), pp 1059-67.

Williams, A. J., Thrower, S. L., Sequeiros, I. M., Ward, A., Bickerton, A. S., Triay, J. M., Callaway, M. P. & Dayan, C. M. 2012. Pancreatic volume is reduced in adult patients with recently diagnosed type 1 diabetes. *J Clin Endocrinol Metab,* 97(11), pp E2109-13.

Wu, H., Liang, S., Liu, S., Pan, Y., Cheng, D. & Zhang, Y. 2013a. ^{18}F-radiolabeled GLP-1 analog exendin-4 for PET/CT imaging of insulinoma in small animals. *Nucl Med Commun,* 34(7), pp 701-8.

Wu, Z., Liu, S., Hassink, M., Nair, I., Park, R., Li, L., Todorov, I., Fox, J. M., Li, Z., Shively, J. E., Conti, P. S. & Kandeel, F. 2013b. Development and evaluation of ^{18}F-TTCO-Cys^{40}-Exendin-4: a PET probe for imaging transplanted islets. *J Nucl Med,* 54(2), pp 244-51.

Wu, Z., Todorov, I., Li, L., Bading, J. R., Li, Z., Nair, I., Ishiyama, K., Colcher, D., Conti, P. E., Fraser, S. E., Shively, J. E. & Kandeel, F. 2011. In vivo imaging of transplanted islets with ^{64}Cu-DO3A-VS-Cys^{40}-Exendin-4 by targeting GLP-1 receptor. *Bioconjug Chem,* 22(8), pp 1587-94.

Xu, G., Kaneto, H., Laybutt, D. R., Duvivier-Kali, V. F., Trivedi, N., Suzuma, K., King, G. L., Weir, G. C. & Bonner-Weir, S. 2007. Downregulation of GLP-1 and GIP receptor expression by hyperglycemia: possible contribution to impaired incretin effects in diabetes. *Diabetes,* 56(6), pp 1551-8.

Young, A. A., Gedulin, B. R., Bhavsar, S., Bodkin, N., Jodka, C., Hansen, B. & Denaro, M. 1999. Glucose-lowering and insulin-sensitizing actions of exendin-4: studies in obese diabetic (ob/ob, db/db) mice, diabetic fatty Zucker rats, and diabetic rhesus monkeys (Macaca mulatta). *Diabetes,* 48(5), pp 1026-34.

Yue, X., Yan, X., Wu, C., Niu, G., Ma, Y., Jacobson, O., Shen, B., Kiesewetter, D. O. & Chen, X. 2014. One-pot two-step radiosynthesis of a new ^{18}F-labeled thiol reactive prosthetic group and its conjugate for insulinoma imaging. *Mol Pharm,* 11(11), pp 3875-84.

Zarkovic, M., Ciric, J., Stojanovic, M., Penezic, Z., Trbojevic, B., Dresgic, M. & Nesovic, M. 1999. Effect of insulin sensitivity on pulsatile insulin secretion. *Eur J Endocrinol,* 141(5), pp 494-501.

Zeng, G. L., Galt, J. R., Wernick, M. N., Mintzer, R. A. & Aarsvold, J. N. 2004. Single-Photon Emission Computed Tomography. *Emission Tomography: Fundamentals of PET and SPECT.* Elsevier Inc.

Zheng, G., Dwoskin, L. P. & Crooks, P. A. 2006. Vesicular monoamine transporter 2: role as a novel target for drug development. *Aaps j,* 8(4), pp E682-92.

Ziegler, A. G., Rewers, M., Simell, O., Simell, T., Lempainen, J., Steck, A., Winkler, C., Ilonen, J., Veijola, R., Knip, M., Bonifacio, E. & Eisenbarth, G. S. 2013. Seroconversion to multiple islet autoantibodies and risk of progression to diabetes in children. *Jama,* 309(23), pp 2473-9.

Annales Universitatis Turkuensis

Turun yliopisto
University of Turku

Painosalama Oy, Turku, Finland 2017

ISBN 978-951-29-6863-3 (PRINT)
ISBN 978-951-29-6864-0 (PDF)
ISSN 0355-9483 (Print) | ISSN 2343-3213 (Online)